Universidade do Minho
Escola de Ciências

Ana Sofia dos Santos Moura

Polymeric nanoparticles for Methotrexate delivery

Outubro de 2018

Ana Sofia dos Santos Moura **Polymeric nanoparticles for Methotrexate delivery**

UMinho | 2018

Universidade do Minho
Escola de Ciências

Ana Sofia dos Santos Moura

Polymeric nanoparticles for Methotrexate delivery

Tese de Mestrado
Mestrado em Bioquímica Aplicada (Área de especialização em Biomedicina)

Trabalho efetuado sob a orientação da
Doutora Ana Isabel Sá Loureiro

e do
Professor Doutor João Carlos Ramos Nunes Marcos

Outubro de 2018

DECLARAÇÃO

Nome: Ana Sofia dos Santos Moura

Endereço eletrónico: sofiamoura17@gmail.com Telefone: 918152267

Cartão do Cidadão: 14375752

Título da dissertação: Polymeric nanoparticles for Methotrexate delivery

Orientadores:

Doutora Ana Isabel Sá Loureiro

Professor Doutor João Carlos Ramos Nunes Marcos

Ano de conclusão: 2018

Mestrado em Bioquímica Aplicada, área de especialização em Biomedicina

Universidade do Minho, 29 de Outubro de 2018

Acknowledgements/Agradecimentos

Ao longo deste ano, de diferentes formas, várias pessoas contribuíram para a realização desta tese de mestrado e eu quero agradecer a todos aqueles que me ajudaram e apoiaram.

Gostaria de agradecer aos meus orientadores, nomeadamente à Dr.ª **Ana Loureiro**, por todo o apoio, orientação, disponibilidade e conselhos dados ao longo do ano. Muito obrigada!

Ao Professor Artur Cavaco Paulo, obrigada pela oportunidade de fazer parte do grupo de investigação Bioprocessos e Bionanotecnologia.

Agradeço a todos os colegas de laboratório, pela receção e ambiente incrível que proporcionaram. Em especial, quero agradecer à **Jennifer** e à **Diana**, por toda a ajuda dada ao longo do ano e por todos os momentos de alegria vividos no laboratório. Obrigada, meninas!

Gostava de agradecer particularmente à **Patrícia**, que tenho o prazer de chamar de amiga, pelo apoio constante, pelos conselhos e incentivo ao longo desta aventura que passámos juntas. Por estares comigo nos bons e maus momentos, sempre pronta a ajudar e por todos os momentos a sorrir juntas (são muitos!). Muito obrigada pela amizade!

A toda a minha família e amigos, obrigada pelo apoio constante. Aos meus queridos **pais** e **irmão**, que sempre me mostraram que com trabalho e dedicação se consegue alcançar os nossos objetivos. Por todo o apoio, paciência e compreensão, muito obrigada. São o meu exemplo de força!

Ao meu **Fábio**, namorado, melhor amigo e companheiro. Pelo amor e amizade ao longo destes anos, pelo apoio incondicional e incentivo em todos os momentos difíceis, pela paciência e dedicação. Obrigada por me ajudares a viver, a ser uma pessoa melhor, e por toda a felicidade que me proporcionas todos os dias! Amo-te.

Muito obrigada a todos, sem vocês não seria possível!

Abstract – POLYMERIC NANOPARTICLES FOR METHOTREXATE DELIVERY

Cancer has one of the highest incidence rates worldwide and chemotherapy remains the main treatment option for most cancers. Chemotherapy has several limitations, such as systemic toxicity, severe side effects and limited efficacy. Nanoparticles (NPs) offer the possibility to encapsulate poorly soluble drugs, protect these therapeutic molecules and modify their blood circulation and tissue distribution profiles. The intravenous (IV) route is the most reliable route of entry for all drug delivery systems (DDS). However, there are multiple biological barriers after IV administration. Due to unique size and amenability to surface functionalization of NPs, they are particularly suitable to overcome these barriers. Body distribution and elimination of NPs depends on several characteristics, but size and surface characteristics are the most important, controlling the fate of the NPs. In general, NPs ranging between 10 and 100 nm, coated with hydrophilic molecules, such as poly(ethylene glycol) (PEG), and modified with a targeting agent at the surface, such as folic acid (FA), can overcome the drawbacks of chemotherapy, allowing an effective treatment for cancer. Methotrexate (MTX) is extensively used for the treatment of cancer and also for the treatment of rheumatoid arthritis (RA). The main objective of this thesis was the development of polymeric NPs as DDS for a specific delivery of MTX. For this, an exhaustive optimization was performed in order to encapsulate high concentrations of MTX in Poloxamer 407 (P407)-based nanoemulsions. P407-MTX conjugate and several MTX derivatives, such as MTX disodium salt (MTX-Na); MTX-dimethyldioctadecylammonium bromide (MTX-DODAB) complex and MTX diethylated (MTX-OEt), were developed and used for the production of the intended NPs. The physicochemical and biological characterization of the developed nanoemulsions demonstrated the production of effective nanoemulsions suitable for MTX delivery applications. Nanoemulsions prepared using a combination between the P407-MTX conjugate and the MTX-OEt derivative demonstrated a great biological effect against cancer cells (Caco-2 cell line). In addition, polymeric micelles were developed, using PEGylated MTX (MTX-PEG_{2000}). Although further optimizations are needed, the preliminary results demonstrated that this conjugate is able to induce the formation of micelles. In conclusion, the work developed in this master thesis allowed the accomplishment of the objectives proposed and the development of promising DDS for therapeutic applications, mainly for cancer therapy.

Resumo – NANOPARTÍCULAS POLIMÉRICAS PARA A ENTREGA DE METOTREXATO

O cancro tem uma das maiores taxas de incidência em todo o mundo e a quimioterapia continua a ser a principal opção de tratamento para a maioria dos cancros. A quimioterapia tem várias limitações, como toxicidade sistémica, efeitos secundários graves e eficácia limitada. As nanopartículas (NPs) oferecem a possibilidade de encapsular drogas pouco solúveis, proteger essas moléculas terapêuticas e modificar a sua circulação sanguínea e os perfis de distribuição nos tecidos. A via intravenosa (IV) é a via de entrada mais confiável para todos os sistemas de libertação de fármacos (DDS, do inglês *drug delivery systems*). No entanto, existem várias barreiras biológicas após a administração IV. Devido ao tamanho único e à facilidade de funcionalização da superfície das NPs, estas são particularmente adequadas para ultrapassar essas barreiras. A distribuição corporal e a eliminação das NPs dependem de várias características, mas o tamanho e as características de superfície são as mais importantes, controlando o destino das NPs. Em geral, NPs variando entre 10 e 100 nm de tamanho, revestidas com moléculas hidrofílicas, como o poli(etilenoglicol) (PEG), e modificadas com um agente de direcionamento na superfície, como o ácido fólico (FA), podem superar as desvantagens da quimioterapia, permitindo um tratamento eficaz para o cancro. Metotrexato (MTX) é amplamente utilizado para o tratamento do cancro e também para o tratamento da artrite reumatóide (RA). O principal objetivo desta tese foi o desenvolvimento de NPs poliméricas como DDS para uma entrega específica de MTX. Para isso, uma otimização exaustiva foi realizada de forma a encapsular altas concentrações de MTX em nanoemulsões baseadas em Poloxamer 407 (P407). O conjugado P407-MTX e vários derivados de MTX, tais como MTX disódio sal (MTX-Na), o complexo MTX-brometo de dimetildioctadecilamónio (MTX-DODAB) e MTX dietilado (MTX-OEt), foram desenvolvidos e utilizados para a produção das NPs pretendidas. A caracterização físico-química e biológica das nanoemulsões desenvolvidas demonstrou a produção de nanoemulsões adequadas para a entrega de MTX. Nanoemulsões preparadas utilizando uma combinação entre o conjugado P407-MTX e o derivado MTX-OEt demonstraram um grande efeito biológico contra células de cancro (linha celular Caco-2). Adicionalmente, foram desenvolvidas micelas poliméricas, utilizando MTX PEGuilado ($MTX\text{-}PEG_{2000}$). Embora sejam necessárias mais otimizações, os resultados preliminares demonstraram que este conjugado é capaz de induzir a formação de micelas. Em conclusão, o trabalho desenvolvido nesta tese de mestrado permitiu a realização dos objetivos propostos e o

desenvolvimento de DDS promissores para aplicações terapêuticas, principalmente para a terapia do cancro.

Table of Contents

Abbreviations and Acronyms Index

0-9

^{1}H NMR, NMR | Proton nuclear magnetic resonance

A

ATCC | American type culture collection

ATP | Adenosine triphosphate

C

CMC | Critical micelle concentration

D

DCC | *N,N'*-dicyclohexylcarbodiimide

DDS | Drug delivery systems

DHB | 2,5-dihydroxybenzoic acid

DHFR | Dihydrofolate reductase

DLS | Dynamic light scattering

DMAP | 4-dimethylaminopyridine

DMEM | Dulbecco's modified Eagle's medium

DMSO | Dimethyl sulphoxide

DMSO-d_6 | Deuterated dimethyl sulphoxide

DNA | Deoxyribonucleic acid

DODAB | Dimethyldioctadecylammonium bromide

E

EE | Encapsulation efficiency

EO | Ethylene oxide

EPR | Enhanced permeability and retention

F

FA | Folic acid, Folate

FBS | Fetal bovine serum

FDA | US Food and drug administration

FR | Folate receptor

G

GRAS | Generally recognized as safe

H

HPH | High pressure homogenization

HPLC | High performance liquid chromatography

I

IV | Intravenous

M

MALDI-TOF MS | Matrix assisted laser desorption ionization time-of-flight mass spectroscopy

MDR | Multidrug resistance

MPS | Mononuclear phagocyte system

MTS | 3-(4,5-dimethylthiazol-2-yl)-5-(3-carboxymethoxyphenyl)-2-(4-sulfophenyl)-2*H*-tetrazolium

MTX | Methotrexate

MTX-Na | MTX disodium salt

MTX-OEt | MTX diethylated

MW | Molecular weight

$MW_{average}$ | Average MW

MWCO | MW cut-off

N

NPs | Nanoparticles

NTA | Nanoparticle tracking analysis

P

P407 | Poloxamer 407

PBS | Phosphate buffered saline

PCS | Photon correlation spectroscopy

PdI | Polydispersity index

PEG | poly(ethylene glycol)

PEO | poly(ethylene oxide)

PES | Polyethersulfone

P-gp | P-glycoprotein

PLA | poly(lactic acid)

PLGA | poly(D,L-lactide-co-glycolic) acid

PNPs | Polymeric nanoparticles

PO | Propylene oxide

PPO | poly(propylene oxide)

R

RA | Rheumatoid arthritis

RES | Reticuloendothelial system

RFC | Reduced folate carrier

RME | Receptor-mediated endocytosis

RT | Room temperature

S

SD | Standard deviation

T

TA | Trifluoroacetic acid

U

UV | Ultraviolet-visible

Z

ZP | Zeta-potential

Figures Index

Tables Index

Equations Index

CHAPTER I

OBJECTIVES AND OUTLINE OF THE THESIS

Chapter I – OBJECTIVES AND OUTLINE OF THE THESIS

1. MOTIVATION AND OBJECTIVES OF THE WORK

Cancer has one of the highest incidence rates worldwide and chemotherapy is still the mainstream anticancer treatment, presenting several limitations and side effects. Thus, new approaches involving nanotechnology are emerging to improve and exploit the advantages of efficient drug delivery. Therefore, the purpose of this work is to develop nanoparticles (NPs) that will be able to provide an effective treatment for cancer. For this, two different types of polymeric NPs (PNPs), nanoemulsions and micelles, were produced. These NPs should present suitable characteristics for intravenous (IV) administration and should be selective to a target cell population. In this way, these nanoemulsions and micelles should present small size, stealth characteristics, ability to entrap methotrexate (MTX) successfully and a targeting agent at the surface. NPs with these characteristics can overcome the limitations and side effects greatly associated with conventional cancer therapy. In order to achieve all these objectives were performed several innovations and optimizations.

In sum, the main aim of this work was the development of PNPs as drug delivery systems (DDS) for a specific delivery of MTX, in order to develop a more effective treatment for cancer and with less side effects associated.

2. OUTLINE OF THE THESIS

In agreement with the goals of this master thesis, this document is divided into 5 chapters. The contents of each chapter are described below.

The current chapter (Chapter I) contains the main purposes and motivation of this work, as well as an introduction to the thesis outline and format. Chapter II presents an overview of the state of art, describing the information needed for a full understanding of the work presented in the following chapters. Chapter III is regarding the produced Poloxamer 407 (P407)-based nanoemulsions and summarizes all the materials and methods used in this work. The results obtained and its discussion are also presented in this chapter, evaluating all of the outcomes obtained and assessing the research work performed. Chapter IV presents the same structure to chapter III but relatively to the developed PEGylated micelles. This master thesis ends with Chapter V, which summarizes the final remarks of the work developed, as wells as the future perspectives for this research work and its possible applications in the future of the nanomedicine.

CHAPTER II

GENERAL INTRODUCTION

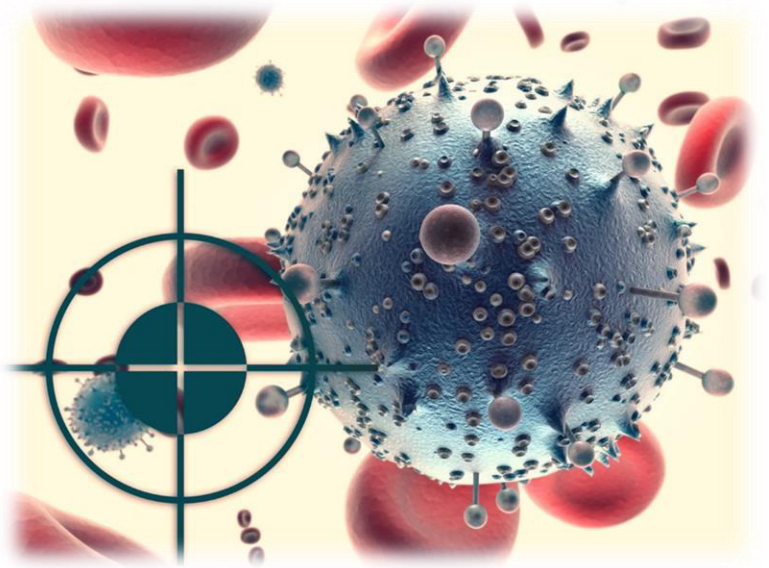

Chapter II – GENERAL INTRODUCTION

1. CANCER AND NANOMEDICINE

Cancer, one of the most devastating diseases in modern society [1], is a complex disease that involves various genetic alterations and cellular anomalies, in which abnormal cells divide without control and are able to invade other tissues in distant parts of the body [2]. Current treatment options for cancer include a combination of surgery, radiation therapy and chemotherapy [3]. Nevertheless, chemotherapy forms the major strategy for treating cancer [4]. However, this conventional therapy has a number of drawbacks such as the limited accessibility of drug to the tumor tissues [5], the requirement of high doses [6], intolerable cytotoxicity [7], the development of multidrug resistance (MDR) [8] and non-specific targeting [9]. Because most current chemotherapeutic agents distribute indiscriminately into virtually all cells of the body, they can damage both malignant and normal cells alike, often inducing sufficient toxicity to cause the patient to discontinue treatment [10]. For effective chemotherapy, it is desirable to suppress the growth of tumors with minimal side-effects on the healthy tissues and organs [11]. In order to improve the therapeutic efficacy of chemotherapeutic drugs, various DDS have been developed [12]. The main goals in the design of DDS are: (i) to decrease the side effects of conventional therapy by decreasing drug concentration in normal tissues; (ii) to enhance the pharmacokinetics and pharmacodynamics profiles; (iii) to allow IV drug administration by increasing drug solubility; (iv) to minimize drug loss in transit and maximize drug concentration in the tumor; (v) to improve drug stability by avoiding drug degradation; (vi) to achieve optimal cellular uptake and intracellular delivery; and (vii) to ensure biocompatibility and biodegradability [13].

Nanotechnology is an emerging interdisciplinary field that combines biology, chemistry and engineering [13]. Nowadays, nanotechnology is frequently used for various applications in fiber and textiles, agriculture, electronics, forensic science, space and medical therapeutics [14]. In recent years there has been an unprecedented expansion in the application of nanotechnology to medicine, commonly referred to as “nanomedicine”, with the development of new NPs for the diagnosis and treatment of cancer [15]. Nanomedicine has gained increasing interest as a means to overcome the problems and potentiate the advantages of efficient drug delivery [16]. One of the major advantages that nanomedicine offers is the development of DDS for the specific site targeted delivery of the therapeutic agents, decreasing the risk of toxicity to the normal tissues around the

lesion and other organs of the patient [17]. These systems also protect the drug from degradation during its transport [13]. In this way, the DDS have many advantages, such as the drug protection from premature degradation and interaction with the biological environment [18], enhancement of the absorption into a selected tissue [15], increase of the bioavailability [19] and circulation time [20], improvement of intracellular penetration [21] and increase of the patient compliance [14]. DDS have unique biological properties and their small size and large surface area-to-volume ratio allows them to bind, absorb and carry compounds, such as small molecule drugs, deoxyribonucleic acid (DNA) and probes, with high efficiency [3]. Over the time, several DDS were developed (figure 1) to improve the pharmacological and therapeutic properties of conventional drugs [22, 23]. Mainly, the past decade has witnessed enormous research efforts, undertaken in the development of nanosized particulate platforms for targeted therapy with minimal toxicity to achieve personalized medicine [24].

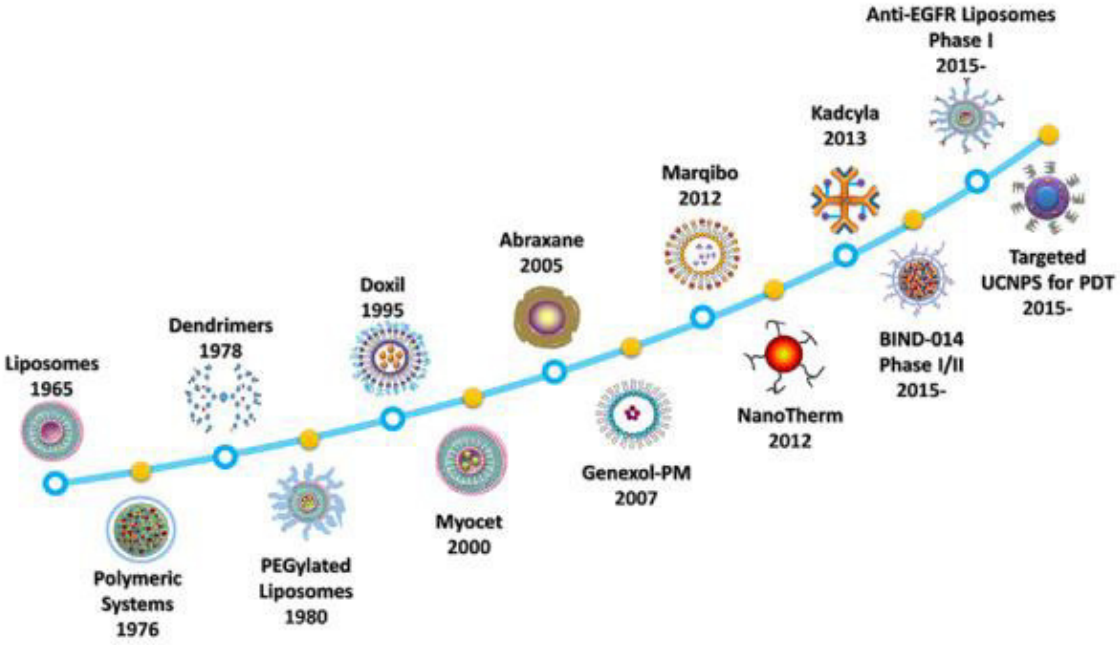

Figure 1 | Timeline of some drug delivery systems (DDS) developed in nanomedicine. [Adapted from Zhen LI *et al.* [25]].

Cancer nanotechnology seeks to characterize the interaction of nanoscale devices with cellular and molecular components specifically related to cancer diagnosis and therapy [26]. Nanoscale complexes have been currently developed, which consist of two main components: the NPs, which are used as the carrier agent, and the chemotherapeutic drug [3]. The use of NPs as DDS allows the administration of smaller but more effective drug doses, minimizing the adverse effects greatly associated to conventional chemotherapy [27].

2. NANOPARTICLES AS DRUG DELIVERY SYSTEMS

NPs are frequently defined as solid, colloidal particles in the range of 10–1000 nm [28]. NPs offer the possibility to encapsulate poorly soluble drugs, protect these therapeutic molecules from degradation and modify their blood circulation and tissue distribution profiles [29]. A wide range of anticancer drugs, such as paclitaxel and doxorubicin, have been loaded onto NPs with a potential effect against various cancers, and a superior therapeutic efficacy than the free drugs [30]. Many original NPs have been developed based on different compositions, both inorganic and organic, and specific biological properties [31]. Examples of NPs used in drug delivery include liposomes and PNPs [15], polymeric micelles and dendrimers [32], quantum dots and gold NPs [33], magnetic NPs and carbon nanotubes [22] (figure 2).

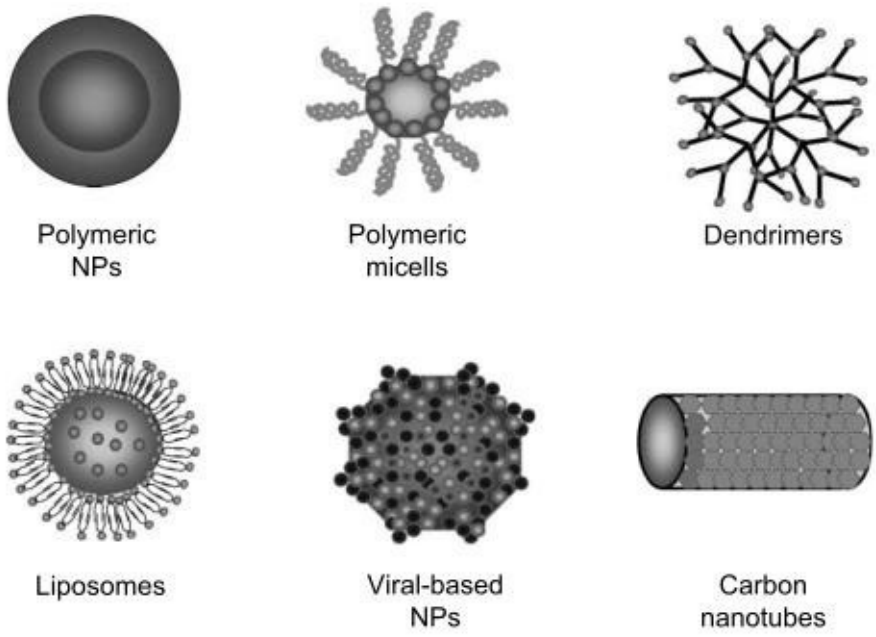

Figure 2 | Examples of nanoparticles (NPs) used as drug delivery systems (DDS). [Adapted from Kwangjae Cho *et al.* [6]].

Liposomes and polymer-based nanoformulations constitute the majority of the NPs based therapeutics available for clinical use [34, 35]. PNPs are a popular topic in the field of drug delivery and controlled drug release, with a diameter ranging from 10 to 100 nm [36]. The PNPs are obtained from synthetic polymers or natural polymers. Synthetic polymers include poly(ethylene glycol) (PEG), poly(lactic acid) (PLA) and poly(D,L-lactide-co-glycolic) acid (PLGA) [37]. Natural polymers, such as chitosan and albumin [38], are less used since they are not naturally pure and homogeneous, requiring a purification step before their use [39].

As a drug carrier, the PNPs have the following advantages: improvement of the absorption and bioavailability and increase of the solubility of drugs [40]; active search out and attack of cancer cells, thereby improving drug targeting [41]; penetration in the tissue and residence in tissues and cells for a long time to release their cargo drugs [40]; furthermore, PNPs can enhance drug stability, exhibiting slow and controlled drug release properties [36].

2.1. Biological Barriers

Pharmacological compounds are applied by enteral method, where the drugs are administered orally [42], or by parenteral method, where the drugs are administered subcutaneously, intramuscularly and intravenously [31]. IV administration is a very important and the most adopted drug delivery route [43]. This route of delivery is the most efficient means of delivering substances because it bypasses the need for solute absorption [44]. Thus, the IV route is the fastest, easiest and most reliable route of entry for all DDS, allowing quick and complete distribution across the body via the systemic circulation [31]. In cancer treatments, NPs are usually administered by IV injection, travelling in the blood stream and passing through biological barriers of the organism in order to reach and activate their molecular targets [13]. Upon administration, the most challenging goal is the passage of the drug molecules across numerous biological barriers that exist to protect the human body from invasion by foreign particles [32, 45]. The biological barriers include the fast renal elimination by glomerular filtration; the clearance by the reticuloendothelial system (RES) [46], also referred to as mononuclear phagocyte system (MPS), comprising the liver and spleen which rapidly remove particles from the circulation [45]; the immune barrier; and the blood vessel wall [31]. The MPS is primarily composed of phagocytic cells (e.g. monocytes and macrophages) and is responsible for engulfing and clearing old cells, cellular debris, foreign substances and pathogens from the bloodstream [8]. The macrophages of the MPS have the ability to remove unprotected NPs from the bloodstream within seconds after the IV administration, rendering them ineffective as site-specific DDS [47]. These macrophages cannot directly identify the NPs themselves, but rather recognize specific opsonin proteins bound to the surface of the NPs [48]. Opsonization of the NPs is a crucial step by which a foreign organism or particle becomes covered with opsonin proteins, thereby making it more visible to phagocytic cells [15, 47]. The process of opsonization, begins immediately after the NPs come in contact with plasma [49], allowing the NPs recognition by the MPS and consequently rapid blood clearance occurs with high liver and spleen accumulation [31, 50].

The MDR is another very common barrier that occurs in cancer therapy, which should be overcome to a successful treatment [51]. MDR is defined as a state of resilience against structurally and/or functionally unrelated drugs [52]. Recent studies have identified that the microenvironment of the tumor can alter the response of cancer cells to chemotherapy and targeted therapies through the production of secreted factors, leading to MDR [53]. The major mechanisms involved in MDR include the activation of the substituted signaling pathway, increased DNA repair capacity, dysfunctional apoptosis, drug efflux mediated by the MDR-related transporters, such as P-glycoprotein (P-gp), and decreased drug uptake (figure 3) [54].

NPs offer a platform for drug delivery that can be optimized to overcome biological barriers and customized to achieve diverse treatment strategies that address the complexities of MDR [52]. Due to their unique size [19], shape [35] and amenability to surface functionalization to incorporate the desired characteristics [39], NPs are particularly well suited to overcome all these barriers.

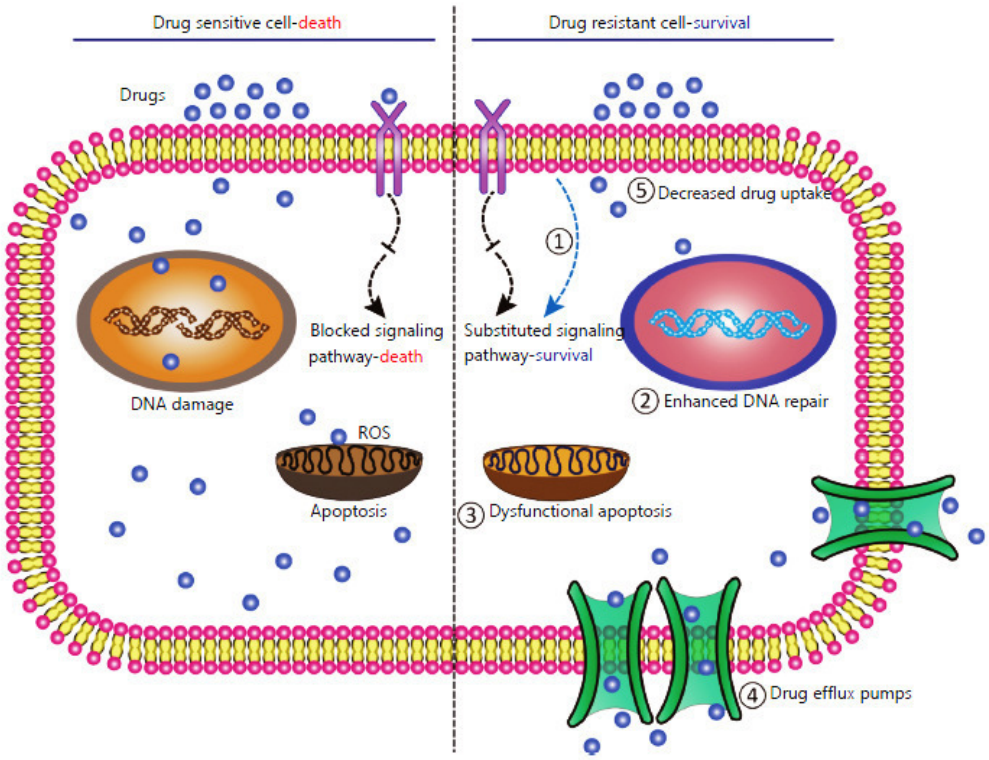

Figure 3 | Various mechanisms involved in tumor multidrug resistance (MDR). [Adapted from Meng Zhang *et al.* [54]].

2.2. Important characteristics of nanoparticles for intravenous administration

The body distribution and elimination of nanocarriers administered intravenously depends on several characteristics of the NPs [40]. Physicochemical properties of the NPs can result in differential uptake and targeting to certain organs, tissues or cells and may be optimized through the effective design of NPs [27]. The physicochemical properties that affect the body distribution of NPs and the drug release include the class, size, shape, surface charge, targeting and activation mechanism (figure 4) [55]. The class determines the basic properties of the particle [56]. Size, shape, surface charge and targeting generally affect the NPs pharmacokinetic and biodistribution [57]. The activation mechanisms can provide improved distribution or bioavailability of encapsulated drugs [58].

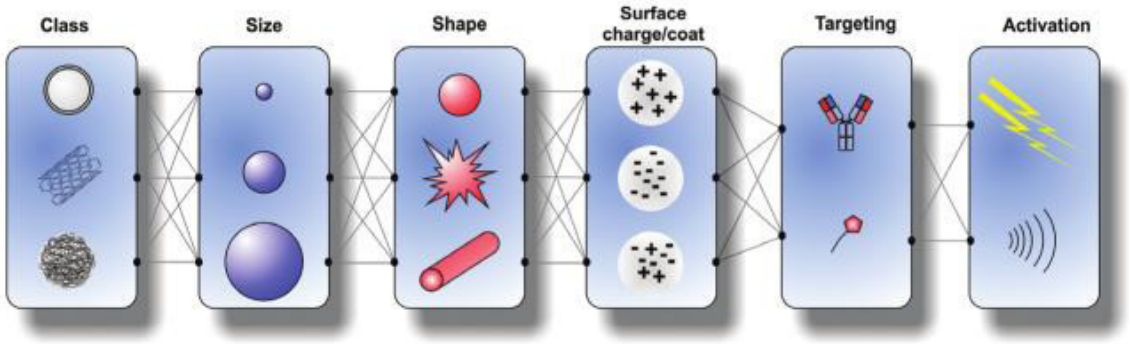

Figure 4 | Physicochemical properties of the nanoparticles (NPs) that affect their body distribution and drug release. [Adapted from Dandan Luo *et al.* [55]].

The fate of NPs injected intravenously can be controlled by adjusting their size and surface characteristics, mainly because these two properties affect the interaction with the blood proteins, which is the initial and most important stage of the journey [6].

2.2.1. Size

One of the advantages of NPs is that their size is tunable [59]. The size of NPs used as DDS should be large enough to prevent their rapid leakage into blood capillaries but small enough to escape capture by fixed macrophages that are lodged in the MPS [6]. After administration, small particles (< 20–30 nm) are eliminated by renal excretion [60, 61]. Larger particles (> 150 nm) can be rapidly taken up by the MPS cells present in the liver, the spleen and to a lesser extent, in the bone marrow [62]. In general, NPs ranging between 10 and 100 nm (figure 5) in size tend to represent an optimal range for the development of NPs for *in vivo* applications [63, 64].

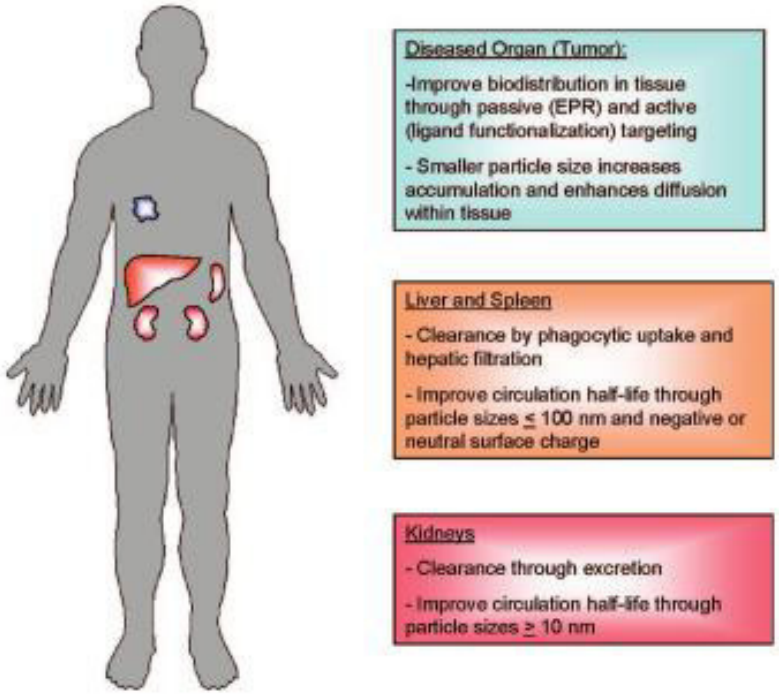

Figure 5 | Biological barriers of the nanoparticles (NPs), after intravenous (IV) administration. The size of the NPs is one of the major factors that affect their biodistribution and clearance. [Adapted from Frank Alexis *et al.* [19]]

The size of the NPs must be taken into consideration early in the design of targeted NPs, because it can affect not only their circulation time and biodistribution but also their cellular uptake [63, 65]. The NPs within this range are also taken up more efficiently by cells [66]. Another important parameter that is used to define the size range of the NPs is called the polydispersity index (PdI) [67]. PdI measures the dispersion of the NPs around the mean diameter and it is defined as the ratio between the standard deviation (SD) and the mean diameter of the distribution of the particles [68]. The numerical value of PdI ranges from 0.0 (for a perfectly uniform sample) to 1.0 (for a highly polydisperse sample with multiple particle size populations) [67]. A major problem in dissecting the effects of the size is high polydispersity of many nanocarriers [69]. Values of PdI of 0.2 and below are most commonly deemed acceptable in practice for polymer-based NPs [67]. However, an optimum condition is reached when PdI is lower or equal to 0.1, where the nanosuspension is seen with highly monodisperse standards [70].

2.2.2. Surface characteristics

It has been established that the physicochemical characteristics of NPs such as surface charge and functional groups can affect its uptake by the cells of the MPS [19], influencing their circulation time and their fate during systemic circulation [6]. The final surface charge affects the efficacy of

the targeted NPs [29]. The presence of surface charge can alter the opsonization profile of the material, its recognition by cells in the organs of the MPS and its overall plasma circulation profile [29]. The zeta-potential (ZP) of a nanoparticle is commonly used to characterize the surface charge property of NPs [71]. NPs with a ZP between −10mV and +10 mV are considered neutral, while NPs with ZP of greater than +30 mV or less than −30 mV are considered strongly cationic and strongly anionic, respectively [72]. Neutral and hydrophilic surface can generate stealth NPs, which are more resistant to macrophage uptake and consequently results in long blood circulation time [73]. Moreover, the opsonization of hydrophobic NPs occurs more quickly comparatively to hydrophilic NPs [63]. In this way, to avoid opsonization, NPs can be coated with a neutral and hydrophilic ligand [69] such as PEG, which is well known to resist to the protein adsorption [74]. PEGylation is the decoration of a particle surface by the covalently grafting, entrapping, or adsorbing of PEG chains [31]. PEG chains create a highly water bound barrier on the particle surface [75], providing steric stabilization and conferring stealth properties that prevent the proteins absorption [19]. The coating of NPs with PEG is a commonly employed strategy to overcome rapid MPS uptake, because it reduces adsorption of opsonins and other serum proteins by a mechanism known as the "steric repulsion effect" [26, 48]. PEG has been validated clinically in many different applications, and is currently listed as "Generally Recognized as Safe" (GRAS) by the US Food and Drug Administration (FDA), making it attractive to researchers [64]. If the PEG density at the NPs surface is low it is said to be in the mushroom regime, when the graft density is high the polymers are said to be in the brush regime (figure 6) [76].

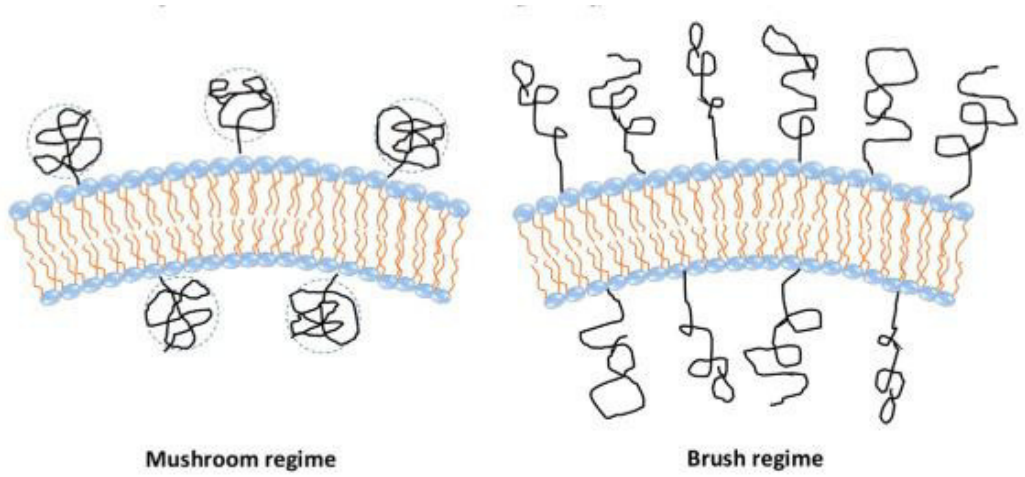

Figure 6 | Possible conformations of poly(ethylene glycol) (PEG) in nanoparticles (NPs) surface, mushroom and brush. [Adapted from Eugénia Nogueira *et al.* [76]].

The increase in density of PEG chains results in a conformation change from mushroom to brush, being the brush conformation described as the most resistant to phagocytosis and that poorly activate the human complement system [31]. Brush configuration in PEGylated NPs would create more effective blocking or repulsion of opsonins than the mushroom one [40]. A reduced recognition of the NPs by MPS, increases the circulation time with benefits for interaction of the NPs with desired biological target, permitting for example an accumulation of NPs in solid tumors [50, 77]. The most important advantages of PEGylation are not only the prolonged residence time in the body and the reduction of immunogenicity, but also the increase in stability towards metabolic enzymes (figure 7) [31].

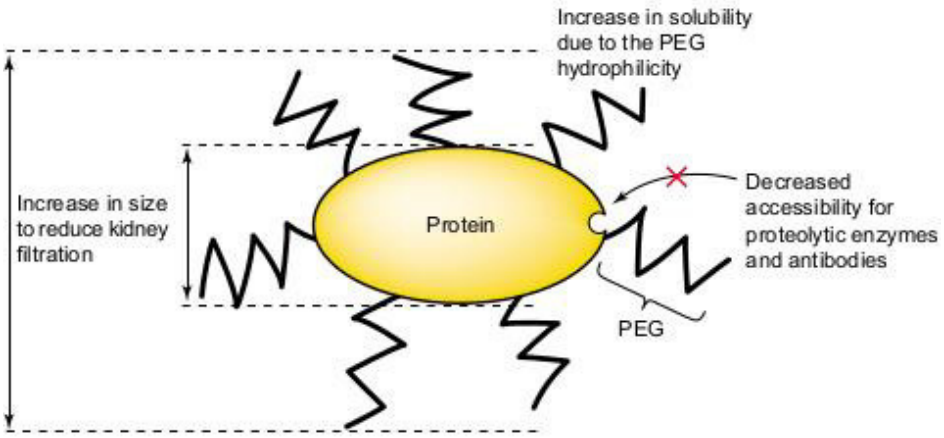

Figure 7 | Main advantages of PEGylation. [Adapted from Francesco M. Veronese *et al.* [78]].

Although the synthetic polymer PEG remains the gold standard for stealth functionalization, PEG chains can also be incorporated on NPs' surfaces using many different types of PEG-containing copolymers, such as Poloxamers [71]. Poloxamer block copolymers have been introduced in the late 1950s and since then they have been proposed for diverse pharmaceutical applications [79]. Poloxamers are triblock copolymers, also known as Pluronics [80]; these are poly(ethylene oxide)-b-poly(propylene oxide)-b-poly(ethylene oxide) type of block copolymers generally expressed as PEO_x-b-PPO_y-b-PEO_x [81], where x and y designate the total average number of the poly(ethylene oxide) (PEO) and poly(propylene oxide) (PPO) repeat units, respectively, and b stands for "block" [82] (figure 8). This arrangement results in an amphiphilic copolymer, in which the number of hydrophilic ethylene oxide (EO) (x) and hydrophobic propylene oxide (PO) (y) units can be altered [80]. Poloxamers containing at least 40 central PO units and PEO segments consisting of at least 70 EO units, such as P407, were described as most effective in suppressing the recognition of NPs by MPS [31].

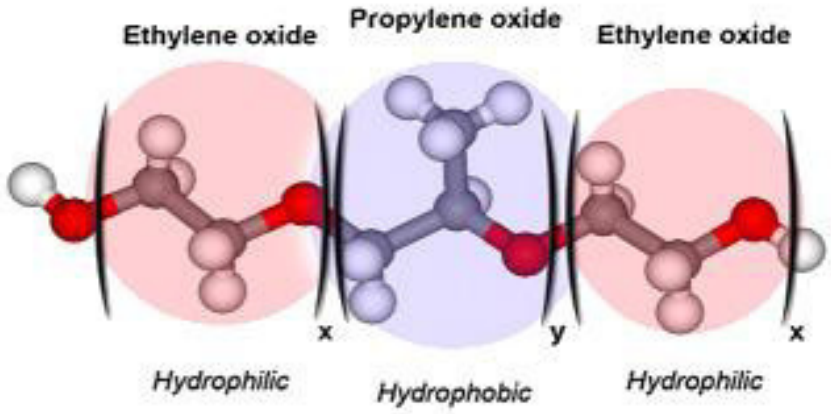

Figure 8 | Representation of the structure of Poloxamers. [Adapted from Elena V. Batrakova *et al.* [83]].

P407, principally available in the registered trademark of Pluronic F127, has a molecular weight (MW) of about 12600 Da [84]. FDA guide has presented P407 as an inactive ingredient for different types of preparations, such as IV, inhalation and oral formulations [79]. Poloxamers are readily available, biocompatible, low toxic [85], biodegradable and present good solubility in aqueous solvents [86]. They have been extensively studied as a potential drug delivery vehicle due to their excellent characteristics suitable for the production of pharmaceutical formulations, such as its amphiphilic micellar behavior, desirable delivery rate, thermo-sensitivity and biocompatibility [87]. Moreover, Poloxamers display a unique set of biological activities and have been shown to be potent sensitizers of MDR cancer cells *in vitro* and *in vivo* [51]. It was found that some Poloxamers copolymers can be used as biological response modifiers [51, 88] that can inhibit the P-gp efflux system by adenosine triphosphate (ATP) depletion in MDR cancerous cells [89]. This results in drastic sensitization of these tumors to anticancer agents, enhancing the activities of chemotherapeutic drugs [85, 90].

3. ENGINEERED NANOPARTICLES FOR CANCER THERAPY

NPs can be engineered to provide adequate features to overcome the main biological barriers and to prevent early clearance, which allow the increase of blood circulation time for long enough to reach or recognize its therapeutic site of action. Moreover, NPs can be also engineered to have enhanced cellular uptake and targeting abilities [31, 91]. To produce NPs that are capable of circulating in the body and reaching target cells, it is necessary to understand the physicochemical properties and their influence in the interaction with biological systems.

Indeed, to design suitable NPs it is crucial to take into account the different factors that influence NPs-cell interactions, such as size, shape, charge, ligand density, receptor expression levels, internalization mechanism and cell properties [92]. NPs can be internalized by cells through different endocytic mechanisms depending on NPs designs, like particle size and surface treatment [24]. Endocytosis can be divided into phagocytosis, macropinocytosis, caveolar-mediated endocytosis, clathrin-mediated endocytosis and clathrin-independent and caveolin-independent endocytosis, as demonstrated in figure 9 [49].

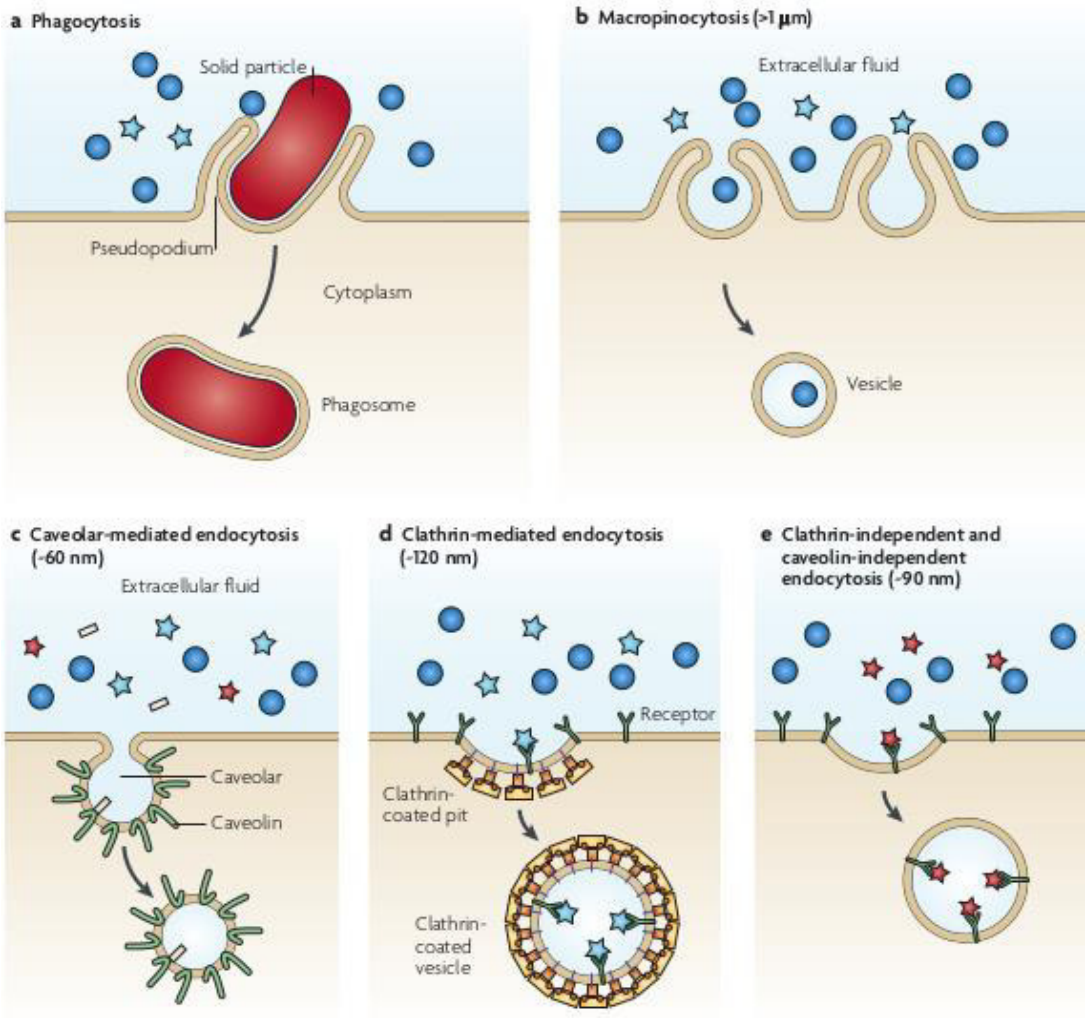

Figure 9 | Internalization of nanoparticles (NPs) through the different types of endocytosis. [Adapted from Robby A. Petros *et al.* [49]].

Internalization of large particles is facilitated by phagocytosis, (figure 9a), which directs the formation of cup-shaped membrane protrusions that gradually surround and close the particles [74]; nonspecific internalization of smaller particles (> 1 μM) can occur through macropinocytosis (figure 9b), which is an actin-regulated process that involves engulfment of a large quantity of extracellular fluid and particles through plasma membrane ruffling [24].

Smaller NPs can be internalized through several pathways, including caveolar-mediated endocytosis (≈ 60 nm) (figure 9c), that involves the assembly of the hairpin-like caveolin coats on the cytosolic side of the plasma membrane, forming a flask-shaped caveolae [49]; clathrin-mediated endocytosis (≈ 120 nm) (figure 9d), in which receptor-ligand binding triggers the recruitment and formation of "coated pits" (clathrin) on the cytosolic side of the plasma membrane [69]; and clathrin-independent and caveolin-independent endocytosis – or receptor-mediated endocytosis (RME) – (≈ 90 nm) (figure 9e), can also occur through receptor-ligand binding [69].
Cytotoxic drugs can distribute non-specifically all over the body and cause the death of normal as well as malignant cells, thereby giving rise to a variety of side effects [93]. Thus, there is need to develop new modalities for cancer treatment that can either passively or actively target cancer cells, enhancing the intracellular concentrations of drugs in cancer cells while avoiding toxicity in normal cells [6]. Drug targeting can be classified as active targeting and passive targeting [94]. A passive targeting strategy takes advantage of the distinct pathophysiological features of a tumor tissue, while an active targeting approach depends on the principle of ligand-receptor recognition, targeting specific receptors that are overexpressed in tumor tissues [7].

3.1. Passive Targeting

The anatomical differences between normal and tumor tissues are responsible for the passive targeting, inducing the delivery of drugs at the therapeutic site [31]. The tumor vasculature is highly heterogeneous in distribution and more permeable in some places, however, large areas of tumors may be poorly perfused [32]. The passive targeting of DDS consists in transporting NPs through leaky tumor capillary fenestrations within the tumor mass to reach cells by passive diffusion [13]. The large pore sizes allow the passage of NPs into the extravascular spaces and accumulation of NPs inside tumors [26]. Meanwhile, the deficient lymphatic recovery system in tumor site can lead to NPs accumulation within the tumor site [85]. The combined effect of a "leaky" defective vascular architecture and poor tumor lymphatic drainage is responsible for the enhanced permeability and retention (EPR) effect [3]. This way, the accumulation of NPs with drug in the tumor site is achieved by the EPR effect [95]. In sum, the EPR effect describes the enhanced accumulation of macromolecules in solid tumors (figure 10) [34], allowing the drug to remain in contact with the tumor for an extended period of time [96].

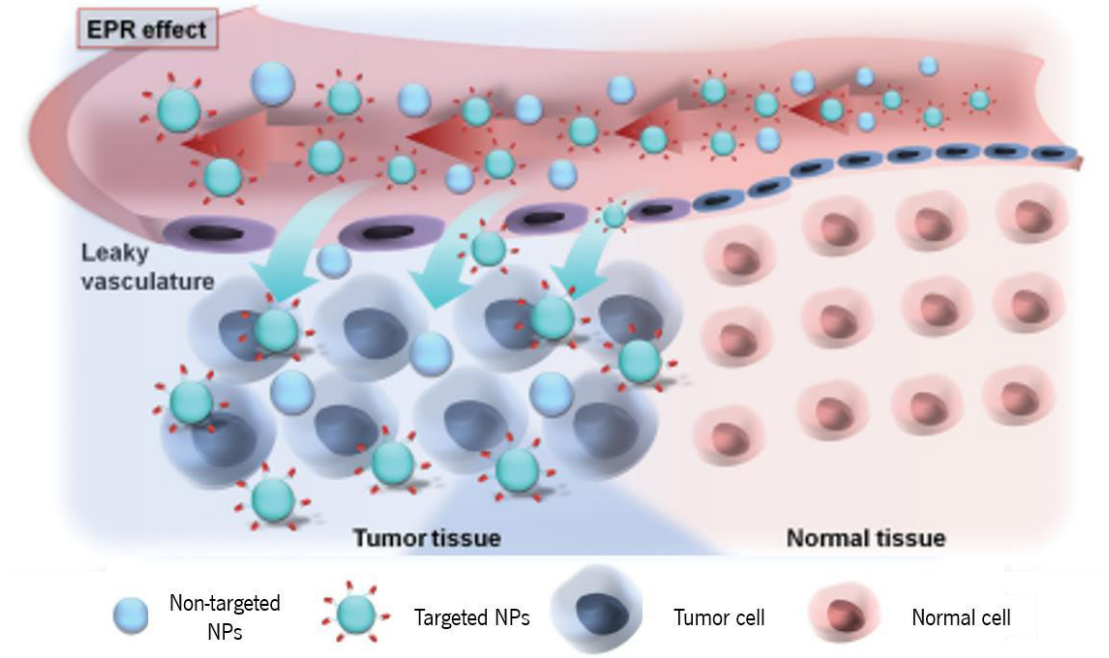

Figure 10 | Representation of passive targeting of nanoparticles (NPs), through enhanced permeability and retention (EPR) effect. [Adapted from Jing Huang *et al.* [97]].

Since its first identification, numerous studies have shown that the EPR effect results in passive accumulation of macromolecules and nanosized particulates (e.g. polymer conjugates, polymeric micelles, dendrimers and liposomes) in solid tumor tissues, increasing the therapeutic index while decreasing side effects [8]. This targeting approach exploits the pathophysiological conditions, such as leaky vasculature, pH, temperature and surface charge surrounding the tumor for specific delivery of NPs [98]. However, the passive targeting encounters many obstacles on the way to their target, such as the mucosal barriers, non-specific uptake of the particles and nonspecific delivery of the drug [99]. Additionally, delivery of the NPs to the interstitial fluid through the EPR effect does not guarantee intracellular delivery of the therapeutic drug [95].

3.2. Active Targeting

In the 19th century, Paul Ehrlich proposed the theory of active targeting by idealizing a DDS that would target drugs to specific areas in the body, describing it as the "magic bullet" [99]. The active targeting mechanism takes advantage of highly specific interactions between the targeting ligand and certain tissues or cells within the body to promote the accumulation of NPs [19]. Tumor cells express many molecules on their surface that distinguishes them from normal cells, which can be used in targeting delivery of NPs by attaching a monoclonal antibody or cell surface receptor ligand [15, 99].

The active targeting can improve the efficient internalization and has demonstrated increased therapeutic activity in some tumor models [100]. The active targeting concept exploits the specific binding affinities of targeting for specific retention and uptake by the disease cells targeted, enhancing intracellular delivery [6, 95]. Certain receptors and antigens are overexpressed in many human cancer cells and can be exploited by active targeting strategies to achieve efficient drug uptake via RME [29, 52], as demonstrated in figure 11. The active targeting using NPs as DDS allows a specific area of the body to be targeted, avoiding one of the drawbacks of current chemotherapy, i.e. the toxic effects in non-malignant organs [13]. Thus, an active area of research involves the functionalization of NPs with targeting agents that identify and bind to receptors overexpressed on tumors or their associated endothelium [96, 101]. Moreover, the decoration of NPs with targeting moieties overcomes MDR and avoids the limitations of passive targeting, since the EPR effect is not produced in certain hypovascular tumors and the permeability of blood vessels can vary in a single tumor [39, 102].

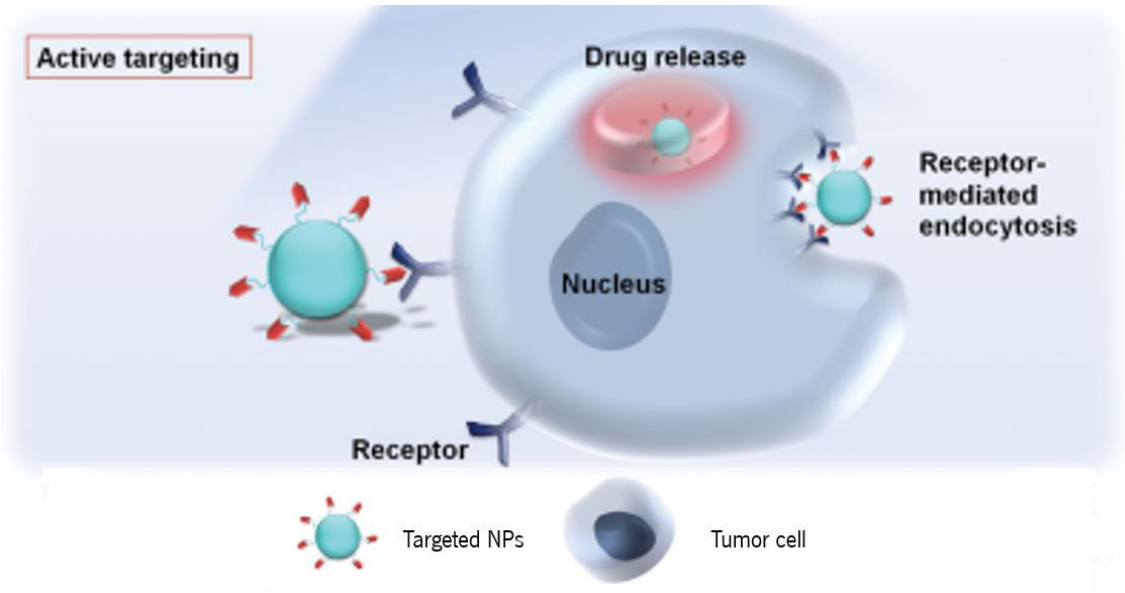

Figure 11 | Representation of active targeting of nanoparticles (NPs), through targeting ligands, leading to receptor-mediated endocytosis (RME). [Adapted from Jing Huang *et al.* [97]].

Targeted NPs have shown exciting results in preclinical studies, demonstrating their potential as therapeutics carriers [99]. The success of drug targeting also depends on the selection of the targeting agent, which should be abundant, have high affinity and specificity of binding to cell surface receptors and should be well suited to chemical modification by conjugation [7].

3.2.1. Folic acid as a targeting agent

While numerous strategies have been proposed to target drugs to tumor cells, one approach that has received considerable attention has been the use of folic acid (FA) to deliver drugs selectively to folate receptor (FR) expressing cancer cells [10]. Due to the ideal characteristics of FA, such as stability in storage and circulation, low cost, non-toxicity, non-immunogenicity, simple conjugation chemistry and high affinity for bind to the FRs at cell surfaces, this molecule has emerged as a potential targeting agent for cancer tissues [76, 98, 103]. FR has been studied extensively as a tumor cellular surface marker for targeted drug delivery [104] because is frequently overexpressed on the surface of a variety of human cancers [29, 82]. Of the four known isoforms (α, β, γ, δ) [105], FR-α and FR-β are anchored to the plasma membrane and bind FA with the highest affinity [106]. It is generally known that higher binding affinity increases targeting efficacy [107]. FA binds both FR-α and FR-β and internalizes into the cells via RME (figure 12) [98].

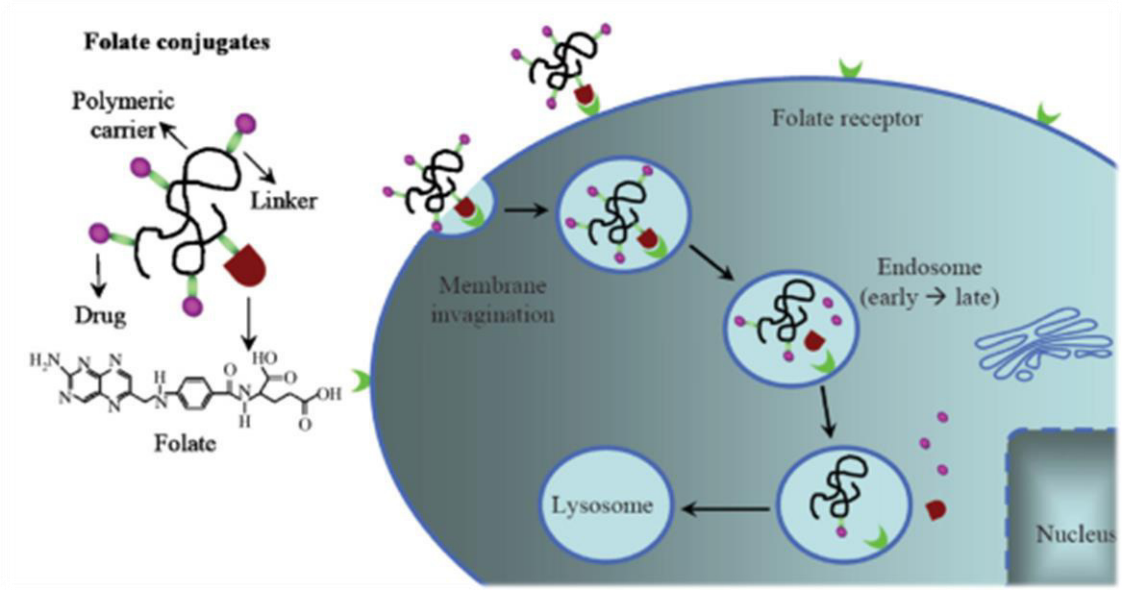

Figure 12 | Representation of receptor-mediated endocytosis (RME), using folate (FA) as a targeting agent. [Adapted from Jae Hyung Park *et al.* [8]].

FR-α is observed on the apical surfaces of several epithelial cells where it is inaccessible to parenterally administered FA and FA conjugates [10]. Moreover, this isoform of the FR has been shown to be overexpressed in various types of human cancers, making it a potential target for cancer [100, 104, 108]. FR-β, in contrast, is expressed on activated macrophages and also on the surfaces of malignant cells of hematopoietic origin [10].

The RME of FA conjugates begins with the conjugate binding to FRs on the cell surface [31]. Then, the plasma membrane invaginates and eventually forms a distinct intracellular compartment [8]. The endocytic vesicles (endosomes) become acidified, allowing the FR to release the FA conjugates [96]. The membrane-bound FRs recycle back to the cell surface, allowing them to mediate the delivery of additional FA conjugates [76]. The FA conjugates released from FRs escape the endosome, resulting in drug deposition in the cytoplasm [92].

In the last years, several studies described the production of FA-tagged NPs that demonstrated a specific internalization by cancer cells and an effective release of the drug inside these cells, being promising NPs for application in cancer therapy [66, 109, 110]. Moreover, FA conjugated PEG-modified NPs have been demonstrated to have a ten-fold higher affinity for FRs compared to free FA affinity for the receptor [52].

4. METHOTREXATE AS A THERAPEUTIC DRUG

MTX is one of the most widely studied and effective therapeutic agents available to treat many solid tumors, hematologic malignancies and autoimmune diseases [111]. MTX, a FA antimetabolite [112], exerts its cytotoxic activity by competitively inhibiting dihydrofolate reductase (DHFR) [85]. The action of MTX depends on active transport into cells through the reduced-folate carrier (RFC) and/or using an endocytic pathway activated by a FR. Subsequently, MTX is converted to a long-lived intracellular polyglutamate, which binds to DHFR [113]. Cell death caused by MTX is dependent on the duration of inhibition of the enzyme, the level of reduction of FA in the cell, and the presence of other factors that inhibit apoptosis [114]. MTX can cease intracellular FA metabolism and finally blocks the synthesis of thymine and purines, leading to impairment of tumor growth and induction of cell death by secondary genotoxic effects or apoptosis [89]. In spite of excellent action mechanism in cancer cell suppression, the utility of MTX in cancer chemotherapy has been restricted due to unexpected adverse effects such as toxicity, low cellular influx, lack of cellular and systemic specificity, and drug resistance [115]. Furthermore, poor aqueous solubility, low permeability and the short circulation half-life (2–10 hours) of the free acid form of MTX are major barriers in developing therapeutically successful formulations [112]. In order to deliver MTX in an efficient way, many studies in the drug delivery community have been carried out, not only to improve drug efficacy and pharmacokinetics, circulation in the blood, controlled release and therapeutic window, but also to overcome drug resistance [115].

MTX has been described as a dual-acting molecule because it can also be used as targeting agent due to its high structural similarity to FA [31], as demonstrated in figure 13. Cellular uptake of MTX is mediated by the α, β and γ FRs isoforms [116]. Pamela *et al.* described the design principle of dual-acting MTX conjugates and provided strong evidence supporting the ability of these conjugates to display the dual activities needed for an effective cancer-targeting delivery and therapeutic platform [117]. Thus, MTX can also be used as a targeting agent [118]. Many efforts have been made to develop macromolecular based DDS for MTX including polymer-drug conjugates and NPs [119].

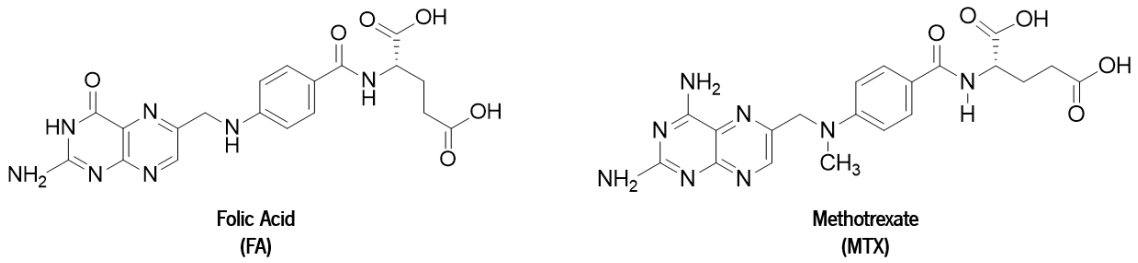

Figure 13 | Structures of folic acid (FA) and methotrexate (MTX).

In this work, it was developed two different PEGylated NPs (P407-based nanoemulsions loaded with MTX and MTX-PEG micelles) that present suitable characteristics for application in cancer therapy. As the commercial MTX presents low solubility either in organic and aqueous solvents [120], several modifications of MTX were performed. A more hydrophilic MTX form (MTX disodium salt (MTX-Na)) was developed, as well as two hydrophobic MTX derivatives (MTX-dimethyldioctadecylammonium bromide (DODAB) and MTX diethylated (MTX-OEt)). These derivatives were more successfully entrapped in the P407-based nanoemulsions than the commercial MTX, allowing higher drug concentrations. Additionally, P407-MTX conjugate was produced in order to obtain nanoemulsions with the ability to carry and specific deliver higher concentrations of drug. MTX-PEG_{2000} was also produced for the development of PEGylated micelles able to deliver MTX.

CHAPTER III

POLOXAMER 407-BASED NANOEMULSIONS FOR AN EFFECTIVE METHOTREXATE DELIVERY

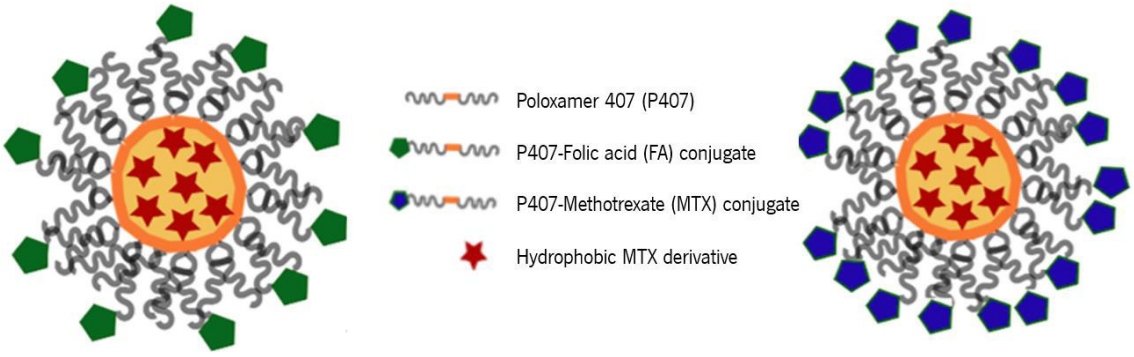

Chapter III – POLOXAMER 407-BASED NANOEMULSIONS FOR AN EFFECTIVE METHOTREXATE DELIVERY

1. FRAMEWORK

In this chapter, several optimizations were performed in order to improve the MTX encapsulation in the P407-based NPs previously developed in our laboratory. Taking into account the production method used, where an aqueous solution and vegetable oil are emulsified by high pressure homogenization (HPH), these NPs were denominated as nanoemulsions. Loureiro *et al.* [66] demonstrated the development of P407-based nanoemulsions by HPH, which showed small size and neutral charge. Due to its lateral PEG hydrophilic chains, P407 provides steric stabilization and prevention of protein adsorption, resulting in less phagocytized NPs and longer half-life in systemic circulation [19]. P407 is a copolymer readily available, biocompatible, and low toxic [85]. Moreover, P407 can interact with MDR cancer cells resulting in chemo-sensitization of cancer cells [79]. This copolymer also allows the NPs surface modification using its hydrophilic PEG chains, in which can be performed the conjugation of targeting agents [5]. Taking into account that FRs are a tumor marker of various types of cancers and the ideal characteristics of FA, such as non-toxicity, non-immunogenicity and high affinity for bind to the FRs at cell surfaces, this molecule has emerged as a potential targeting agent for cancer therapy [31]. Thus, a conjugate of P407-FA was produced in order to obtain FA-tagged nanoemulsions, allowing a specific target to cancer cells. MTX, as a potent anticancer agent [113], was the pharmacological compound chosen to be encapsulated in these P407-based nanoemulsions. The PPO central hydrophobic chain of P407 induces the formation of a hydrophobic core allowing the encapsulation of lipophilic drugs. Furthermore, as the oil phase is totally incorporated in the nanoemulsions, hydrophobic derivatives of MTX were produced in order to achieve a higher concentration of entrapped drug. MTX has been described as a dual-acting molecule because it can also be used as targeting agent due to its high structural similarity to FA [31]. Thus, another approach performed was the conjugation of MTX with P407, increasing the drug concentration present in the initial formulation and maintaining the ability to specific target cancer cells. The nanoemulsions developed should have desirable characteristics to be use as DDS for IV administration in cancer therapy.

2. MATERIALS AND METHODS

2.1. Reagents and equipment

2.1.1. Reagents

FA, P407, 4-dimethylaminopyridine (DMAP), pyridine, lipase from *Thermomyces lanuginosus*, dialysis tubes and membranes, 2,5-dihydroxybenzoic acid (DHB) (suitable for matrix assisted laser desorption ionization time-of-flight mass spectroscopy (MALDI-TOF MS)), trifluoroacetic acid (TA), NaOH, all culture media and supplements were purchased from Sigma-Aldrich, USA. *N,N'*-dicyclohexylcarbodiimide (DCC), DODAB and MTX were obtained from TCI Chemicals, Belgium. Acetonitrile (high performance liquid chromatography (HPLC) grade) and HCl 37 % were obtained from Fisher Scientific, USA. Anhydrous dimethyl sulphoxide (DMSO) was bought from Acros Organics, Belgium. Phosphate buffered saline (PBS) was acquired from Biochrom GmbH, Germany. Ultrapure water was obtained from a Milli-Q Water Purification System, Germany. Deuterated DMSO (DMSO-d_6) was purchased from Cortecnet, France. Human colorectal adenocarcinoma cells (Caco-2 cell line) were obtained from American Type Culture Collection (ATCC), UK. T75 flasks and 96-well tissue culture polystyrene plates were acquired from SPL Life Sciences, Korea. CellTiter 96® AQueous Non-Radioactive Cell Proliferation [3-(4,5-dimethylthiazol-2-yl)-5-(3-carboxymethoxyphenyl)-2-(4-sulfophenyl)-2*H*-tetrazolium, inner salt] (MTS) assay was purchased from Promega, USA.

2.1.2. Equipment

Centrifugations were performed using Beckman Allegra X 155 centrifuge from Beckman Coulter, USA. Ultrafiltration was performed in a solvent-resistant stirred cell using Ultracel 10 kDa regenerated cellulose ultrafiltration discs, 47 mm, from Merck Millipore, Ireland. Lyophilization was executed in FreeZone 2.5 Freeze Dryer from Labconco, USA. Proton nuclear magnetic resonance (^{1}H NMR) spectra were recorded using a Bruker Avance III 400 (400 MHz) from Bruker Daltonics GmbH, Germany. MALDI-TOF mass spectra were acquired on a Bruker Autoflex Speed instrument, equipped with a 337 nm nitrogen laser, from Bruker Daltonics GmbH, Germany. HPH was executed using APV-2000 Homogenizer from SPX, Denmark. Dynamic light scattering (DLS) analysis were performed in a Malvern zetasizer NS from Malvern Instruments, UK. Nanoparticle tracking analysis

(NTA) were acquired using a NanoSight NS500 instrument from Salisbury, UK. Absorbance measurements were conducted in a Synergy Mx Multi-Mode Reader from BioTek, USA.

2.2. Preparation and characterization of Poloxamer 407-Folic acid and Poloxamer 407-Methotrexate conjugates for nanoemulsions preparation

2.2.1. Production of Poloxamer 407-Folic acid and Poloxamer 407-Methotrexate conjugates

The production of the conjugates was based on the conjugation method previously described by Loureiro *et al.* [121]. Commercial FA/MTX (10 equivalents) was dissolved in anhydrous DMSO (20 mL) with DCC (10 equivalents) and DMAP (10 equivalents). After stirring for 2 hours, P407 (1 equivalent) was added to the solution and the reaction proceeds overnight. All reactions were executed at 40℃ and 700 rpm, under nitrogen atmosphere and shielded from the light. Afterwards, the solution was filtered by gravity (Prat Dumas, France) and dialyzed (MW cut-off (MWCO) = 2 kDa) for 7 days against PBS to remove the excess of FA/MTX and other reactants. Then, the solution was centrifuged (6000 rpm for 30 minutes at 25℃) and subsequently was purified through ultrafiltration (MWCO = 10 kDa). The purified conjugates were obtained as orange (P407-FA) and yellow (P407-MTX) aqueous solutions. Several optimizations were performed in order to improve the conjugation of P407 with FA and MTX, including the test of different equivalents of the reactants. The amount of FA and MTX linked to P407 was determined by measuring the absorbance at 330 nm and 350 nm, respectively. The characterization of the conjugates was performed by ^{1}H NMR and MALDI-TOF.

2.2.2. ^{1}H NMR analysis

P407, FA, MTX, P407-FA and P407-MTX conjugates were characterized by ^{1}H NMR spectroscopy. DMSO-d_6 was used as deuterated solvent, using the peak solvent as internal reference. Pyridine was used as internal standard, which was added to the NMR tube for P407, MTX and FA quantification.

2.2.3. MALDI-TOF analysis

Mass/charge of P407, FA, MTX and P407-FA and P407-MTX conjugates was verified by MALDI-TOF using DHB as matrix. A saturated solution of DHB was mixed with a solution of acetonitrile/TA

0.1 % (30:70) containing the sample. The samples were analyzed using the positive or negative linear mode.

2.3. Preparation and characterization of Methotrexate derivatives

2.3.2. Production of Methotrexate disodium salt

In order to obtain the solubilization of MTX in water 2 equivalents of NaOH were added and then the solution was vortexed. Afterwards, the pH was corrected with a solution of HCl (5 M) until pH 7. Finally, the solution is freeze-dried to obtain the MTX-Na as orange solid. The characterization of MTX-Na derivative was performed by ^{1}H NMR, using DMSO-d_6 as deuterated solvent, and by absorbance measurements.

2.3.3. Production of Methotrexate-Dimethyldioctadecylammonium bromide complex

MTX-Na and DODAB were dissolved in a molar ratio 1:2 using a mixture 50/50 (v/v) of water and ethanol. After 70 minutes of agitation at 70 °C and 700 rpm, the produced complex precipitated in water. The precipitate was then filtered by gravity (Prat Dumas, France) and dried overnight to obtain the MTX-DODAB complex as yellow solid. The characterization of MTX-DODAB complex was performed by ^{1}H NMR, using DMSO-d_6 as deuterated solvent, and by absorbance measurements. The yield (η) of the reaction was calculated using the equation 1, where the limiting reagent corresponds to DODAB.

$$\eta\,(\%) = \frac{nº\ of\ moles\ of\ MTX - DODAB\ complex}{nº\ of\ moles\ of\ limiting\ reagent} * 100$$

Equation 1 | Determination of the reaction yield.

Initially, this production method was developed using chloroform as organic solvent but its substitution for ethanol was executed in order to develop a green method. Other optimizations were performed in order to obtain the best results in terms of yield of the reaction, namely the reaction scale.

2.3.4. Production of Methotrexate diethylated

This MTX derivative was produced by a colleague in the laboratory (unpublished work). The characterization of MTX-OEt was performed by ^{1}H NMR and absorbance measurements. For the ^{1}H NMR analysis, DMSO-d_6 was used as deuterated solvent.

2.4. Preparation and characterization of Poloxamer 407-based nanoemulsions

2.4.2. Production of nanoemulsions by high pressure homogenization

The production of the nanoemulsions was performed as previously described by Loureiro *et al.* [121]. An aqueous solution of P407 at 5 mg/mL in PBS (pH 7.4) was emulsified with an organic phase (vegetable oil). The emulsification was performed subjecting this initial formulation to 36 homogenization cycles at high pressures (250 and 600 bar, two stages of pressure) using the high pressure homogenizer. The aqueous solution/vegetable oil ratio (v/v) of 99.5/0.5 was used. In order to obtain nanoemulsions with FA at their surface, the solution of P407-FA conjugate was added to the aqueous phase at final FA concentration of 12 μg/mL. For the preparation of nanoemulsions containing the P407-MTX conjugate, the aqueous phase was a solution of this conjugate where the concentration of the copolymer (P407) was maintained at 5 mg/mL. For the entrapment of pharmacological compounds in nanoemulsions, the hydrophilic compounds were dissolved in the aqueous phase and the hydrophobic compounds in the organic phase of the initial formulation. The free drug was separated from the nanoemulsions using PD-10 desalting columns containing Sephadex G-25 Medium (MWCO = 5 kDa) from GE Healthcare, UK. At last, the nanoemulsions were filtered under sterile conditions using 0.22 μm polyethersulfone (PES) filter from Merck Millipore, Ireland.

2.4.3. Determination of the encapsulation efficiency of the pharmacological compounds

After separation of the free drug from the nanoemulsions, the drug present in the aqueous phase was quantified by measuring the absorbance at the maximum wavelength of the MTX or MTX derivatives (λ_{max} = 303 nm). The encapsulation efficiency (EE) was determined using the equation 2, where $[drug]_{initial}$ and $[drug]_{free}$ are the total concentration of drug added in the initial formulation and the concentration of the free drug in aqueous phase solution after separation in PD-10 desalting columns, respectively.

$$EE\ (\%) = \frac{[drug]_{initial} - [drug]_{free}}{[drug]_{initial}} * 100$$

Equation 2 | Determination of the encapsulation efficiency (EE).

2.4.4. Determination of size, polydispersity index and zeta-potential

The nanoemulsions were analyzed for their size distribution and ZP, at pH 7.4 and 25℃, by photon correlation spectroscopy (PCS) and electrophoretic laser Doppler anemometry, respectively. The values for viscosity and refractive index were taken as 0.8616 cP and 1.350, correspondingly. The concentration of P407 was kept constant at 1 mg/mL. Nanoemulsions, in suspension, were stored at 4 ℃ for a period of 16 weeks. After predetermined storage times, the stability parameters (particles size, PdI and ZP) were determined as described above. Each sample was measured in triplicate and the results are presented as mean value ± SD.

2.4.5. Determination of size distribution and particle concentration by nanoparticle tracking analysis

The NTA measurements were made at room temperature (RT) and video sequences were captured over 60 seconds with manual shutter and gain adjustments. The samples were diluted with water and then injected into the system. Each sample was measured in triplicate and the results are presented as mean value ± SD.

2.4.6. Release profile of Methotrexate

The MTX release profile of the most promising nanoemulsions was evaluated by dialysis against PBS in a hot room at 37 °C, using dialysis tubes (MWCO = 1 kDa). Aliquots were taken at different time points, for 440 hours, and the absorbance was measured in a 96-quartzo microplate at 303 nm. The percentage of release was quantified as follows:

$$Release\ (\%) = \frac{[Released\ MTX]}{[Total\ MTX]} * 100$$

Equation 3 | Determination of methotrexate (MTX) released.

2.4.7. Release of Methotrexate in the presence of lipase

The release of MTX from nanoemulsions produced using P407-MTX conjugate was assessed by the incubation of the nanoemulsions with an esterase, namely lipase. For this, each sample was transferred to a dialysis tube (MWCO = 1 kDa) and incubated with lipase from *Thermomyces*

lanuginosus (activity: 407 µmol/mL/min) at 37 °C in a hot room, accomplishing the reactions by dialysis against PBS. Aliquots were taken at different time points and the absorbance was measured at 303 nm. The percentage of release was quantified using equation 3. The PBS was replaced and the release proceed for 440 hours. A control condition was performed without the addition of the lipase.

2.5. Evaluation of the biological effect

In order to evaluate the biological effect of the nanoemulsions loaded with MTX-OEt, the most promising nanoemulsions, MTS assay was performed using Caco-2 cell line.

2.5.2. Cells and culture conditions

Caco-2 cell line was maintained in a humidified atmosphere of 5 % CO_2 in air at 37 °C, growing in T75 flasks.

Table 1 | Composition of cell culture medium for Caco-2 cell line

Cell Line	Medium	Supplements
Caco-2	Dulbecco's modified Eagle's medium (DMEM)	20 % (v/v) of Fetal Bovine Serum (FBS); 1 % (v/v) of penicillin/streptomycin solution; 1 % (v/v) of non-essential aminoacids

In figure 14 are represented images of low and high cell density of Caco-2 cell line. This figure represents a guideline that indicates the expected cell morphology and suitable cell density to proceed the cellular experiments with success.

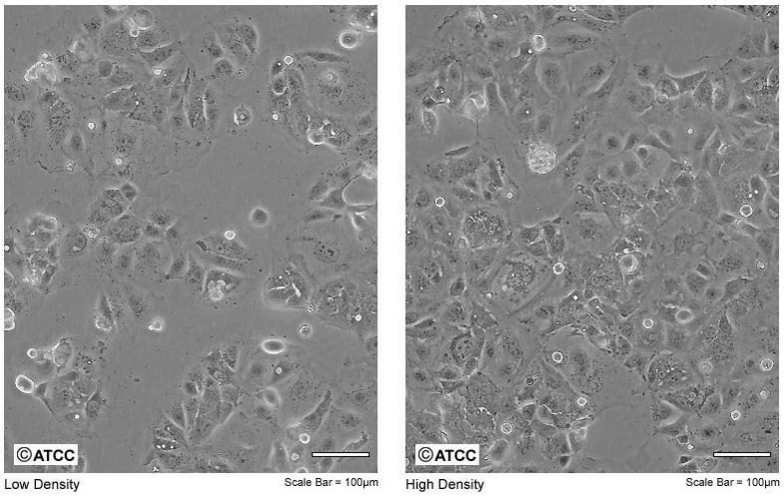

Figure 14 | Caco-2 cell line. [Adapted from ATCC, [122]].

2.5.3. Cell viability assay

Cell viability was studied using the MTS assay, which is a colorimetric method for determining the number of viable cells. MTS, a tetrazolium compound, is bioreduced by metabolically active cells into a colored formazan (figure 15), which is soluble in the culture medium. The quantity of formazan is measured by absorbance at 490 nm, being directly proportional to the number of living cells [123].

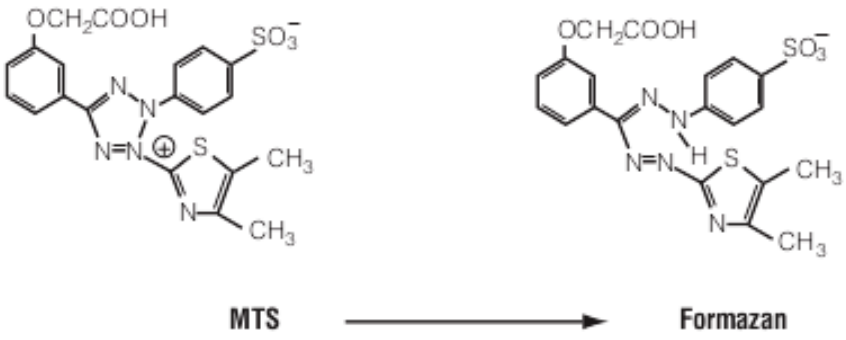

Figure 15 | Reactional scheme of the reduction of MTS to form formazan. [Adapted from Promega, [123]].

Caco-2 cells were seeded in 96-well tissue culture polystyrene plates at a density of 1×10^4 cells/well and incubated overnight to promote cell adhesion. The cells were incubated with different concentrations of nanoemulsions containing MTX and/or MTX derivatives and respective controls. After 48 and 72 hours of incubation, an MTS mixture was added and the cells were further incubated for 4 hours at 37℃. After this period, the absorbance of the formazan product was read at 490 nm using the microplate reader. Each sample was measured in triplicate and the results

are presented as mean value ± SD. Cell viability was calculated using equation 4 and expressed as a percentage relative to the negative control (untreated control cells).

$$Cell\ viability\ (\%) = \frac{Absorbance\ of\ sample\ (mean)}{Absorbance\ of\ control\ (mean)} * 100$$

Equation 4 | Determination of cell viability as a percentage relative to the negative control.

3. RESULTS AND DISCUSSION

3.1. Production and characterization of Poloxamer 407-Folic acid and Poloxamer 407-Methotrexate conjugates for nanoemulsions preparation

The major drawback of the current cancer therapy strategies is the inability to specific deliver the drug to the target, occurring several side effects [5]. While numerous strategies have been proposed to target drugs to tumor cells, one approach that has received considerable attention has been the use of FA to deliver attached drugs selectively to FR-expressing cancer cells [10]. Thus, in order to obtain P407-based nanoemulsions with the ability to specific delivery MTX, P407-FA conjugate was produced and added in the initial formulation for nanoemulsions production. In figure 16 is represented a proposal scheme of the mechanism of conjugation between P407 and FA.

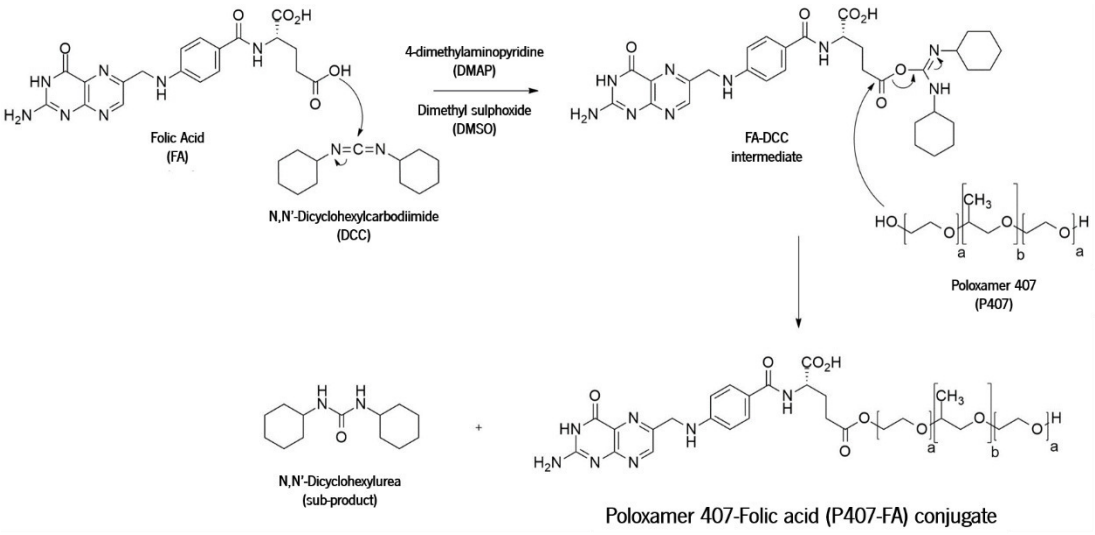

Figure 16 | Scheme of the proposed mechanism of Poloxamer 407-Folic acid (P407-FA) conjugate synthesis.

MTX is extensively used for the treatment of cancer but also for the treatment of rheumatoid arthritis (RA), psoriasis and autoimmune diseases [114]. However, the free form of MTX has poor aqueous solubility, low permeability and short circulation half-life (2–10 hours), limited effectiveness, undesirable side effects, and lack of selectivity [40, 112]. In order to deliver MTX in an efficient way, many studies have been performed to improve drug efficacy and pharmacokinetics, circulation in the blood and controlled release [115], minimize side effects, and also to overcome drug resistance [12].

The development of P407-based nanoemulsions with the ability to carry and specific delivery high concentrations of MTX was tested through the production of P407-MTX conjugate that was used for the nanoemulsions preparation. A proposal scheme of the mechanism of conjugation between P407 and MTX is represented in figure 17.

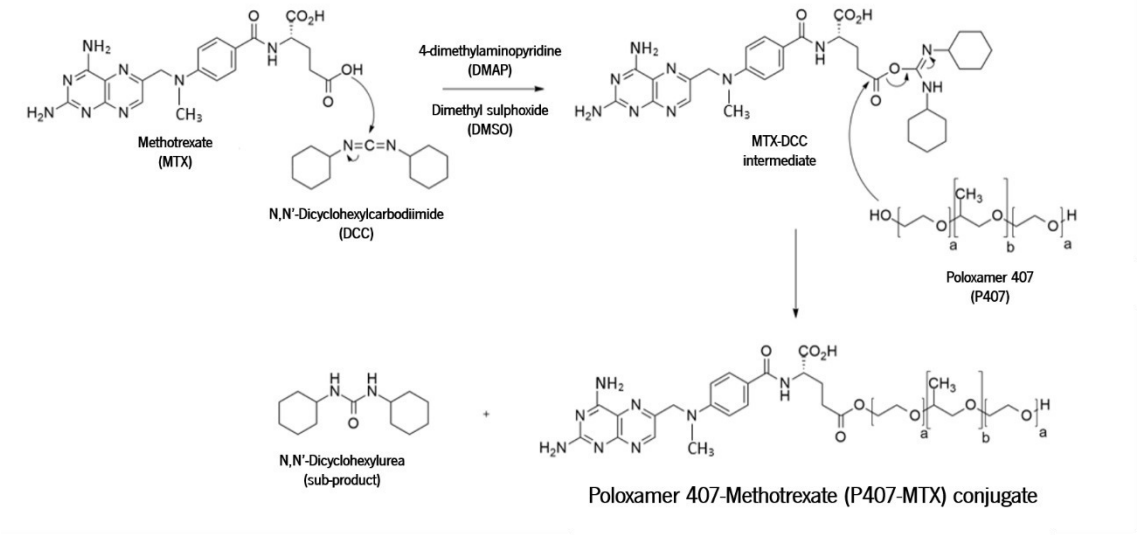

Figure 17 | Scheme of the proposed mechanism of Poloxamer 407-Methotrexate (P407-MTX) conjugate synthesis.

The reactions of conjugation occurred by an esterification reaction between one of the carboxylic groups of MTX/FA and the terminal hydroxyl group of P407, resulting in a strong covalent bond. The products resulting from these reactions were the conjugates and urea, as subproduct. As reported by Abdulrahman *et al.* and Noro *et al.*, when the modification occurs on just one of the carboxylic groups of MTX, it is on the γ-position carbonyl group, since it is the most reactive carboxyl group of the glutamic acid portion of MTX [70, 124].

^{1}H NMR and MALDI-TOF were executed to characterize P407-FA and P407-MTX conjugates. Also, the amount of FA and MTX linked to P407 was determined by measuring the absorbance at 330 nm and 350 nm, respectively.

3.1.1. Characterization of Poloxamer 407-Folic acid conjugate

^{1}H NMR spectra of FA, P407 and P407-FA conjugate are presented as stacked spectra in figure 18.

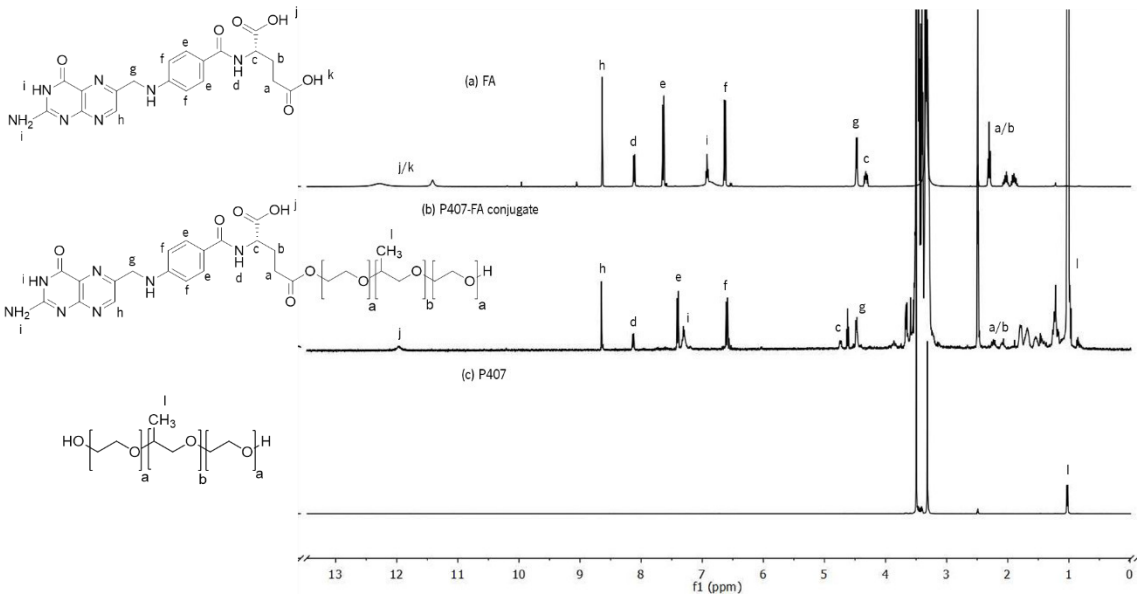

Figure 18 | ^{1}H NMR spectra of (a) folic acid (FA), (b) Poloxamer 407-Folic acid (P407-FA) conjugate and (c) Poloxamer 407 (P407) in DMSO-d_6.

The peaks labeled in lowercase letters correspond to the protons indicated in the structures of FA and P407.

It is possible to detect the differences among the conjugate (figure 18b) and its reactants (figure 18a and 18c) spectra. The main difference when comparing the conjugate spectrum (figure 18b) with the spectrum of FA (figure 18a) is the disappearance of one of the carboxylic group peaks. In the spectrum of the conjugate product there is only one peak corresponding to this group (j). Other protons, such as (a/b) and (c) appear at a different chemical shift after the conjugation reaction. All other protons have a similar chemical shift as the FA spectrum. In the conjugate spectrum (figure 18b) it is also possible to detect protons (l) that corresponds to the CH_3 group of P407 (figure 18c). All these results confirm the conjugation reaction via the esterification reaction described.

NMR spectroscopy can be used for the qualitative as well as quantitative estimation of the drugs [125]. This way, the quantification of FA and P407 in the purified conjugate was also performed by ^{1}H NMR using pyridine as internal standard (δ_H = 7.77 ppm). Taking into account the specific peaks of FA (δ_H = 6.60 ppm) and P407 (δ_H = 1.02 ppm) it was verified that the conjugate presents 0.24 mg/mL of FA and 20.37 mg/mL of P407. This corresponds to 0.388 moles of FA per 1 mole of P407, meaning that 38.8 % of P407 was modified with FA.

MALDI-TOF has allowed for a new era in the analysis of diverse molecules because of its high sensitivity, rapid analysis, simplicity of operation and utility for automatic high-throughput screening [126]. MALDI-TOF MS of P407 and P407-FA conjugate was performed and the resulting stacked spectra is presented in figure 19.

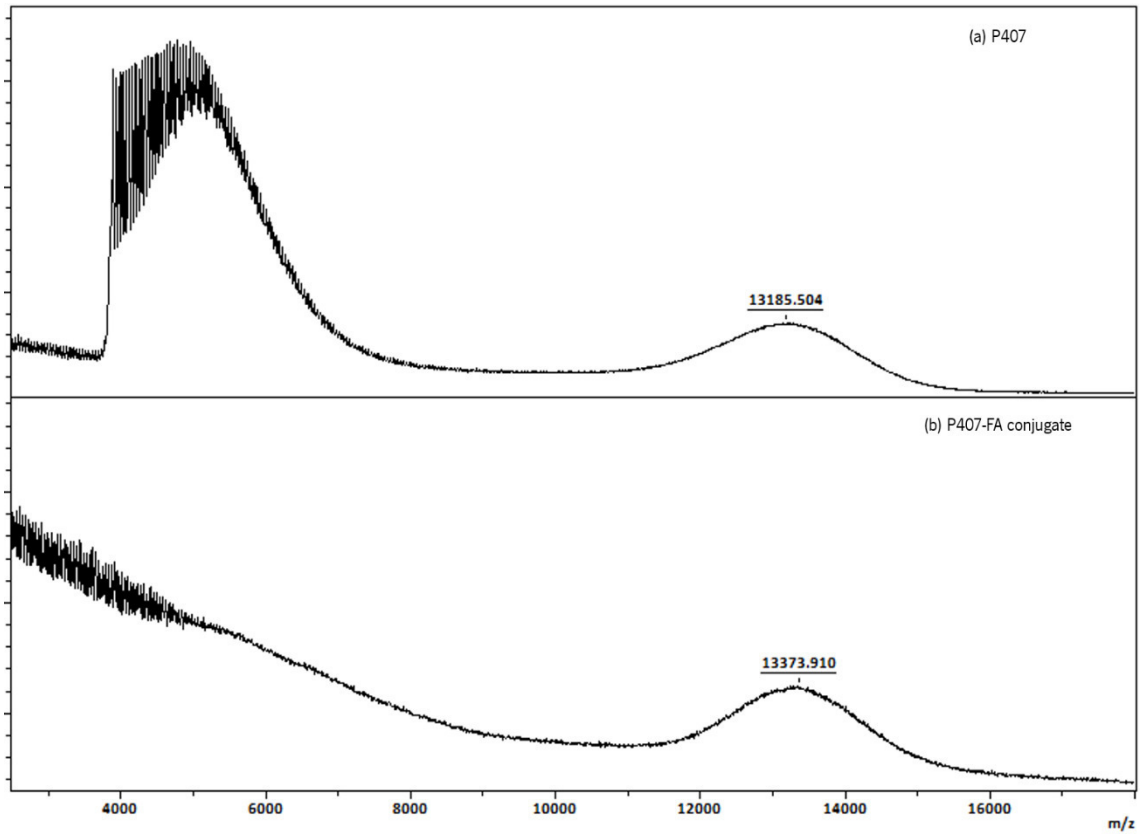

Figure 19 | MALDI-TOF mass spectra of (a) Poloxamer 407 (P407) and (b) Poloxamer 407-Folic acid (P407-FA) conjugate, acquired in linear positive mode.

MALDI-TOF spectra demonstrated that the average molecular weight ($MW_{average}$) obtained for the P407 was 13185.504 Da (figure 19a) and for the P407-FA conjugate was 13373.910 Da (figure 19b). The mass difference between P407 and P407-FA conjugate was 188.406 Da, corresponding to one molecule of FA conjugated with each molecule of P407. This mass value was lower than the $MW_{average}$ obtained for the FA measured by MALDI-TOF (450.998 Da) (figure 20). The difference observed occurred because the sample was analyzed using linear mode, which allows to infer only the medium value of the molecular mass. Taking into account these results obtained by MALDI-TOF analysis it is possible to infer that 41.8 % of P407 molecules were modified with a molecule of FA.

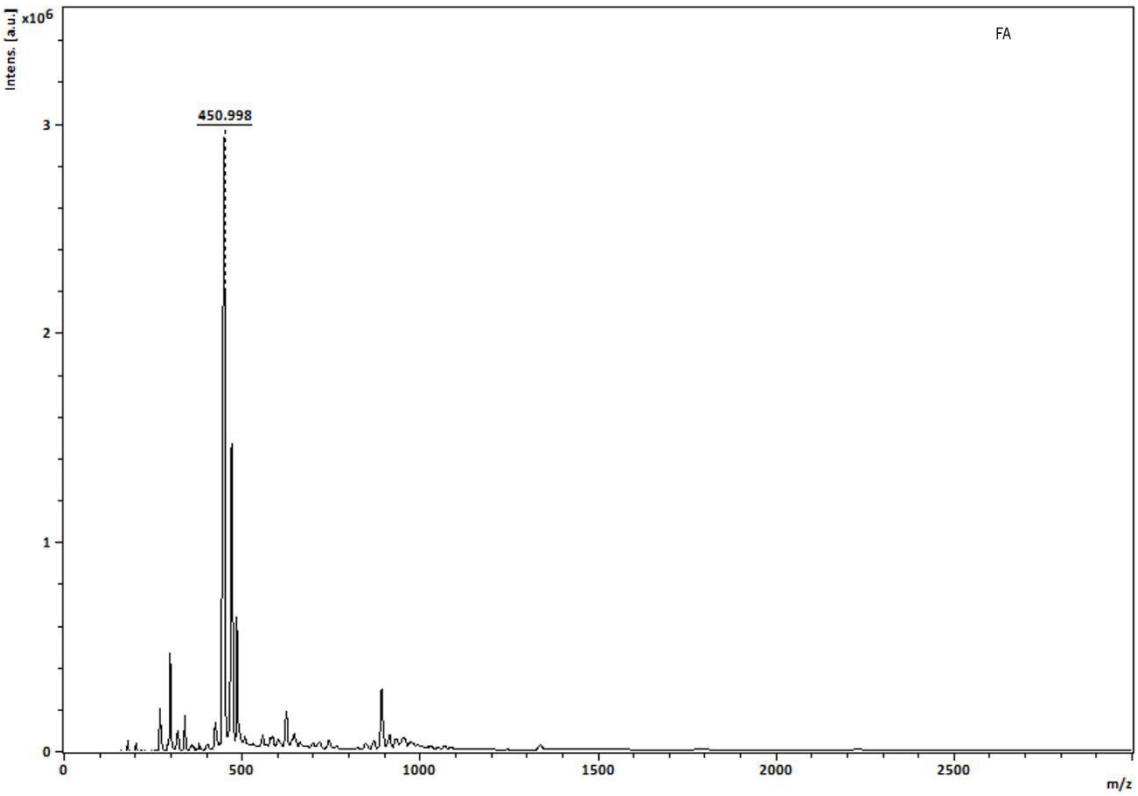

Figure 20 | MALDI-TOF mass spectrum of folic acid (FA), acquired in linear positive mode.

The percentage of modified P407 was calculated using ^{1}H NMR and MALDI-TOF analysis and both demonstrated that around 40 % of molecules were successfully modified.

It has been reported that ultraviolet-visible (UV) spectroscopy is a fast, reliable and accurate technique for the quantification of compounds [127]. In this way, the quantification of FA conjugated with P407 was also performed by absorbance measurements. The absorbance spectra of FA and P407-FA conjugate revealed that the wavelength of maximum absorbance obtained for the FA conjugated with P407 was 330 nm and for the free FA was 350 nm (figure 21). The absorbance spectra of P407 demonstrated that this compound not interfere with the quantification of FA.

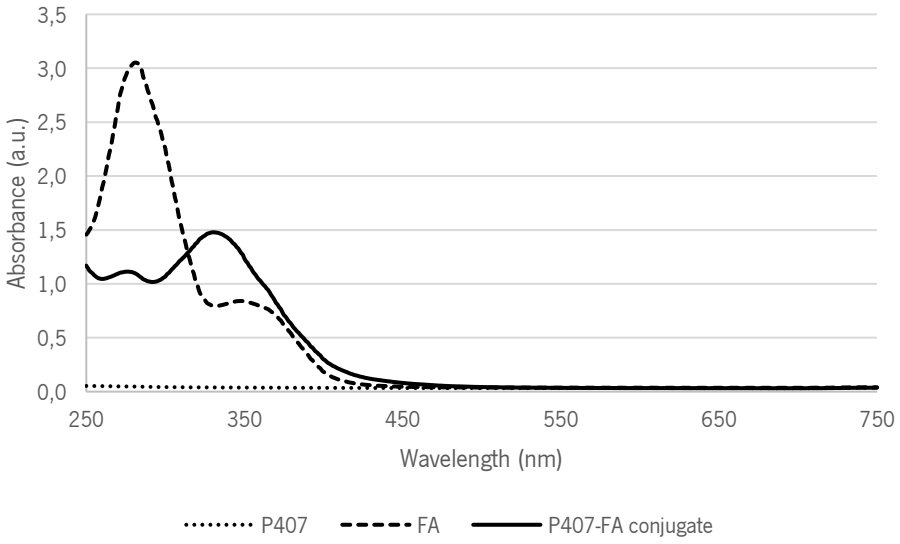

Figure 21 | Absorbance spectra of Poloxamer (P407), folic acid (FA) and Poloxamer 407-Folic acid (P407-FA) conjugate in PBS. [P407] = 1.02 mg/mL; [FA] = 0.4 mg/mL.

In this way, the quantification of FA conjugated with P407 was performed at 330 nm and the results demonstrated that the conjugate presents 0.26 mg/mL of FA.

Table 2 shows a comparison of the values of FA concentration obtained by ^{1}H NMR spectroscopy and the absorbance method.

Table 2 | Comparison of Poloxamer (P407) and folic acid (FA) concentrations determined using different methods (^{1}H NMR and absorbance)

Method	[FA] (mg/mL)	[P407] (mg/mL)
^{1}H NMR spectroscopy	0.24	20.37
Absorbance method	0.26	n.d.*

* Not determined.

FA quantification is more accurate when performed by ^{1}H NMR spectroscopy because the concentration was determined based in a single peak that corresponds to the FA molecule. In this quantification the interference of the other components in solution does not occur. Using the absorbance method for the FA quantification, the calibration curve and the conjugate sample have to be measured at different wavelengths, corresponding to the maximum absorbance of each. In this way, the ^{1}H NMR spectroscopy is the best method for the FA quantification when the molecule was conjugated. Nevertheless, when comparing both methods the values of FA concentration are quite similar. There is no procedure described in the literature for the quantification of P407 by

absorbance, therefore its concentration was not determined by this method. This highlights another advantage of the quantification by NMR since one single analysis allows the quantification of both compounds.

3.1.2. Characterization of Poloxamer 407-Methotrexate conjugate

^{1}H NMR spectra of MTX, P407 and P407-MTX conjugate were achieved and are presented as stacked spectra in figure 22.

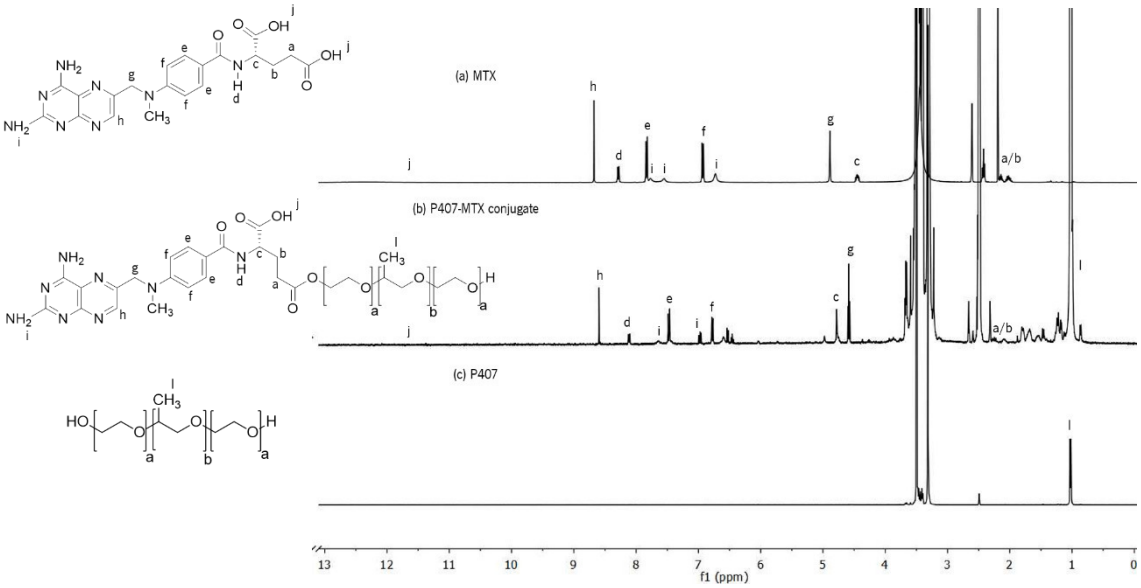

Figure 22 | ^{1}H NMR spectra of (a) methotrexate (MTX), (b) Poloxamer 407-Methotrexate (P407-MTX) conjugate and (c) Poloxamer 407 (P407) in DMSO-d_6. The peaks labeled in lowercase letters correspond to the protons indicated in the structures of MTX and P407.

Comparing the conjugate spectrum (figure 22b) with the spectrum of MTX (figure 22a) it is possible to see the same main differences observed in the conjugation of the FA with P407. The decrease in intensity of proton (j) and the deviation of the chemical shift of the protons (a/b) and (c) were the main differences due to the conjugation reaction. Concerning the similarity of the P407-FA and P407-MTX spectra, it is possible conclude that the conjugation reaction between P407 and MTX occurs via the esterification reaction described. By ^{1}H NMR spectroscopy was also performed the quantification of MTX and P407. Taking into account the specific peaks of MTX (δ_H = 6.78 ppm) and P407 (δ_H = 1.02 ppm) it was verified that the conjugate presents 0.36 mg/mL of MTX and 30 mg/mL of P407. This corresponds to 0.386 moles of MTX per 1 mole of P407, demonstrating that 38.6 % of P407 was modified with MTX.

Figure 23 shows the spectra of P407 and P407-MTX conjugate obtained by MALDI-TOF mass spectrometry.

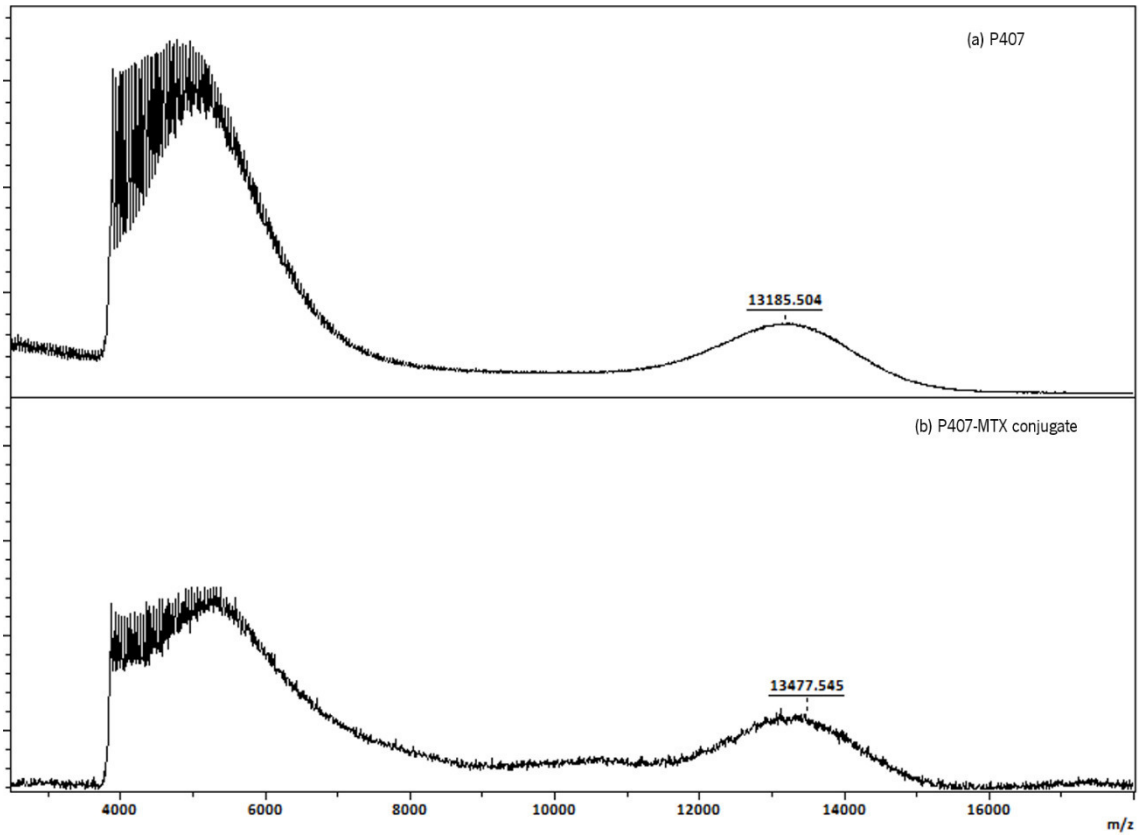

Figure 23 | MALDI-TOF mass spectra of (a) Poloxamer 407 (P407) and (b) Poloxamer 407-Methotrexate (P407-MTX) conjugate, acquired in linear negative mode.

By analysis of MALDI-TOF spectra one could infer that 43.6 % of the P407 molecules were modified with a molecule of MTX, revealing a $MW_{average}$ of 13477.545 Da (figure 23b) for the P407-MTX conjugate. Just one molecule of MTX was conjugated with each molecule of P407 since the mass difference between P407 and P407-MTX was very low (292.041 Da). This mass difference was lower than the $MW_{average}$ of MTX obtained by MALDI-TOF analysis (431.783 Da) (figure 24) because the sample was analyzed using the linear mode.

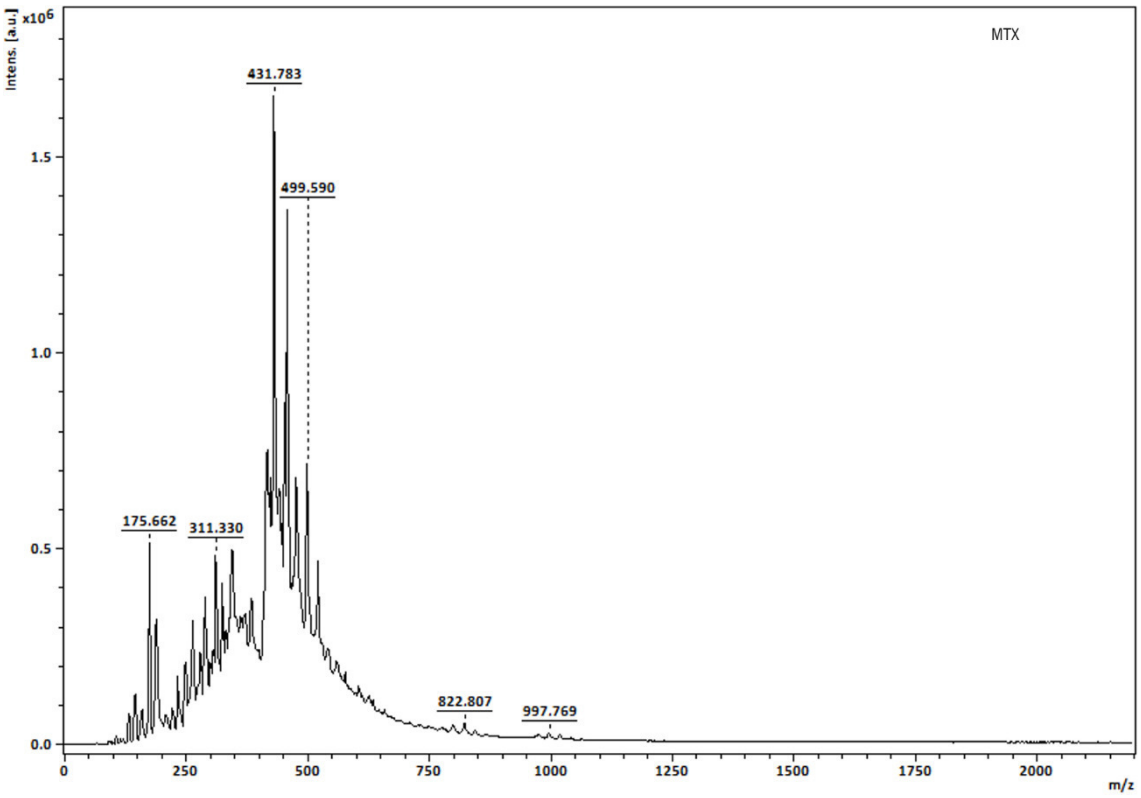

Figure 24 | MALDI-TOF mass spectrum of methotrexate (MTX), acquired in linear negative mode.

Regarding the percentage of modified P407, both ^{1}H NMR spectroscopy and MALDI-TOF analysis demonstrated that around 40 % of molecules were successfully modified.

For the quantification of the MTX conjugated with P407, absorbance measurements were also performed. Comparing the absorbance spectra of MTX and P407-MTX conjugate, it was observed a deviation of the wavelength of maximum absorbance from 303 nm for the free MTX to 350 nm for the conjugated MTX (figure 25).

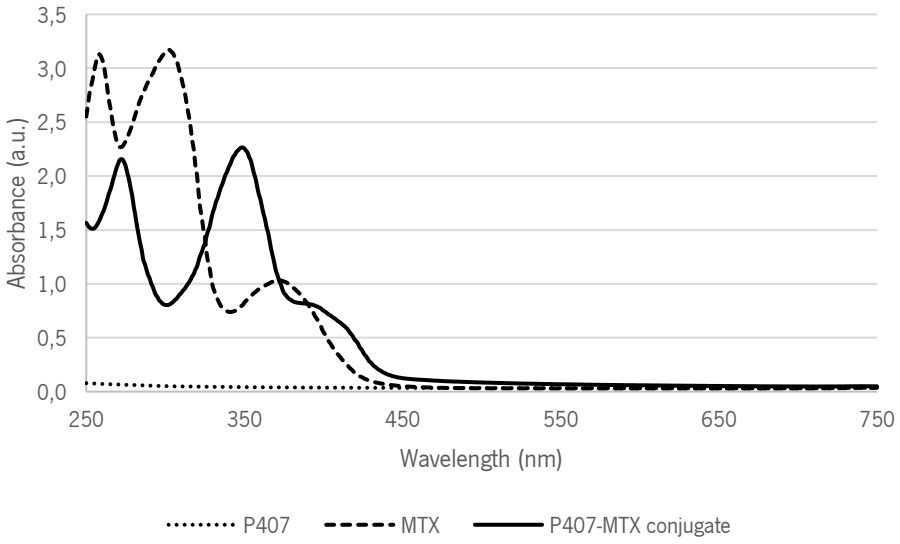

Figure 25 | Absorbance spectra of Poloxamer 407 (P407), methotrexate (MTX) and Poloxamer 407-Methotrexate (P407-MTX) conjugate in PBS. [P407 = 6.74 mg/mL; [MTX] = 0.084 mg/mL.

The quantification of the MTX linked to P407 using the absorbance values demonstrated that the conjugate presents 0.29 mg/mL of MTX.

For the case of the P407-MTX conjugate, when compared the values of MTX concentration obtained by NMR and by absorbance was observed a higher difference than P407-FA conjugate (table 3).

Table 3 | Comparison of Poloxamer 407 (P407) and methotrexate (MTX) concentrations determined using different methods (^{1}H NMR and absorbance)

Method	[MTX] (mg/mL)	[P407] (mg/mL)
^{1}H NMR spectroscopy	0.36	30
Absorbance method	0.29	n.d.*

* Not determined.

These different values of MTX concentration are explained by the differences between the two methods of quantification, as previously described for the P407-FA conjugate.

3.2. Production and characterization of Methotrexate derivatives

Different MTX derivatives were produced in order to allow a higher encapsulation of the MTX in the previously developed P407-based nanoemulsions. The commercial MTX presents low solubility either in organic and aqueous solvents, as mentioned before. Thus, a more hydrophilic MTX form

(MTX-Na) was developed by the addition of 2 equivalents of NaOH in an aqueous suspension of MTX and in figure 26 is represented the reactional scheme of its formation. Using this MTX-Na it was possible the solubilization of a higher concentration of MTX in the aqueous phase used for the nanoemulsions preparation. In this way, it was expected a higher concentration of MTX in the final formulation.

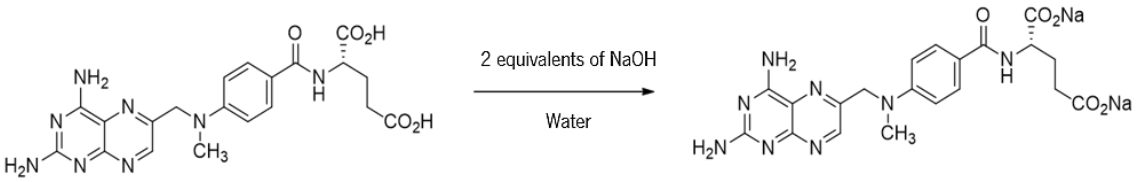

Figure 26 | Reactional scheme of methotrexate disodium salt (MTX-Na) preparation.

Also, two hydrophobic MTX derivatives (MTX-DODAB and MTX-OEt) were also developed. These MTX derivatives can be dissolved in the organic phase used for the nanoemulsions preparation, being successfully entrapped in the nanoemulsions. The reactional scheme for MTX-DODAB complex formation is represented in figure 27.

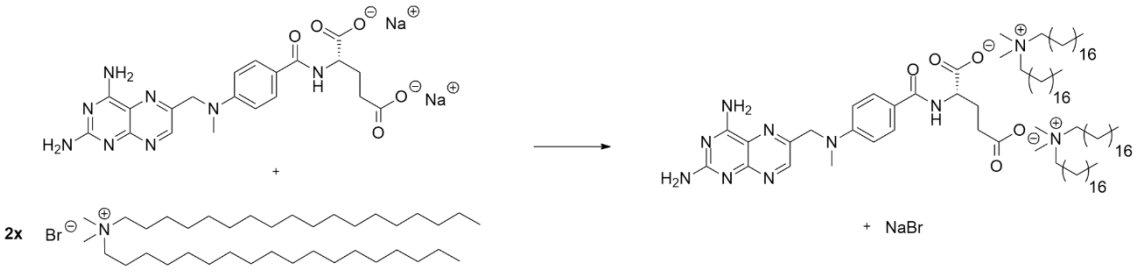

Figure 27 | Reactional scheme of methotrexate-dimethyldioctadecylammonium bromide (MTX-DODAB) complex formation.

The MTX presents negative charge (carboxylic groups) which is favorable to its ionic interaction with the cationic lipid DODAB. Moreover, this lipid has a quaternary amine that prevents the formation of a covalent bond with other molecules. In this way, the ionic interaction is the most favorable interaction with the DODAB molecule. After the ethanol evaporation, it was obtained a yellow solid precipitated in the aqueous medium which was isolated and characterized. The yield of MTX-DODAB production was η = 45.5 %.

These 3 MTX derivatives were analyzed by ^{1}H NMR spectroscopy in order to confirm their structure and purity. Figure 28 shows the stacked spectra of MTX and its derivatives.

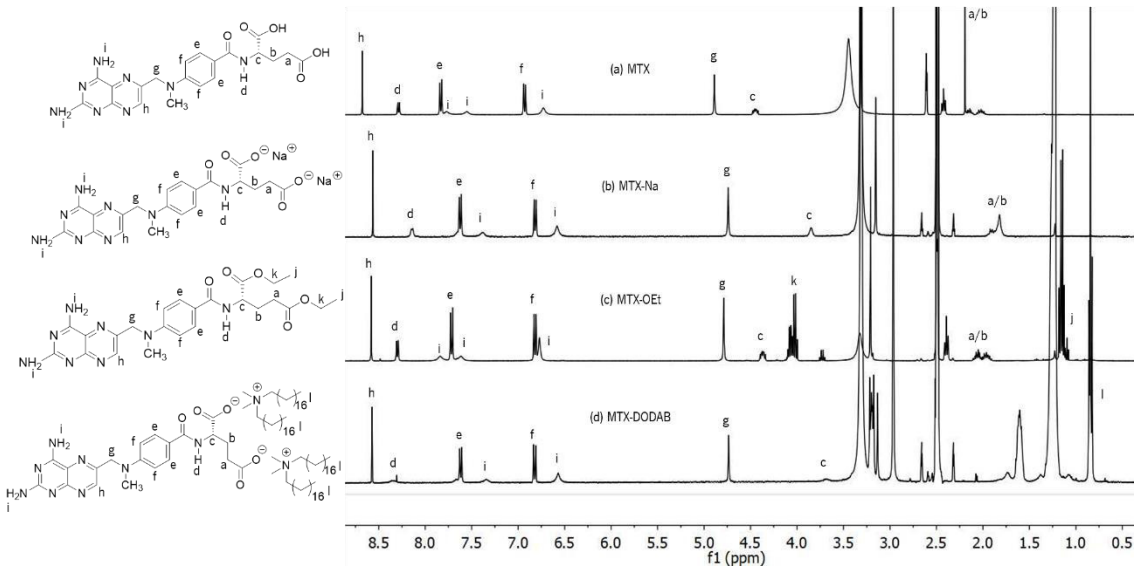

Figure 28 | ^{1}H NMR stacked spectra of (a) methotrexate (MTX), (b) methotrexate disodium salt (MTX-Na), (c) methotrexate diethylated (MTX-OEt) and (d) methotrexate-dimethyldioctadecylammonium bromide (MTX-DODAB) in DMSO-d_6. The peaks labeled in lowercase letters correspond to the protons indicated in the structures of MTX and its derivatives.

Comparing the MTX-Na spectrum (figure 28b) with the commercial MTX spectrum (figure 28a), the main difference is that protons such as (a/b) and (c) appear at different chemical shift, which indicated the MTX modification. All other protons have similar chemical shift as the MTX spectrum and no differences among pattern were detected, as expected. In the spectrum of the MTX-OEt derivative (figure 28c) were detected the protons (j) and (k) that correspond to the CH_3 and CH_2 groups of the ethyl moiety, respectively. The protons (a/b) and (c) also suffer a deviation of the chemical shift, as happened in the spectrum of MTX-Na. Finally, comparing the MTX-DODAB complex spectrum (figure 28d) with the MTX spectrum (figure 28a), it was verified the same behavior observed to the other modifications. A deviation of the chemical shift of the proton (c) was observed, while all other protons maintain a similar chemical shift. Proton (l), which corresponds to the CH_3 group of DODAB appears in the spectrum of the MTX-DODAB complex. All of these results support the isolation of the hydrophilic MTX derivative (MTX-Na) and the two hydrophobic MTX derivatives (MTX-OEt and MTX-DODAB).

In order to verify if the wavelength of maximum absorbance of the commercial MTX is the same of the MTX derivatives were acquired the absorbance spectra of these 4 compounds. The absorbance spectra (figure 29) demonstrated that all MTX derivatives showed the same wavelength of maximum absorbance (303 nm) than MTX.

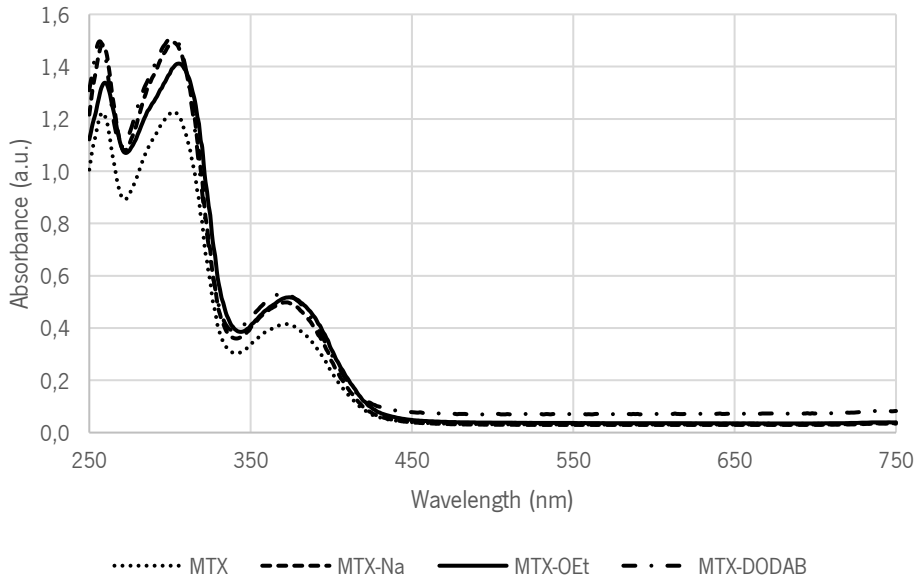

Figure 29 | Absorbance spectra of methotrexate (MTX) and its derivatives (methotrexate disodium salt (MTX-Na), methotrexate diethylated (MTX-OEt) and methotrexate-dimethyldioctadecylammonium bromide (MTX-DODAB) complex) at 0.1 mM of MTX.

All spectra revealed very similar behavior, indicating that the MTX derivatives can be quantified by absorbance using the same wavelength (303 nm) used for the quantification of the MTX.

3.3. Preparation and characterization of Poloxamer 407-based nanoemulsions loaded with Methotrexate

3.3.1. Production of nanoemulsions loaded with Methotrexate by high pressure homogenization

P407 features several advantages like biocompatibility and high solubility in aqueous solvents [86]. Moreover, Loureiro *et al.* described the development of P407-based nanoemulsions with suitable characteristics for IV therapeutic applications, using HPH [121]. These nanoemulsions also showed to be efficiently internalized by cancer cells. Thus, in order to produce P407-based nanoemulsions loaded with high concentrations of MTX, the several MTX modifications developed (table 4) were tested.

Table 4 | Representation of the structures of methotrexate (MTX) and its derivatives (MTX disodium salt (MTX-Na), MTX-dimethyldioctadecylammonium bromide (MTX-DODAB) complex, MTX diethylated (MTX-OEt) and Poloxamer 407-Methotrexate (P407-MTX) conjugate) and their molecular weights (MW)

Compound	Molecular Weight (g/mol)	Structure
MTX	454.44	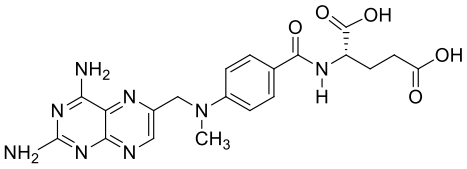
MTX-Na	498.4	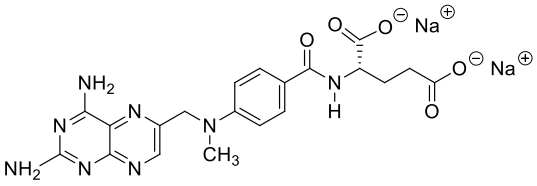
MTX-DODAB	1554.52	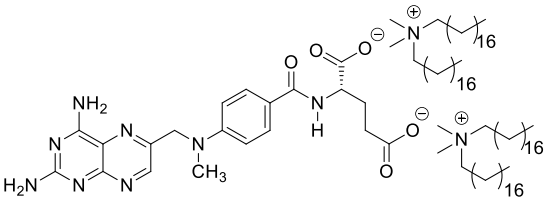
MTX-OEt	510.55	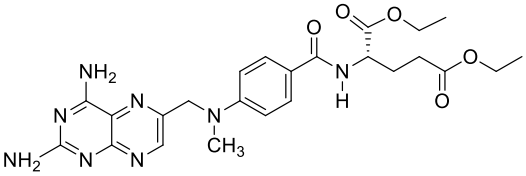
P407-MTX	13477.545	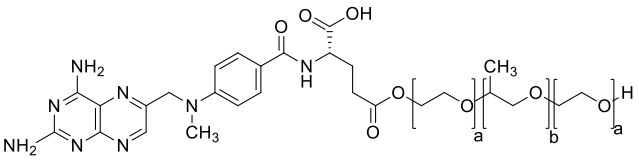

Figure 30 shows a schematic representation of all the process performed for the production of P407-based nanoemulsions loaded with MTX.

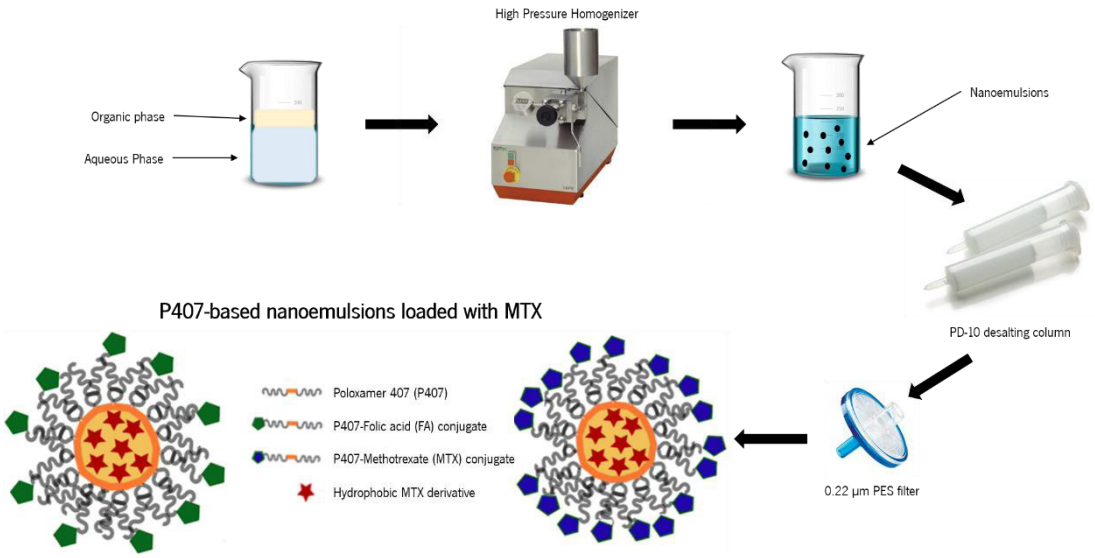

Figure 30 | Schematic illustration of the preparation of Poloxamer 407 (P407)-based nanoemulsions loaded with methotrexate (MTX) or its derivatives.

Different initial formulations were tested in order to optimize the encapsulation of MTX in these promising nanoemulsions (table 5).

Table 5 | Different formulations prepared during the optimization process, regarding the aqueous and organic phases

Aqueous Phase	Organic Phase
Aqueous solution of P407	Vegetable oil containing a hydrophobic MTX derivative (MTX-OEt or MTX-DODAB)
Aqueous solution of P407 containing P407-FA conjugate	
Aqueous solution of P407-MTX conjugate	
Aqueous solution of P407 containing hydrophilic MTX (commercial MTX or MTX-Na)	Vegetable oil

The hydrophilic MTX derivative (MTX-Na) was dissolved in the aqueous phase, while the hydrophobic derivatives (MTX-OEt and MTX-DODAB) were dissolved in the organic phase (vegetable oil). In order to produce FA-tagged nanoemulsions were also prepared formulations in which was added a percentage of the P407-FA conjugate to the aqueous phase. Another strategy to increase the concentration of encapsulated MTX was the preparation of nanoemulsions using as aqueous phase a solution of P407-MTX conjugate. Nanoemulsions without MTX were also prepared as control.

3.3.2. Determination of encapsulation efficiency of Methotrexate

As the main objective of this work is the encapsulation of a high concentration of MTX in the P407-based nanoemulsions, the first characterization performed was the determination of final concentration of MTX in the several produced formulations. Table 6 shows the results obtained for the nanoemulsions produced using MTX with different hydrophilic properties (commercial MTX and MTX disodium salt).

Table 6 | Methotrexate (MTX) concentrations and encapsulation efficiency (EE) of nanoemulsions produced using hydrophilic MTX. Values represent the mean ± SD of two independent experiments

	Initial [drug]		Final [drug] *		Encapsulation
	(mg/mL)	(mM)	(mg/mL)	(mM)	Efficiency (%)
P407 nanoemulsions + MTX	0.125	0.275	0.009 ± 0.004	0.020 ± 0.008	10.2 ± 4.2
P407 nanoemulsions + MTX-Na	0.125	0.251	0.014 ± 0.003	0.032 ± 0.006	16.3 ± 3.3

* Values in the final nanoemulsions after dilution of 1.4 in PD-10 desalting columns.

For the preparation of these two formulations was weighted the same mass of MTX and MTX-Na that was dissolved in the P407 aqueous solution, resulting in a concentration of 0.125 mg/mL. As the MTX has a smaller MW (454.44 g/mol) than MTX-Na (498.4 g/mol), the initial molar concentration of MTX was higher in the first case (0.275 mM). After production and separation using the PD-10 columns, it was observed that the use of MTX-Na resulted in a higher EE than the commercial MTX. The P407-based nanoparticles produced using MTX-Na showed a higher concentration of MTX (0.028 mM), indicating that this simple MTX modification can improve its encapsulation in these nanoemulsions.

Table 7 shows the values of drug concentrations (initial and final) as well as the EE obtained when the nanoemulsions were prepared using the hydrophobic MTX derivatives (MTX-OEt and MTX-DODAB). In this case, the MTX derivatives were dissolved in the vegetable oil and it was tested the maximum solubility of each compound. The initial concentration of these two hydrophobic MTX derivatives was different because the MTX-DODAB complex presented a lower solubility than MTX-OEt. Moreover, the MW of MTX-DODAB (1554.52 g/mol) is higher than MTX-OEt (510.55 g/mol), which results in a higher difference on the molar concentration. In this way, in the initial formulations were achieved 0.245 mM of MTX-OEt and 0.064 mM of MTX-DODAB. After separation of the free drug using the PD-10 desalting columns was showed that the EE obtained in the case

of MTX-DODAB (superior to 90 %) was much higher than in the case of MTX-OEt. However, the final concentration of drug is the most important parameter and it was obtained a higher concentration (superior to 0.070 mM) when the MTX-OEt derivative was used.

Table 7 | Concentrations of methotrexate (MTX) derivatives and the encapsulation efficiency (EE) of nanoemulsions prepared using the hydrophobic MTX derivatives. Values represent the mean ± SD of two independent experiments

	Initial [drug]		Final [drug] *		Encapsulation
	(mg/mL)	(mM)	(mg/mL)	(mM)	Efficiency (%)
P407 nanoemulsions + MTX-OEt	0.125	0.245	0.041 ± 0.018	0.078 ± 0.040	44.3 ± 22.9
FA-P407 nanoemulsions + MTX-OEt	0.125	0.245	0.032 ± 0.006	0.059 ± 0.017	33.5 ± 9.8
P407 nanoemulsions + MTX-DODAB	0.100	0.064	0.066 ± 0.001	0.042 ± 0.000	92.0 ± 0.9
FA-P407 nanoemulsions + MTX-DODAB	0.100	0.064	0.067 ± 0.001	0.043 ± 0.000	94.1 ± 0.9

* Values in the final nanoemulsions after dilution of 1.4 in PD-10 desalting columns.

Comparing the hydrophilic MTX derivatives with the hydrophobic derivatives it is possible to verify that the concentration of encapsulated drug is much higher when used either hydrophobic derivatives. Moreover, the MTX-OEt seems to be an effective approach for an efficient encapsulation of MTX in the P407-based nanoemulsions.

In order to achieve a higher final concentration of drug, a formulation was produced using the P407-MTX conjugate as aqueous solution for the nanoemulsions production. Nanoemulsions prepared using this conjugate in combination with MTX-OEt dissolved in vegetable oil was an important strategy tested. Table 8 shows the results obtained for these nanoemulsions produced using the P407-MTX conjugate.

Using the strategy of combination of the P407-MTX conjugate with the MTX-OEt was achieved a higher initial MTX concentration (0.355 mM) than in other all conditions tested. Taking into account the control formulation (prepared only with the P407-MTX conjugate) can be observed a high EE (around 90%), which indicates that almost all conjugate was used in the nanoemulsions formulation. Even if the EE of the formulation prepared using the combination of P407-MTX conjugate with MTX-OEt derivative was lower, the final drug concentration was greater (0.046 ± 0.003 mg/mL). In this case, it's not possible to calculate the molar concentration because there

are two different types of MTX that we cannot distinguish using indirect quantification by absorbance.

Table 8 | Drug concentrations and encapsulation efficiency (EE) of nanoemulsions prepared using Poloxamer 407-methotrexate (P407-MTX) conjugate. Values represent the mean ± SD of two independent experiments

	Initial [drug]		Final [drug] *		Encapsulation
	(mg/mL)	(mM)	(mg/mL)	(mM)	Efficiency (%)
P407-MTX nanoemulsions	0.050 ± 0.015	0.110	0.031 ± 0.005	0.067 ± 0.011	89.0 ± 10.2
P407-MTX nanoemulsions + MTX-OEt	0.175 ± 0.015	0.355	0.046 ± 0.003	- **	36.3 ± 1.6

* Values in the final nanoemulsions after dilution of 1.4 in PD-10 desalting columns; ** not possible to determine.

Comparing these results with the previously observed for the P407 nanoemulsions + MTX-OEt, it is possible to conclude that this new approach improved the results, as expected. This strategy allowed the production of P407-based nanoemulsions loaded with a greater concentration of the pharmacological compound.

Other two methods used for the quantification of pharmacological compounds, HPLC and ^{1}H NMR, were also tested for the quantification of MTX in the nanoemulsions. However, this quantification was not successful, probably due to the low concentration of drug.

3.3.3. Determination of size, polydispersity index, zeta-potential and long-time stability

Particle size is an important parameter as it can directly affect the physical stability, cellular uptake, biodistribution and drug release from the NPs [128]. DLS is a technique that measures the Brownian motion of macromolecules in solution and relates this motion to the size of particles [129]. DLS is a noninvasive technique, which offers good statistics with respect to measurements of the size distribution and PdI of NPs [130]. Therefore, DLS has become the preferred technique to routinely determine the size of NPs [21]. Using this technique, the size and PdI of the several formulations of nanoemulsions were analyzed (table 9).

Table 9 | Physicochemical characterization of the nanoemulsions evaluated by dynamic light scattered (DLS) analysis. Values represent the mean ± SD of two independent experiments

	Z-average (d.nm)	PdI	Stability
P407 nanoemulsions	98.4 ± 2.9	0.176 ± 0.041	> 16 weeks
FA-P407 nanoemulsions	92.3 ± 3.7	0.118 ± 0.001	> 16 weeks
P407 nanoemulsions + MTX	97.3 ± 10.8	0.105 ± 0.020	> 16 weeks
P407 nanoemulsions + MTX-Na	105.9 ± 11.5	0.129 ± 0.034	> 16 weeks
P407 nanoemulsions + MTX-OEt	86.7 ± 6.7	0.096 ± 0.013	> 16 weeks
FA-P407 nanoemulsions + MTX-OEt	86.1 ± 1.7	0.096 ± 0.023	> 16 weeks
P407 nanoemulsions + MTX-DODAB	94.7 ± 4.1	0.094 ± 0.013	> 16 weeks
FA-P407 nanoemulsions + MTX-DODAB	95.1 ± 7.9	0.099 ± 0.008	> 16 weeks
P407-MTX nanoemulsions	91.3 ± 24.4	0.122 ± 0.003	> 16 weeks
P407-MTX nanoemulsions + MTX-OEt	84.0 ± 12.7	0.132 ± 0.003	> 16 weeks

NPs larger than 100 nm can be easily cleared-off by macrophages and other MPS cells and cleared from circulation by phagocytosis [48]. Additionally, NPs below 10 nm have a higher tendency to be excreted by the kidneys [67]. Therefore, for IV administration, the range between 10 nm and 100 nm is the most appropriate to reach the desired cells. PdI values of 0.2 and below are acceptable for polymer-based NPs [67], but values of 0.1 and below represent a very monodisperse population of nanoemulsions [70], being the latter an ideal condition. Therefore, all nanoemulsions formulations developed (table 9) showed suitable characteristics for IV therapeutic applications, demonstrating monodisperse populations of small nanoemulsions.

The delivery efficiency of NPs exhibiting neutral ZPs, defined from −10 to +10 mV, tends to be higher than the delivery efficiency of NPs with positive (>10 mV) or negative (<−10 mV) ZPs [131]. Neutral NPs have been associated to much lower opsonization rates than charged NPs and, consequently, lower clearance from the blood circulation [31]. The ZP of the nanoemulsions was also analyzed and all formulations demonstrated a ZP close to zero (0 ± 2 mV), meaning that all formulations present neutral surface charge [72]. A neutral and hydrophilic surface can lead to a

longer half-life in the blood circulation [48], being this neutral and hydrophilic surface conferred by the presence of PEG chains of the P407.

The nanoemulsions containing FA at the surface and non-targeted nanoemulsions showed very similar values of size, PdI and ZP. All formulations revealed high stability along time, even after 16 weeks of storage the nanoemulsions maintained their characteristics. Moreover, the leakage of the MTX was evaluated along time and for all formulations was not detected leakage.

The nanoemulsions that demonstrated higher concentrations of encapsulated MTX as well as the respective controls were also analyzed using NTA (table 10). NTA is an innovative system for sizing particles from about 30 to 1000 nm, allowing direct visualization of a liquid NPs suspension [132] and offering an estimated particle concentration [21].

Table 10 | Physicochemical characterization of the nanoemulsions prepared using methotrexate diethylated (MTX-OEt) and Poloxamer 407-methotrexate (P407-MTX) conjugate and respective controls, evaluated by nanoparticle tracking analysis (NTA). Values represent the mean ± SD of two independent experiments

	Mean size (nm)	SD (nm)	Concentration (E^{12} particles/mL)
P407 nanoemulsions	98.0 ± 10.1	43.5 ± 16.8	2.8 ± 0.38
FA-P407 nanoemulsions	98.8 ± 8.4	43.5 ± 15.1	2.7 ± 0.23
P407 nanoemulsions + MTX-OEt	95.8 ± 7.4	51.3 ± 13.8	1.8 ± 0.35
FA-P407 nanoemulsions + MTX-OEt	92.5 ± 9.3	41.0 ±18.7	2.4 ± 0.15
P407-MTX nanoemulsions	97.0 ± 5.7	39.0 ± 3.9	5.1 ± 0.61
P407-MTX nanoemulsions + MTX-OEt	92.3 ± 6.3	31.5 ± 4.2	2.3 ± 0.18

The values of size obtained by NTA corroborates the results obtained by DLS. In this way, using two different methods it was verified that the nanoemulsions present narrow and small size making them suitable for IV application. NTA also allows to quantify the NPs concentration on each sample, and similar concentrations of particles per mL were obtained for all nanoemulsions, except for P407-MTX nanoemulsions. It seems that the use of P407-MTX conjugate induces the formation of more NPs however the use of MTX-OEt in combination with the conjugate can interfere with the nanoemulsions formation. Using the HPH method, the nanoemulsions are formed due to molecular interactions, such as intramolecular hydrogen, hydrophobic and electrostatic interactions, between

all of the components [31]. Thus, one possible explanation for this result can be that the presence of more molecules in the formulation can result in different nanoemulsions populations.

Concluding, all formulations tested revealed suitable physicochemical characteristics for IV therapeutic applications. However, taking into account the concentration values of drug encapsulated, only the nanoemulsions produced using MTX-OEt and using a combination of P407-MTX conjugate with this MTX derivative were used for posterior assays.

3.3.4. Study of release profile of Methotrexate

The *in vitro* drug release was evaluated at 37 °C using the dialysis method and PBS as release medium, as previously described. MTX release was evaluated for the nanoemulsions loaded with MTX-OEt prepared using P407 and P407-MTX conjugate. As control was also evaluated the MTX release for the P407-MTX conjugate and for the nanoemulsions prepared using this conjugate without MTX-OEt. The release profile of the MTX from these formulations is represented in figure 31.

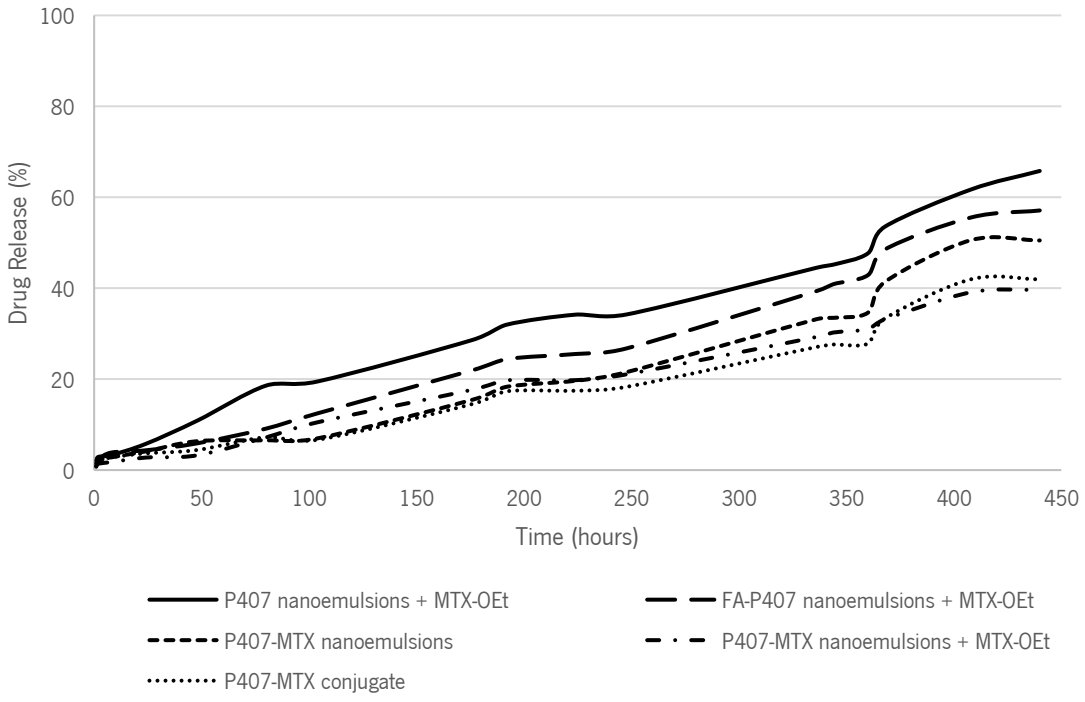

Figure 31 | Release of methotrexate (MTX) from the nanoemulsions over time. Values represent the results of one experiment.

Analyzing the data obtained, it can be observed a slow drug release rate for all samples, comparable to a sustained release. Taking into account the MTX release percentage, the P407-based nanoemulsions loaded with MTX-OEt revealed a higher value (approximately 60 % after 440

hours) than the nanoemulsions prepared using the P407-MTX conjugate. It seems to reveal that the release of MTX is easier when was used the MTX-OEt dissolved in the vegetable oil than when the MTX was covalently bond to P407. In conclusion, the delayed release of MTX observed in all samples allows to infer that the MTX is shielded by P407, indicating that the MTX molecules were indeed entrapped in the nanoemulsions. As evidenced from the *in vitro* release profile, P407 nanoemulsions may have the potential to serve as a sustained release matrix. This type of drug release is much sought after because it reduces dosing frequency, increasing patient compliance.

3.3.5. Study of the Methotrexate release in the presence of lipase

The nanoemulsions prepared using the P407-MTX conjugate demonstrated a slower MTX release, probably due to the strong ester linkage between the P407 and MTX. Moreover, in a biological environment the NPs are in contact with different hydrolytic enzymes that can induce their hydrolysis and degradation [133]. Recent evidences demonstrate that various esterases are involved in drug metabolism [134]. In this way, it was studied the MTX release from these nanoemulsions in the presence of lipase. Lipase is an esterase, therefore it was expected that its presence would accelerate the release of MTX present in the conjugate used for the nanoemulsions production. Figure 32 shows the results obtained for empty P407-MTX nanoemulsions and loaded with MTX-OEt, for the P407-MTX conjugate and for the respective controls performed in the absence of lipase.

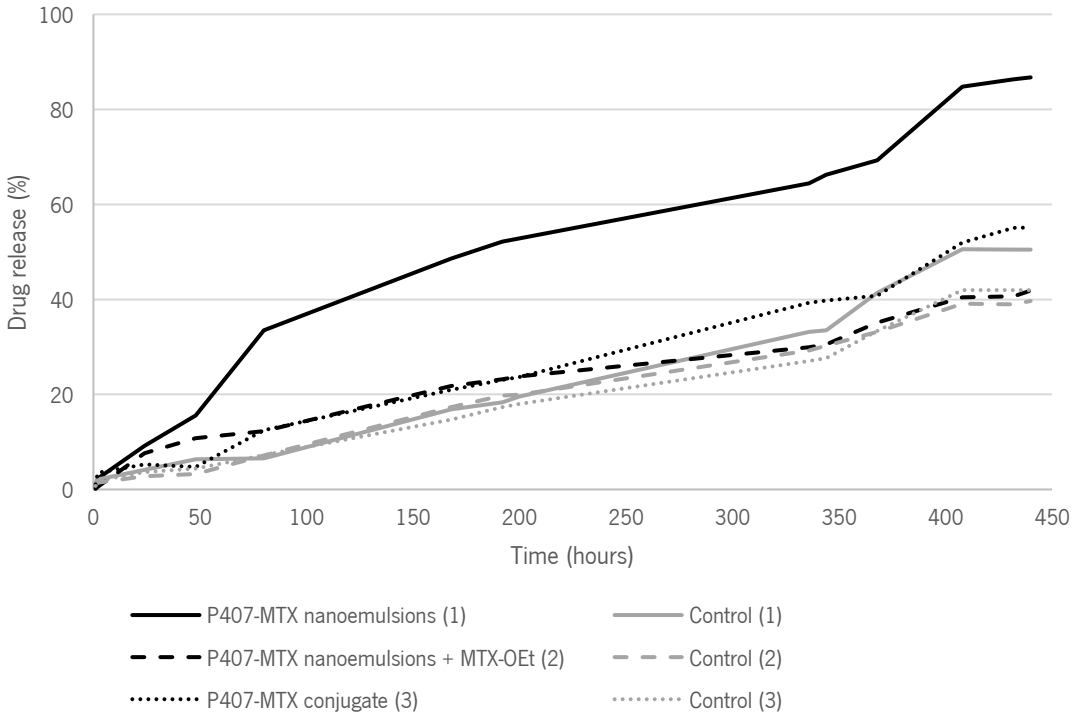

Figure 32 | Release of methotrexate (MTX) from the nanoemulsions prepared using the poloxamer 407-methotrexate (P407-MTX) conjugate in the presence of lipase and respective controls (in the absence of lipase). Values represent the results of one experiment.

The P407-MTX nanoemulsions incubated with lipase showed a significant increase in the MTX release percentage (approximately 86 % of release after 440 hours) when compared with the respective control (approximately 50 %). Furthermore, the drug release rate was faster than in the control condition, indicating that the lipase catalyst was able to cleave the ester linkage occurring the MTX release. For the P407-MTX conjugate, even in the presence of lipase, was observed the release of a lower percentage of MTX after 440 hours of incubation (approximately 55 %). It can be speculated that the P407-MTX nanoemulsions can be easily hydrolyzed by lipase probably due to an increase of the surface area available for hydrolysis created during the nanoemulsions formation. Thus, these structures are more easily hydrolyzed by the lipase and hence a higher amount of MTX is released. It was observed a higher MTX release from the P407-MTX nanoemulsions than that of the nanoemulsions loaded with MTX-OEt (approximately 42 % after 440 hours). This result allows to infer that this latter form of MTX it is present in the core of the nanoemulsions and only the MTX conjugated with P407 present at the surface can be released after the hydrolysis by lipase. During the entire assay the enzyme used remains active concerning previous stability studies realized in our laboratory (maintain 100 % of initial activity after 440 hours).

3.4. Biological effect of Poloxamer 407-based nanoemulsions containing Methotrexate in Caco-2 cell line

The cytotoxicity test is one of the most important indicators of the biological evaluation *in vitro*, being a requirement for the application of NPs as DDS [135]. This test is simple, fast, has a high sensitivity and can save animals from toxicity [136]. Loureiro *et al.* demonstrated that P407-based NPs (up to 900 µg/mL) did not induce cytotoxicity in immortalized human normal cells, even after 72 hours of incubation [121]. In this way, the next step of this work was the evaluation of the biological effect of these nanoemulsions containing the MTX derivatives.

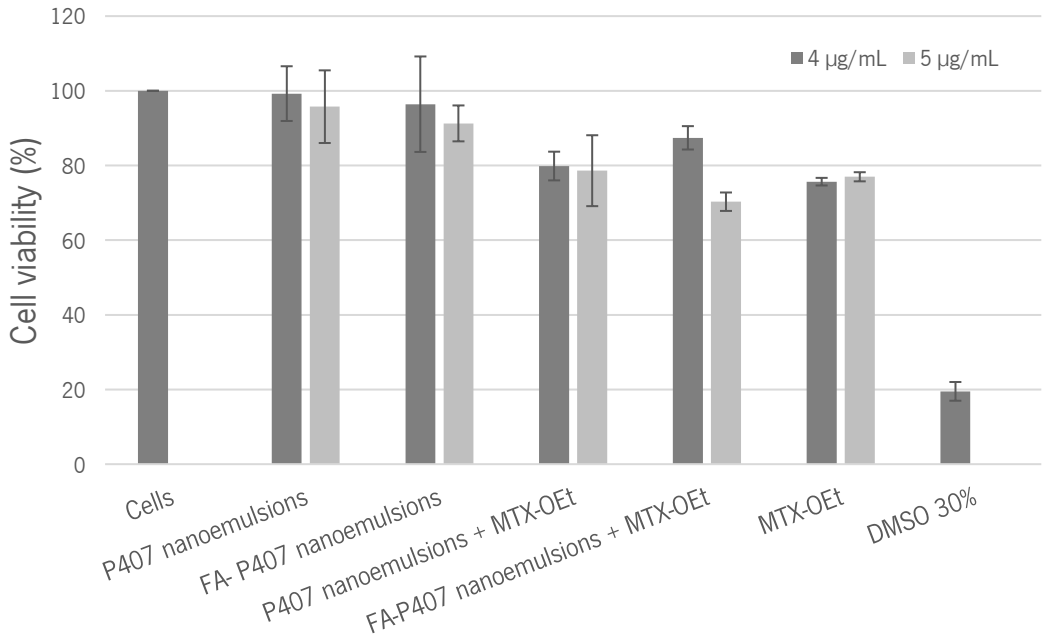

Figure 33 | Caco-2 cell viability after 48 hours of contact with Poloxamer 407 (P407)-based nanoemulsions containing or not 4 and 5 µg/mL of methotrexate diethylated (MTX-OEt) and with the methotrexate (MTX) derivative alone at same concentrations, compared with cells (negative control) and cells incubated with 30 % (v/v) of DMSO (death control), determined by MTS assay. Values are the mean ± SD of two independent experiments.

Figure 33 represents the biological effect of the P407-based nanoemulsions loaded with MTX-OEt (containing or not FA at their surface) in Caco-2 cell line. The results demonstrated that the empty nanoemulsions with and without FA did not induce a significant less of cell viability, as expected. Nanoemulsions loaded with MTX-OEt and the drug alone demonstrated very similar values of cell viability. These results indicate that occurs an effective release of the MTX-OEt from the nanoemulsions *in vitro*. The FA-nanoemulsions loaded with 5 µg/mL of MTX-OEt seem to have a slight tendency of a higher biological effect. This difference is very low, which can be explained by

the very small concentrations of MTX-OEt applied. For this reason, it is very important to increase the MTX concentration loaded in the P407-based nanoemulsions.

Using the P407-MTX conjugate for the production of the nanoemulsions it was possible to obtain a higher concentration of drug in the final formulation, as previously observed. Thus, the biological effect of these nanoemulsions was also tested in Caco-2 cells applying a higher concentration of drug (8 μg/mL).

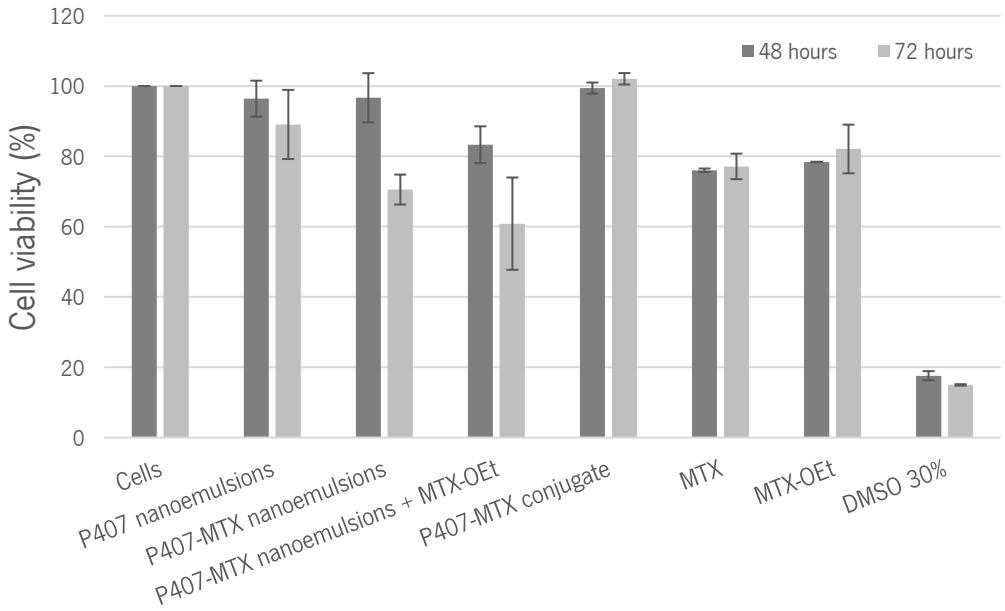

Figure 34 | Caco-2 cell viability after 48 and 72 hours of contact with Poloxamer 407-methotrexate (P407-MTX) nanoemulsions containing or not 8 μg/mL of drug, with the P407-MTX conjugate and with the two types of methotrexate (MTX) at the same concentration, compared with cells (negative control) and cells incubated with 30 % (v/v) of DMSO (death control), determined by MTS assay. Values are the mean ± SD of two independent experiments.

Figure 34 shows that the P407-MTX nanoemulsions loaded with MTX-OEt and the two types of MTX demonstrated very similar values of cell viability after 48 hours of incubation. For this time point all the other conditions (P407 nanoemulsions, P407-MTX nanoemulsions and P407-MTX conjugate) did not induce loss of cell viability. After 72 hours of incubation, the P407-MTX nanoemulsions with and without MTX-OEt revealed similar values of cell viability, being the value for the case of nanoemulsions loaded with MTX-OEt slightly smaller. Taking into account these results it can be speculated that a higher time of incubation can contribute to the release of the MTX conjugated with P407. The cells incubated with the conjugate showed 100 % of cell viability

even after 72 hours. A possible explanation can be that this conjugate not formulated in nanoemulsions was not internalized by the cells.

4. CONCLUSIONS

In summary, with this work it was successfully produced two different P407 conjugates (P407-FA and P407-MTX) by an esterification reaction. The conjugation of P407 with FA was performed in order to produce FA-tagged nanoemulsions for a specific drug delivery into cancer cells. In the other hand, P407-MTX conjugate was produced in order to increase the MTX concentration in the nanoemulsions. Additionally, several MTX modifications were performed with success in order to produce different MTX derivatives. These strategies resulted in higher concentrations of MTX encapsulated, being the best approach the production of nanoemulsions using P407-MTX conjugate as aqueous phase combined with the addition of MTX-OEt in vegetable oil. After an exhaustive physicochemical characterization of all P407-based nanoemulsions, it was observed that they present suitable characteristics for IV therapeutic applications. MTX release studies were performed using the most promising nanoemulsions and it was observed a slow drug release rate for all samples. The incubation of P407-MTX nanoemulsions with lipase from *Thermomyces lanuginosus* induced a faster release of MTX, maintaining the drug release for a long period of time. The evaluation of the biological effect of these most promising nanoemulsions revealed that the P407-MTX nanoemulsions loaded with MTX-OEt can be a good strategy for the IV application of MTX in cancer therapy.

All these characteristics of the produced nanoemulsions can overcome the problems associated with therapies using free MTX, by increasing its half-life in systemic circulation, protecting the drug from degradation and also reducing the potential side effects due to the specific cell targeting. Overall, the P407-MTX nanoemulsions loaded with MTX-OEt have the potential to be implemented as DDS in cancer therapy, as supported by the cellular viability assays performed. In the future, *in vivo* experiments using these nanoemulsions could be performed and could be also evaluated their biological effects in other diseases that express FRs, such as RA.

CHAPTER IV

DEVELOPMENT OF PEGYLATED MICELLES FOR METHOTREXATE DELIVERY

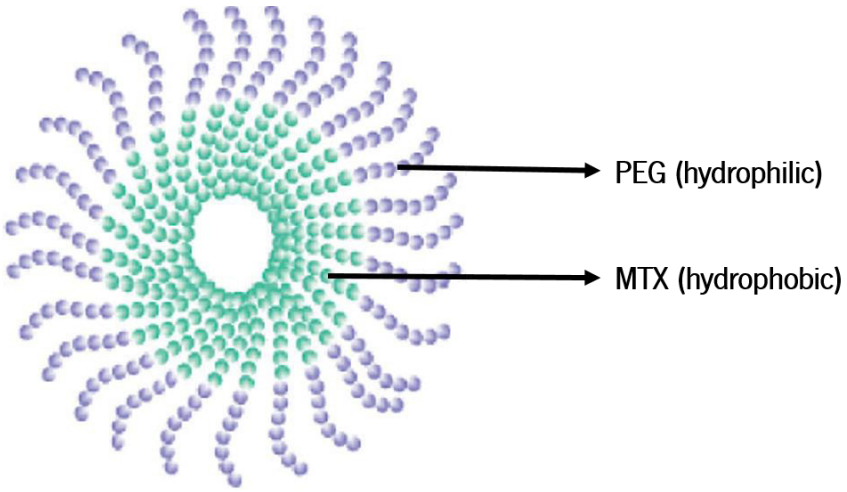

Chapter IV – DEVELOPMENT OF PEGYLATED MICELLES FOR METHOTREXATE DELIVERY

1. FRAMEWORK

In this chapter it will be described the development of PEGylated micelles containing MTX, which were produced by two high energy methods (sonication and HPH) and ethanol injection. In order to develop a new approach for the therapeutic application of MTX was produced MTX-PEG_{2000} conjugate. As this new molecule presents amphiphilic properties was tested the production of micelles using this conjugate. Polymeric micelles are promising vehicles for the delivery of poorly soluble cytotoxic drugs that allow a controlled drug release [39]. In this way, was tested the production of this new type of PEGylated micelles containing MTX in the core. PEG gives stealth properties to the micelles, allowing them to avoid uptake by the MPS, which is crucial for achieving long circulation time in blood [82]. Additionally, PEGylated NPs were found to be capable of specific extravasation in diseased tissues as a result of the EPR [137]. Thus, the PEG molecules conjugated with MTX provides stabilization and stealth behavior to the developed micelles. These micelles as DDS not only protect the MTX from degradation but may also allow a controlled release.

2. MATERIALS AND METHODS

2.1. Reagents and equipment

2.1.1. Reagents

Ultrapure water and deionized water were obtained from Milli-Q Water Purification Systems, Germany. DMSO-d_6 was purchased from Cortecnet, France. DHB (suitable for MALDI-TOF analysis) as well as TA were purchased from Sigma-Aldrich, USA. Acetonitrile (HPLC grade) and ethanol were obtained from Fisher Scientific, USA.

2.1.2. Equipment

Determination of refractive index was performed in a digital refractometer RX-9000α from ATAGO, UK. Sonication was executed in a USC600TH ultrasonic bath from VWR International Ltd, USA, at 120 W and using a frequency of 45 kHz. Sonication with ultrasonic probe was performed using a VC 505/VC 750 Sonics Vibracell Ultrasonic Processor from Sonics & Materials, USA. The probe of choice was a titanium probe Vibracell CV 33, 20 kHz (3 mm of diameter) from Sonics & Materials, USA. ^{1}H NMR spectra were recorded using a Bruker Avance III 400 (400 MHz) from Bruker Daltonics GmbH, Germany. MALDI-TOF mass spectra were acquired on a Bruker Autoflex Speed instrument, equipped with a 337 nm nitrogen laser, from Bruker Daltonics GmbH, Germany. DLS analysis were performed in a Malvern zetasizer Nano ZS from Malvern Instruments, UK. All absorbance measurements were conducted in a Synergy Mx Multi-Mode Reader from BioTek, USA.

2.2. Production and characterization of PEGylated Methotrexate

In an effort to maximize the drug loading capacity of PNPs, a polymeric drug conjugate was developed. MTX-PEG_{2000} was produced by a colleague in the laboratory (unpublished work). MTX and MTX-PEG_{2000} were characterized by ^{1}H NMR spectroscopy, being the DMSO-d_6 used as deuterated solvent, using the peak solvent as internal reference. Mass/charge of MTX-PEG_{2000} was verified by MALDI-TOF using DHB as matrix. The matrix and sample solution were prepared by dissolving a saturated solution of DHB in acetonitrile/TA 0.1 % (30:70). The samples were analyzed using the linear positive mode. The refractive index was also determined and absorbance measurements were performed.

2.3. Preparation and characterization of PEGylated Methotrexate micelles

2.3.1. Critical micelle concentration determination of PEGylated Methotrexate (MTX-PEG_{2000})

Critical micelle concentration (CMC) of the MTX-PEG_{2000} was determined using two different techniques (absorbance and DLS measurements). The same stock solution of MTX-PEG_{2000} was used for both techniques, allowing a lower error associated between the methods. MTX-PEG_{2000} stock solution was prepared dissolving the conjugate in water at RT, at a concentration of 1 mM. After this preparation, the solution was sonicated for 60 minutes in the ultrasonic bath. Using this stock solution, several dilutions were made in order to test different concentrations (from 0.001 to 1000 μM).

The methods used for CMC determination were based on Karimi *et al.* [138] and Patist *et al.* [139] for absorbance measurements and on Topel *et al.* for DLS measurements [140].

2.3.2. Production of micelles by high energy methods (sonication and high pressure homogenization)

MTX-PEG_{2000} was dissolved in water at different concentrations (1 and 5 mg/mL). For the sonication method, the solutions were submitted to sonication using the probe for 5 minutes with pulses (2 seconds on/2 seconds off) using different temperatures (30 °C, 60 °C and in ice). For the HPH method, the solutions were submitted to 10 minutes of homogenization cycles at high pressures (250 and 600 bar), using the high pressure homogenizer. A combination between these two methods was also tested (5 minutes of sonication at 30 °C and 5 minutes of HPH). The size reduction of the micelles was performed after their production using different methods (filtration using filters with different pore sizes and extrusion). The method that demonstrated better results was the filtration using the 0.22 μm PES filter.

2.3.3. Production of micelles by ethanol injection

MTX-PEG_{2000} was dissolved in ethanol and injected dropwise in water, at 70 °C. After the ethanol evaporation for 10 minutes were obtained the micelles, which were subsequently filtered using 0.22 μm PES filter (Merck Millipore, Ireland). Different concentrations (1 and 5 mg/mL) and agitation speeds (250, 500 and 750 rpm) were tested in order to optimize the production of micelles.

2.3.4. Determination of size and polydispersity index

The micelles were analyzed for their size distribution, at 25 ℃, by PCS, using DLS. The values for viscosity and refractive index were taken as 0.8872 cP and 1.333, respectively. Each sample was measured in triplicate and the results are presented as mean value ± SD.

3. RESULTS AND DISCUSSION

3.1. Characterization of the PEGylated Methotrexate

The addition of PEG to the NPs surface has been used as a method to create a hydrophilic protective layer against opsonization [50]. This coating provides an active "cloud" of hydrophilic and neutral chains at the NPs surface which repels plasma proteins, resulting in invisibility against MPS [40]. These PEGylated NPs have a long blood residence time and a high rate of extravasation into permeable tissues [19]. Therefore, in order to obtain PEGylated micelles with the ability to maintain the MTX more time in the systemic circulation, the MTX-PEG_{2000} conjugate was produced and its structure is represented in figure 35.

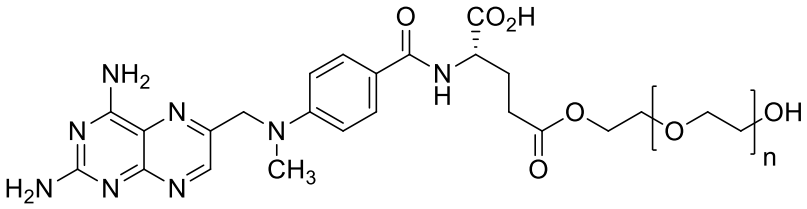

Figure 35 | Structure of MTX-PEG_{2000} conjugate.

^{1}H NMR spectroscopy and MALDI-TOF analysis were executed to characterize the MTX-PEG_{2000} conjugate. ^{1}H NMR spectra of MTX and MTX-PEG_{2000} are presented as stacked spectra in figure 36. The main difference when comparing the MTX spectrum (figure 36a) with the spectrum of the MTX-PEG_{2000} (figure 36b) is the decrease in the intensity of proton (j), which corresponds to the carboxylic groups of MTX. This difference indicated that the conjugation occurred in one of the carboxylic groups. Other protons, such as (a/b) and (c) have a different chemical shift due to the conjugation reaction. All other protons have similar chemical shift as the MTX spectrum. Also, in the conjugate spectrum (figure 36b) it is possible to detect proton (k) that corresponds to the CH_2 repetition groups of PEG. All these results indicated that the conjugation between PEG_{2000} and MTX was successfully achieved. By the integration of the specific peaks of MTX (δ_H = 8.56 ppm) and PEG_{2000} (δ_H = 3.48 ppm) was possible to verify that there is still 50% of unreacted PEG.

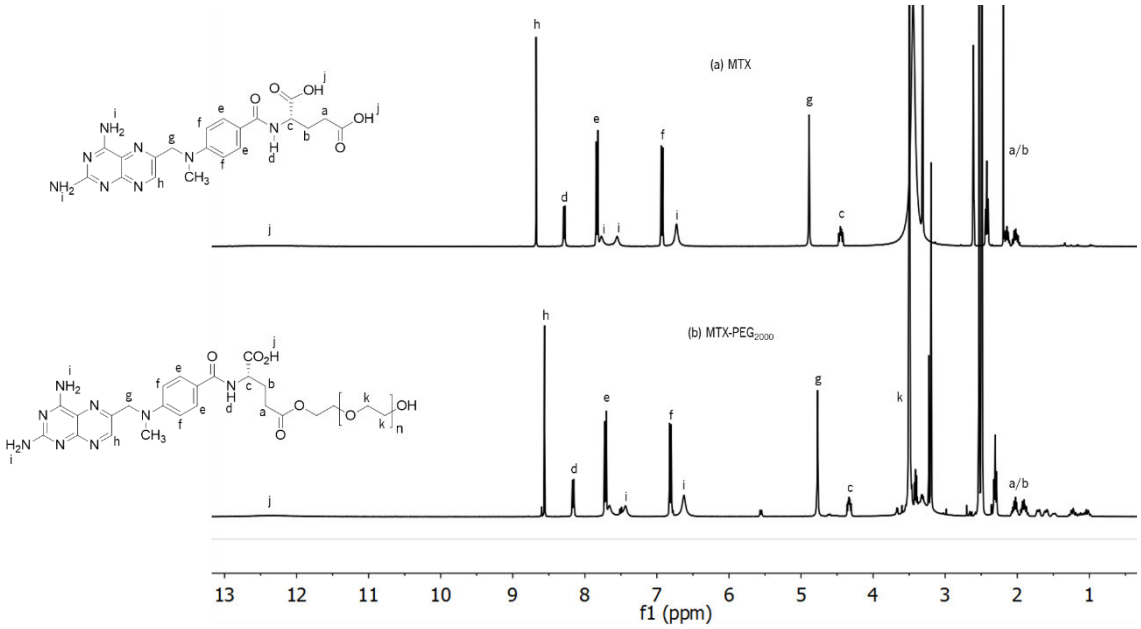

Figure 36 | ^{1}H NMR stacked spectra of (a) methotrexate (MTX) and (b) MTX-PEG$_{2000}$ in DMSO-d$_6$. The peaks labeled in lowercase letters correspond to the protons indicated in the structures.

MALDI-TOF MS of MTX-PEG$_{2000}$ was performed and the spectrum is presented in figure 37.

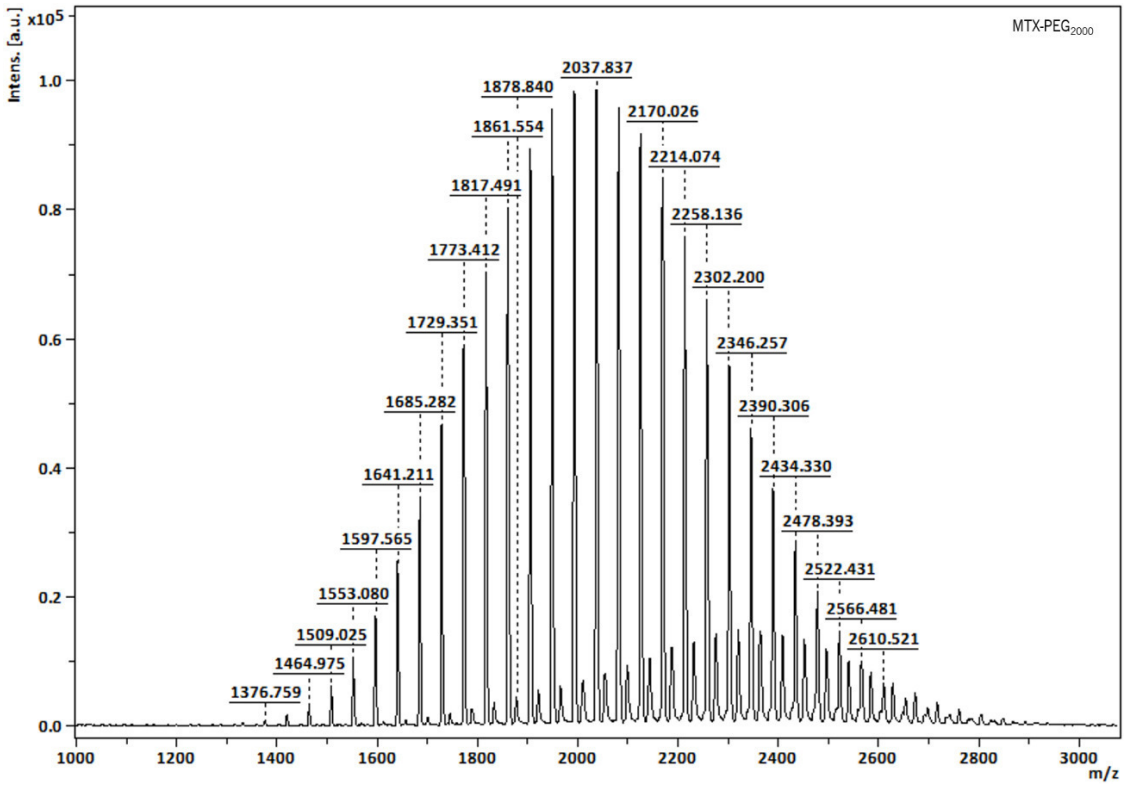

Figure 37 | MALDI-TOF mass spectrum of MTX-PEG$_{2000}$, acquired in linear positive mode.

It is possible to observe that MTX-PEG_{2000} has a $MW_{average}$ of 2434.330 Da (figure 37). Considering the previous results of NMR that indicated 50% of unreacted PEG it is also possible to see the $MW_{average}$ of this compound (2037.837 Da) in the MALDI-TOF spectrum.

Absorbance spectra of MTX and PEGylated MTX (figure 38) were performed in order to determine if the PEGylation of MTX modifies the wavelength of maximum absorbance.

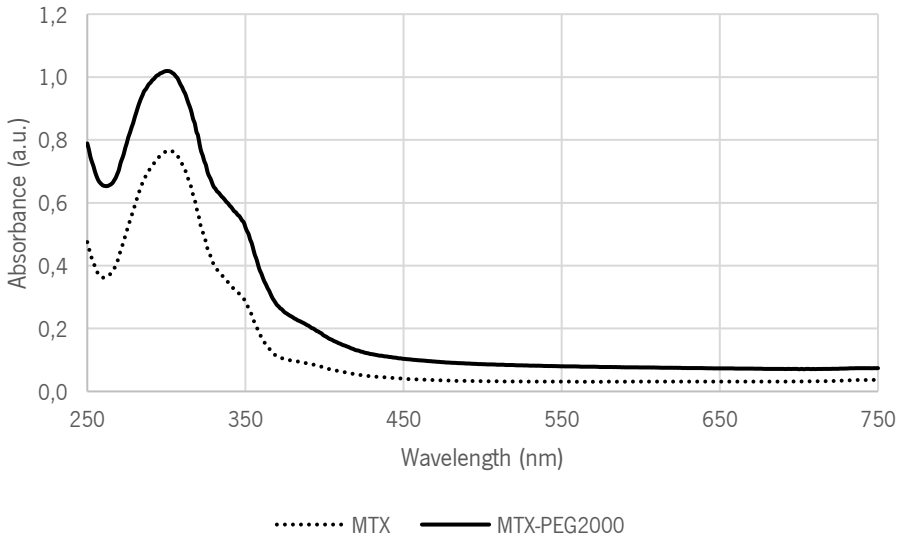

Figure 38 | Absorbance spectra of methotrexate (MTX) and MTX-PEG_{2000} conjugate in water, at 0.1 mM of MTX.

The results demonstrated that both compounds present the same wavelength of maximum absorbance of 303 nm, which was used for the quantification of MTX by absorbance.

3.2. Determination of the critical micelle concentration of PEGylated Methotrexate (MTX-PEG_{2000})

The CMC can be defined as the concentration below which only single chains are present but above which both single chains and micellar aggregates can be found [140]. At CMC point, some properties of surfactant solutions, like conductivity, surface tension, absorption and fluorescence, as a function of concentration, suffer abrupt changes due to the micelle formation [80, 141]. Therefore, CMC determination as an important characteristic of a surfactant is of great importance [138]. The applicable methods depend on the nature of the surfactant [142]. Experimentally, the CMC is found by plotting a graph of a suitable physical property as a function of the surfactant concentration and an abrupt change of slope marks the CMC [141]. There are many methods to measure the CMC such as tensiometry, spectroflourometry, conductometry and DLS, which are all based on the abrupt change in the related physical properties upon micelle formation [140].

One of the techniques used in this work for the determination of the CMC was the absorbance method. The absorbance spectra of the several solutions at different concentrations of MTX-PEG_{2000} were performed and it was verified that the wavelength of maximum absorbance is 303 nm for all samples. Using these absorbance values at 303 nm for each sample were performed the best fit lines drawn through the data points (figure 39). The intersection of these fit lines indicates the CMC value. The CMC obtained for MTX-PEG_{2000} compound using this method was 47.2 μM.

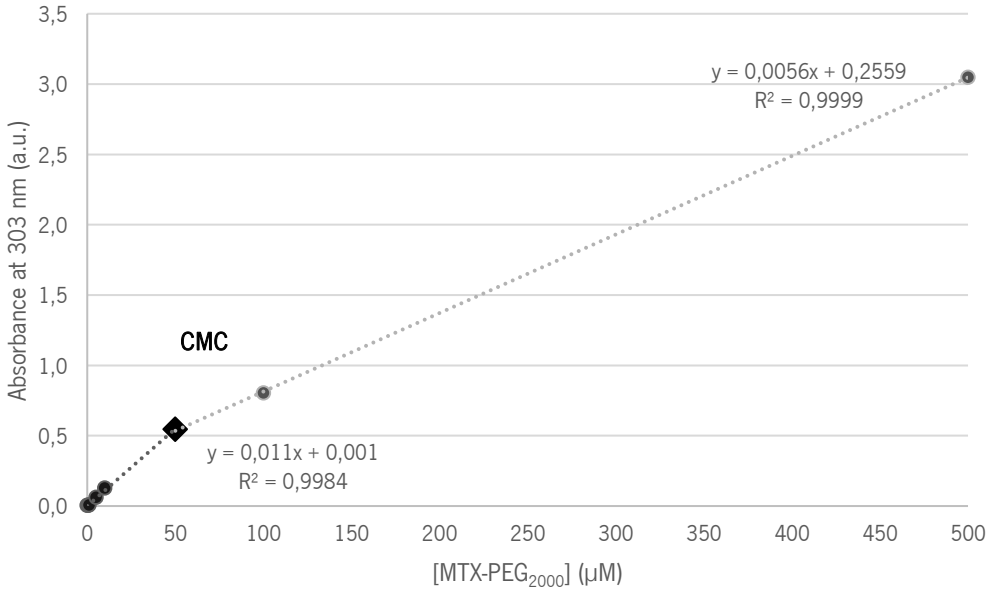

Figure 39 | Critical micelle concentration (CMC) determination of MTX-PEG_{2000} (CMC = 47.2 μM) using the absorbance method (at 303 nm). Values represent the results of one experiment.

DLS can also be used for determination of the CMC values of micelle formed in solution, since there is a sudden increase in intensity of scattered light when the CMC is reached [140]. For this, a plot of intensity as a function of the concentration of MTX-PEG_{2000} was done (figure 40). Using this method, the intersection of best fit lines, which corresponds to the CMC value, was 99.7 μM.

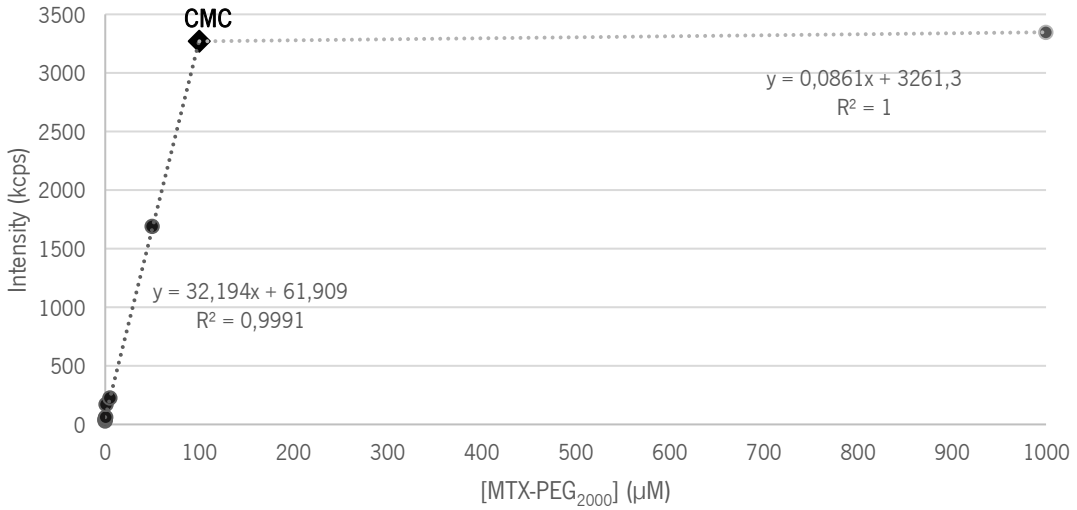

Figure 40 | Scattered intensity (kcps) as a function of MTX-PEG_{2000} concentration. The critical micelle concentration (CMC) obtained using the dynamic light scattered (DLS) analysis method was 99.7 μM. Values represent the results of one experiment.

Different values of CMC were obtained using these two methods. It is very common to observe a large difference between the CMC values of nonionic surfactants when are used different determination methods [139]. This can be explained by the broad MW distribution of these compounds and the possible presence of impurities [139]. This assumption can be extrapolated for our case considering that the PEG coupled to MTX has a MW distribution from 1500 to 2800 Da (see figure 37). Moreover, the MTX-PEG_{2000} conjugate can be considered a nonionic surfactant because no charge is present in the MTX.

Other methods for CMC determination were performed, such as the surface tension measurements using the tensiometer and the fluorescence probe technique using pyrene as fluorescence dye. However, the successful determination of the CMC was not possible using these two methods.

3.3. Preparation and characterization of PEGylated Methotrexate micelles

The minimum MTX-PEG_{2000} concentration used for the micelles production was 1 mg/mL (410.4 μM), being a value significantly higher than the CMC values determined. Several optimizations were performed for the production of PEGylated micelles using high energy methods (figure 41).

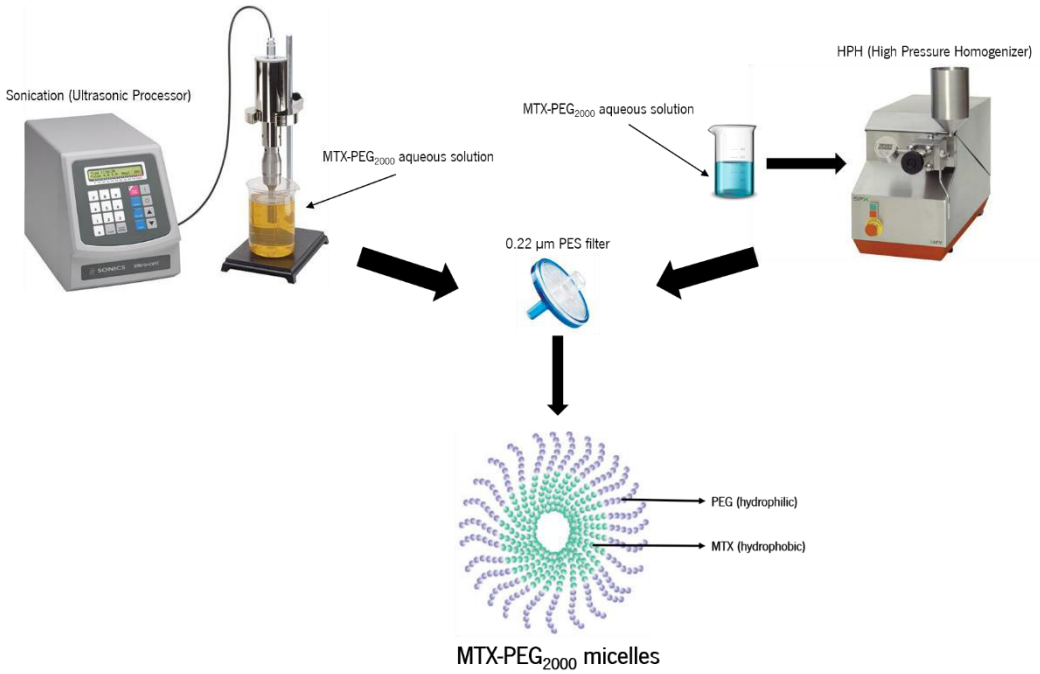

Figure 41 | Schematic representation of micelles production using high energy methods (sonication and high pressure homogenization (HPH)).

High energy approaches use mechanical devices capable of generating intense disruptive forces, forming small droplets e.g., high-pressure homogenizers and sonication [143]. HPH is pointed as the most appropriate high energy method for industrial applications, due to the facility of operation, scalability and reproducibility [144]. This technique makes use of high pressure homogenizer to produce NPs of extremely low particle size [145]. The surfactant type and concentration, as well as the homogenization conditions of pressure, temperature and number of cycles, have influence on the physicochemical properties of the NPs formed [146]. Sonication has received increased attention in the last few years due to high efficiency, economic performance and low instrumental requirements [147]. Sonication also generates intense shear forces, due to cavitation, facilitating the production of fine and stable NPs in the presence of surfactants [147]. It was tested the micelles production using sonication, HPH and a combination between these two processes, being the best results presented in table 11.

Table 11 | Size and polydispersity index (PdI) values of different MTX-PEG_{2000} micelles prepared using high energy methods (sonication and high pressure homogenization (HPH). Values represent the results of one experiment

	Initial [MTX-PEG_{2000}] (mg/mL)	High energy method	Size * (nm)	PdI *	Size ** (nm)	PdI **
A	1	Sonication at 30 °C	363.2	0.185	206.2	0.152
B	1	Sonication in ice	335.2	0.350	201.2	0.218
C	5	Sonication in ice	403.7	0.178	373.9	0.060
D	1	HPH	3121.0	0.214	173.5	0.261
E	1	Sonication (30 °C) + HPH	399.0	0.358	394.0	0.596

* After production; ** after production and filtration using the 0.22 μm filter.

A solution of MTX-PEG_{2000} at 1 mg/mL submitted to sonication at 30 °C (test A) resulted in PEGylated micelles with small size (206.2 nm) and an acceptable PdI value (PdI = 0.152), after filtration using 0.22 μm filter. A higher temperature of sonication (60 °C) was tested but it was observed worse results. So, a lower temperature (ice) was evaluated (test B), which resulted in very similar values of size and PdI compared to sonication at 30 °C. In order to verify if a higher concentration of MTX-PEG_{2000} could influence the results, the sonication of a solution containing 5 mg/mL of this conjugate was tested. It was verified that the increase of the concentration (test C) improved the results in terms of PdI, showing a monodisperse population (PdI < 0.1), but did not improve the size of the micelles. Afterwards, a different high energy method, HPH, was tested (test D) using 1 mg/mL of MTX-PEG_{2000}. The results demonstrated that this technique did not present better results than the sonication at 30 °C, mainly when compared the PdI values (PdI > 0.2). A combination of both production methods was performed (test E) and it was verified that the junction of two different approaches leads to poorer results.

In conclusion, the best conditions for the production of MTX-PEG_{2000} micelles, using high energy methods, were the sonication at 30 °C using 1 mg/mL of the PEGylated MTX.

Many other techniques have been reported for NPs preparation including ethanol injection, which is based on the replacement of organic solvents by aqueous media [148]. This method has several advantages, such as simplicity, fast implementation and reproducibility [148].

In order to determine if the use of another production method allows the development of micelles with more suitable characteristics for IV therapeutic applications was tested the ethanol injection method (figure 42).

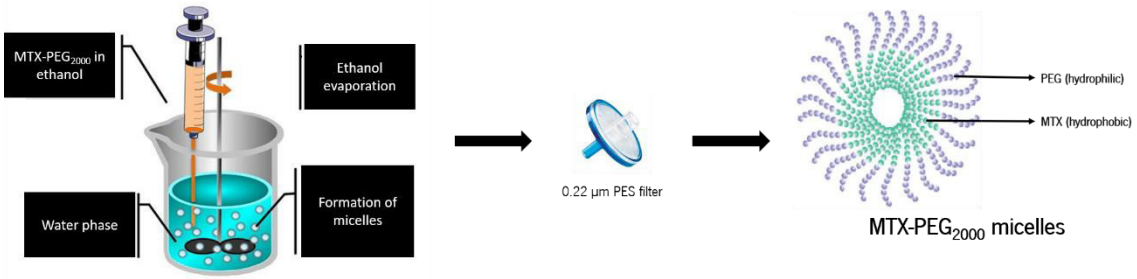

Figure 42 | Schematic representation of micelles production using ethanol injection method.

Table 12 shows that the samples prepared using 1 mg/mL of MTX-PEG_{2000} and an agitation speed of 250 rpm (test A) resulted in a monodisperse population (PdI < 0.1) of small micelles (261.2 nm), after filtration using 0.22 µm filter. In order to verify if an increase of the conjugate concentration can result in smaller micelles was tested the micelles production using 5 mg/mL. However, the results demonstrated that the presence of more MTX-PEG_{2000} resulted in higher size and PdI values (test B).

Table 12 | Size and polydispersity index (PdI) values of different MTX-PEG_{2000} micelles prepared using ethanol injection method. Values represent the results of one experiment

	Initial [MTX-PEG_{2000}] (mg/mL)	Rotation (rpm)	Size * (nm)	PdI *	Size ** (nm)	PdI **
A	1	250	331.2	0.331	261.2	0.079
B	5	250	1561	0.735	452.4	0.292
C	1	500	824.1	0.519	203.8	0.240
D	1	750	1006	0.494	221.1	0.051

*after production; ** after production and filtration using the 0.22 µm filter.

Previous studies performed in our laboratory demonstrated that the agitation speed influence the size and PdI values of the NPs prepared using the ethanol injection method. In this way, it was tested the production of micelles using 1 mg/mL of MTX-PEG_{2000} and the agitation speeds of 500

and 750 rpm (tests C and D, respectively). It was observed that high agitations speeds resulted in micelle solutions with higher size and PdI values before the filtration process. However, after the filtration using the 0.22 μm filter it was observed a significant reduction of size and PdI of the sample prepared using 750 rpm (test D).

Concluding, using the ethanol injection method was possible the production of PEGylated micelles with more suitable characteristics than using the high energy methods. These preliminary results allowed to conclude that this PEGylated MTX is able to induce the micelles formation. However, more optimizations are needed in order to obtain smaller micelles and it is also very important to repeat all these tests to evaluate their reproducibility. Additionally, in the future it is expected to perform the full characterization of these micelles, including the determination of the MTX concentration entrapped in the micelles and the evaluation of their biological characterization.

4. CONCLUSIONS

In conclusion, with this part of the work was possible the successful characterization of the PEGylated MTX produced in our laboratory. By ^{1}H NMR spectroscopy was confirmed the structure of the MTX-PEG_{2000} conjugate and the MALDI-TOF analysis allowed to confirm the MW of this compound. The CMC of this conjugate was also determined using two different techniques. An optimization of the micelles production was performed using different methods and the ethanol injection method using 1 mg/mL of MTX-PEG_{2000} and agitation speeds of 250 or 750 rpm resulted in monodisperse populations of small size micelles.

In the future, more optimizations are needed in order to achieve micelles with more suitable characteristics for IV therapeutic applications. Moreover, it is very important to perform the full characterization of the most promising micelles, including their biological characterization.

CHAPTER V

CONCLUSIONS

Chapter V – CONCLUSIONS

1. FINAL REMARKS

The main objective of this thesis was the development of PNPs as DDS for a specific delivery of MTX. P407-based nanoemulsions are a type of PNPs previously developed in our laboratory that showed suitable characteristics for IV therapeutic applications.

In this master thesis was performed an exhaustive optimization in order to encapsulate high concentrations of MTX in these nanoemulsions. P407-MTX conjugate and several MTX derivatives (MTX-Na, MTX-DODAB and MTX-OEt) were developed and used for the production of the intended NPs. The physicochemical and biological characterization of the developed nanoemulsions demonstrated the production of effective nanoemulsions suitable for MTX delivery applications. The nanoemulsions prepared using a combination between the P407-MTX conjugate and the MTX-OEt derivative revealed a great biological effect in cancer cells.

Additionally, it was performed the development of other PNPs using PEGylated MTX (MTX-PEG_{2000}). The preliminary results obtained demonstrated that this compound is able to induce micelles formation, but further optimizations are needed. Concluding, the work developed in this master thesis allowed the achievement of the proposed objectives and give a positive contribution towards the development of novel DDS for therapeutic applications.

2. FUTURE PERSPECTIVES

In the future, some optimizations can be performed in order to achieve more efficient DDS, mainly in the case of the micelles produced using MTX-PEG_{2000}. As the P407-MTX nanoemulsions loaded with MTX-OEt demonstrated an excellent biological effect *in vitro*, the next step can be the realization of *in vivo* experiments.

Moreover, as these developed nanoemulsions represent a promising tool for cancer therapy, their application can also be explored in other relevant diseases. For example, in RA the activated macrophages are the key effect cells, which also express FR at the surface [104]. Additionally, the MTX is the first-line drug therapy for the treatment of RA [31]. In this way, in the future can be studied the application of these promising nanoemulsions in RA therapy.

References

1. Luong, D., *et al.*, *Folic acid conjugated polymeric micelles loaded with a curcumin difluorinated analog for targeting cervical and ovarian cancers.* Colloids and Surfaces B: Biointerfaces, 2017. **157**: p. 490-502.
2. Estanqueiro, M., *et al.*, *Nanotechnological carriers for cancer chemotherapy: The state of the art.* Colloids and Surfaces B: Biointerfaces, 2015. **126**: p. 631-648.
3. Thakor, A.S. and S.S. Gambhir, *Nanooncology: The future of cancer diagnosis and therapy.* CA: A Cancer Journal for Clinicians, 2013. **63**(6): p. 395-418.
4. Kim, J., *et al.*, *Polymeric biomaterials for the delivery of platinum-based anticancer drugs.* Biomaterials Science, 2015. **3**(7): p. 1002-1017.
5. Lee, J.J., L. Saiful Yazan, and C.A. Che Abdullah, *A review on current nanomaterials and their drug conjugate for targeted breast cancer treatment.* International Journal of Nanomedicine, 2017. **12**: p. 2373-2384.
6. Cho, K., *et al.*, *Therapeutic Nanoparticles for Drug Delivery in Cancer.* Clinical Cancer Research, 2008. **14**(5): p. 1310-1316.
7. Chandana, M., *et al.*, *Receptor Mediated Tumor Targeting: An Emerging Approach for Cancer Therapy.* Current Drug Delivery, 2011. **8**(1): p. 45-58.
8. Park, J.H., *et al.*, *Polymeric nanomedicine for cancer therapy.* Progress in Polymer Science, 2008. **33**(1): p. 113-137.
9. Pelt, J., *et al.*, *Chloroquine and nanoparticle drug delivery: A promising combination.* Pharmacology & Therapeutics, 2018. **191**: p. 43-49.
10. Low, P.S. and S.A. Kularatne, *Folate-targeted therapeutic and imaging agents for cancer.* Current Opinion in Chemical Biology, 2009. **13**(3): p. 256-262.
11. Misra, R. and S. Mohanty, *Sustained release of methotrexate through liquid-crystalline folate nanoparticles.* Journal of Materials Science: Materials in Medicine, 2014. **25**(9): p. 2095-2109.
12. Ramasamy, T., *et al.*, *Cationic drug-based self-assembled polyelectrolyte complex micelles: Physicochemical, pharmacokinetic, and anticancer activity analysis.* Colloids and Surfaces B: Biointerfaces, 2016. **146**: p. 152-160.
13. Boulaiz, H., *et al.*, *Nanomedicine: Application Areas and Development Prospects.* International Journal of Molecular Sciences, 2011. **12**(5): p. 3303-3321.

14. Kumari, A., S.K. Yadav, and S.C. Yadav, *Biodegradable polymeric nanoparticles based drug delivery systems.* Colloids and Surfaces B: Biointerfaces, 2010. **75**(1): p. 1-18.
15. Sandhiya, S., S.A. Dkhar, and A. Surendiran, *Emerging trends of nanomedicine – an overview.* Fundamental & Clinical Pharmacology, 2009. **23**(3): p. 263-269.
16. Huang, D., *et al.*, *Acetal-linked PEGylated paclitaxel prodrugs forming free-paclitaxel-loaded pH-responsive micelles with high drug loading capacity and improved drug delivery.* Materials Science and Engineering: C, 2018. **82**: p. 60-68.
17. Alam, F., *et al.*, *Unique roles of nanotechnology in medicine and cancer-II.* Indian Journal of Cancer, 2015. **52**(1): p. 1-9.
18. Li, J., *et al.*, *A review on phospholipids and their main applications in drug delivery systems.* Asian Journal of Pharmaceutical Sciences, 2015. **10**(2): p. 81-98.
19. Alexis, F., *et al.*, *Factors Affecting the Clearance and Biodistribution of Polymeric Nanoparticles.* Molecular Pharmaceutics, 2008. **5**(4): p. 505-515.
20. Tan, Y.F., *et al.*, *Controlled-release nanotherapeutics: State of translation.* Journal of Controlled Release, 2018. **284**: p. 39-48.
21. Filipe, V., A. Hawe, and W. Jiskoot, *Critical Evaluation of Nanoparticle Tracking Analysis (NTA) by NanoSight for the Measurement of Nanoparticles and Protein Aggregates.* Pharmaceutical Research, 2010. **27**(5): p. 796-810.
22. Wilczewska, A.Z., *et al.*, *Nanoparticles as drug delivery systems.* Pharmacological Reports, 2012. **64**(5): p. 1020-1037.
23. Prasad, M., *et al.*, *Nanotherapeutics: An insight into healthcare and multi-dimensional applications in medical sector of the modern world.* Biomedicine & Pharmacotherapy, 2018. **97**: p. 1521-1537.
24. Zhang, S., H. Gao, and G. Bao, *Physical Principles of Nanoparticle Cellular Endocytosis.* ACS nano, 2015. **9**(9): p. 8655-8671.
25. Li, Z., *et al.*, *Cancer drug delivery in the nano era: An overview and perspectives.* Oncology Reports, 2017. **38**(2): p. 611-624.
26. Cuenca, A.G., *et al.*, *Emerging implications of nanotechnology on cancer diagnostics and therapeutics.* Cancer, 2006. **107**(3): p. 459-466.
27. Kim, K.Y., *Nanotechnology platforms and physiological challenges for cancer therapeutics.* Nanomedicine: Nanotechnology, Biology and Medicine, 2007. **3**(2): p. 103-110.

28. Rao, J.P. and K.E. Geckeler, *Polymer nanoparticles: Preparation techniques and size-control parameters.* Progress in Polymer Science, 2011. **36**(7): p. 887-913.
29. Bertrand, N., *et al.*, *Cancer Nanotechnology: The impact of passive and active targeting in the era of modern cancer biology().* Advanced drug delivery reviews, 2014. **66**: p. 2-25.
30. Jurj, A., *et al.*, *The new era of nanotechnology, an alternative to change cancer treatment.* Drug Design, Development and Therapy, 2017. **11**: p. 2871-2890.
31. Ana, L., *et al.*, *Albumin-Based Nanodevices as Drug Carriers.* Current Pharmaceutical Design, 2016. **22**(10): p. 1371-1390.
32. Desai, N., *Challenges in Development of Nanoparticle-Based Therapeutics.* The AAPS Journal, 2012. **14**(2): p. 282-295.
33. Singh, S.K., *et al.*, *Drug delivery approaches for breast cancer.* International Journal of Nanomedicine, 2017. **12**: p. 6205-6218.
34. Pitto-Barry, A. and N.P.E. Barry, *Pluronic® block-copolymers in medicine: from chemical and biological versatility to rationalisation and clinical advances.* Polymer Chemistry, 2014. **5**(10): p. 3291-3297.
35. Sanna, V., N. Pala, and M. Sechi, *Targeted therapy using nanotechnology: focus on cancer.* International journal of nanomedicine, 2014. **9**: p. 467-483.
36. Li, Q., *et al.*, *A Review of the Structure, Preparation, and Application of NLCs, PNPs, and PLNs.* Nanomaterials, 2017. **7**(6): p. 122-147.
37. Batrakova, E.V., *et al.*, *Polymer Micelles as Drug Carriers*, in *Nanoparticulates as Drug Carriers*. 2006, PUBLISHED BY IMPERIAL COLLEGE PRESS AND DISTRIBUTED BY WORLD SCIENTIFIC PUBLISHING CO. p. 57-93.
38. Banerjee, A., *et al.*, *Strategies for targeted drug delivery in treatment of colon cancer: current trends and future perspectives.* Drug Discovery Today, 2017. **22**(8): p. 1224-1232.
39. Pérez-Herrero, E. and A. Fernández-Medarde, *Advanced targeted therapies in cancer: Drug nanocarriers, the future of chemotherapy.* European Journal of Pharmaceutics and Biopharmaceutics, 2015. **93**: p. 52-79.
40. Bhatia, S., *Nanoparticles Types, Classification, Characterization, Fabrication Methods and Drug Delivery Applications*, in *Natural Polymer Drug Delivery Systems: Nanoparticles, Plants, and Algae*, S. Bhatia, Editor. 2016, Springer International Publishing: Cham. p. 33-93.

41. Alexis, F., *et al.*, *Nanoparticle Technologies for Cancer Therapy*, in *Drug Delivery*, M. Schäfer-Korting, Editor. 2010, Springer Berlin Heidelberg: Berlin, Heidelberg. p. 55-86.
42. Hickey, J.W., *et al.*, *Control of polymeric nanoparticle size to improve therapeutic delivery.* Journal of Controlled Release, 2015. **219**: p. 536-547.
43. Dhand, C., *et al.*, *Role of size of drug delivery carriers for pulmonary and intravenous administration with emphasis on cancer therapeutics and lung-targeted drug delivery.* RSC Advances, 2014. **4**(62): p. 32673-32689.
44. Turner, P.V., *et al.*, *Administration of Substances to Laboratory Animals: Routes of Administration and Factors to Consider.* Journal of the American Association for Laboratory Animal Science : JAALAS, 2011. **50**(5): p. 600-613.
45. Barua, S. and S. Mitragotri, *Challenges associated with Penetration of Nanoparticles across Cell and Tissue Barriers: A Review of Current Status and Future Prospects.* Nano today, 2014. **9**(2): p. 223-243.
46. Byrne, J.D., T. Betancourt, and L. Brannon-Peppas, *Active targeting schemes for nanoparticle systems in cancer therapeutics.* Advanced Drug Delivery Reviews, 2008. **60**(15): p. 1615-1626.
47. Owens, D.E. and N.A. Peppas, *Opsonization, biodistribution, and pharmacokinetics of polymeric nanoparticles.* International Journal of Pharmaceutics, 2006. **307**(1): p. 93-102.
48. Zahr, A.S., C.A. Davis, and M.V. Pishko, *Macrophage Uptake of Core–Shell Nanoparticles Surface Modified with Poly(ethylene glycol).* Langmuir, 2006. **22**(19): p. 8178-8185.
49. Petros, R.A. and J.M. DeSimone, *Strategies in the design of nanoparticles for therapeutic applications.* Nature Reviews Drug Discovery, 2010. **9**: p. 615-627.
50. Wacker, M., *Nanocarriers for intravenous injection—The long hard road to the market.* International Journal of Pharmaceutics, 2013. **457**(1): p. 50-62.
51. Alakhova, D.Y. and A.V. Kabanov, *Pluronics and MDR Reversal: An Update.* Molecular Pharmaceutics, 2014. **11**(8): p. 2566-2578.
52. Milane, L., *et al.*, *Multi-modal strategies for overcoming tumor drug resistance: Hypoxia, the Warburg effect, stem cells, and multifunctional nanotechnology.* Journal of Controlled Release, 2011. **155**(2): p. 237-247.
53. Iyer, A.K., *et al.*, *Role of integrated cancer nanomedicine in overcoming drug resistance.* Advanced Drug Delivery Reviews, 2013. **65**(13): p. 1784-1802.

54. Zhang, M., *et al.*, *Nanotechnology-based combination therapy for overcoming multidrug-resistant cancer.* Cancer Biology & Medicine, 2017. **14**(3): p. 212-227.

55. Luo, D., K.A. Carter, and J.F. Lovell, *Nanomedical engineering: shaping future nanomedicines.* Wiley interdisciplinary reviews. Nanomedicine and nanobiotechnology, 2015. **7**(2): p. 169-188.

56. Korsmeyer, R., *Critical questions in development of targeted nanoparticle therapeutics.* Regenerative Biomaterials, 2016. **3**(2): p. 143-147.

57. Huang, Y., *et al.*, *Current applications and future prospects of nanomaterials in tumor therapy.* International Journal of Nanomedicine, 2017. **12**: p. 1815-1825.

58. Couvreur, P. and C. Vauthier, *Nanotechnology: Intelligent Design to Treat Complex Disease.* Pharmaceutical Research, 2006. **23**(7): p. 1417-1450.

59. Thanuja, M.Y., C. Anupama, and S.H. Ranganath, *Bioengineered cellular and cell membrane-derived vehicles for actively targeted drug delivery: So near and yet so far.* Advanced Drug Delivery Reviews, 2018. p. 1-78.

60. Johnson, J.L.K.M.S.S.P.R.G., *Biology*. 9th ed. 2008, Boston: McGraw-Hill Higher Education.

61. White, P.T.A.M.A.B.M., *Molecular Biology*. 3rd ed. 2005, New York: Taylor & Francis.

62. Gaumet, M., *et al.*, *Nanoparticles for drug delivery: The need for precision in reporting particle size parameters.* European Journal of Pharmaceutics and Biopharmaceutics, 2008. **69**(1): p. 1-9.

63. Duan, X. and Y. Li, *Physicochemical Characteristics of Nanoparticles Affect Circulation, Biodistribution, Cellular Internalization, and Trafficking.* Small, 2012. **9**(9-10): p. 1521-1532.

64. Kamaly, N., *et al.*, *Targeted polymeric therapeutic nanoparticles: design, development and clinical translation.* Chemical Society reviews, 2012. **41**(7): p. 2971-3010.

65. Movassaghian, S., O.M. Merkel, and V.P. Torchilin, *Applications of polymer micelles for imaging and drug delivery.* Wiley Interdisciplinary Reviews: Nanomedicine and Nanobiotechnology, 2015. **7**(5): p. 691-707.

66. Loureiro, A., *et al.*, *Size controlled protein nanoemulsions for active targeting of folate receptor positive cells.* Colloids and Surfaces B: Biointerfaces, 2015. **135**: p. 90-98.

67. Danaei, M., *et al.*, *Impact of Particle Size and Polydispersity Index on the Clinical Applications of Lipidic Nanocarrier Systems.* Pharmaceutics, 2018. **10**(2): p. 57-68.

68. Della Porta, G., R. Campardelli, and E. Reverchon, *Monodisperse biopolymer nanoparticles by Continuous Supercritical Emulsion Extraction.* The Journal of Supercritical Fluids, 2013. **76**: p. 67-73.

69. Sahay, G., D.Y. Alakhova, and A.V. Kabanov, *Endocytosis of Nanomedicines.* Journal of controlled release : official journal of the Controlled Release Society, 2010. **145**(3): p. 182-195.

70. Abdulrahman, L.A.O.B.M., *The Chemical Approach of Methotrexate Targeting.* American Institute of Science, 2016. **1**(2): p. 50-73.

71. Singh, R. and J.W. Lillard, *Nanoparticle-based targeted drug delivery.* Experimental and Molecular Pathology, 2009. **86**(3): p. 215-223.

72. Clogston, J.D. and A.K. Patri, *Zeta Potential Measurement*, in *Characterization of Nanoparticles Intended for Drug Delivery*, S.E. McNeil, Editor. 2011, Humana Press: Totowa, NJ. p. 63-70.

73. Nogueira, E., *et al.*, *Liposome and protein based stealth nanoparticles.* Faraday Discussions, 2013. **166**(0): p. 417-429.

74. Verma, A. and F. Stellacci, *Effect of Surface Properties on Nanoparticle–Cell Interactions.* Small, 2009. **6**(1): p. 12-21.

75. Letchford, K. and H. Burt, *A review of the formation and classification of amphiphilic block copolymer nanoparticulate structures: micelles, nanospheres, nanocapsules and polymersomes.* European Journal of Pharmaceutics and Biopharmaceutics, 2007. **65**(3): p. 259-269.

76. Nogueira, E., *et al.*, *Folate-targeted nanoparticles for rheumatoid arthritis therapy.* Nanomedicine: Nanotechnology, Biology and Medicine, 2016. **12**(4): p. 1113-1126.

77. Sorin Emilian, L., *Nanotechnology for Delivery of Drugs and Biomedical Applications.* Current Clinical Pharmacology, 2010. **5**(4): p. 257-280.

78. Veronese, F.M. and G. Pasut, *PEGylation, successful approach to drug delivery.* Drug Discovery Today, 2005. **10**(21): p. 1451-1458.

79. Dumortier, G., *et al.*, *A Review of Poloxamer 407 Pharmaceutical and Pharmacological Characteristics.* Pharmaceutical Research, 2006. **23**(12): p. 2709-2728.

80. Kabanov, A.V., E.V. Batrakova, and V.Y. Alakhov, *Pluronic® block copolymers as novel polymer therapeutics for drug and gene delivery.* Journal of Controlled Release, 2002. **82**(2): p. 189-212.

81. Kabanov, A.V., E.V. Batrakova, and V.Y. Alakhov, *Pluronic® block copolymers for overcoming drug resistance in cancer.* Advanced Drug Delivery Reviews, 2002. **54**(5): p. 759-779.

82. Kedar, U., *et al.*, *Advances in polymeric micelles for drug delivery and tumor targeting.* Nanomedicine: Nanotechnology, Biology and Medicine, 2010. **6**(6): p. 714-729.

83. Batrakova, E.V. and A.V. Kabanov, *Pluronic Block Copolymers: Evolution of Drug Delivery Concept from Inert Nanocarriers to Biological Response Modifiers.* Journal of controlled release : official journal of the Controlled Release Society, 2008. **130**(2): p. 98-106.

84. Bodratti, A.M. and P. Alexandridis, *Formulation of Poloxamers for Drug Delivery.* Journal of Functional Biomaterials, 2018. **9**(1): p. 11.

85. Ren, J., *et al.*, *A micelle-like structure of poloxamer–methotrexate conjugates as nanocarrier for methotrexate delivery.* International Journal of Pharmaceutics, 2015. **487**(1): p. 177-186.

86. Breitenbach, B.B., I. Schmid, and P.R. Wich, *Amphiphilic Polysaccharide Block Copolymers for pH-Responsive Micellar Nanoparticles.* Biomacromolecules, 2017. **18**(9): p. 2839-2848.

87. Kamboj, V.K.V., Prabhakar., *Poloxamers based nanocarriers for drug delivery system.* Der Pharmacia Lettre, 2015. **7**(2): p. 264-269.

88. Yan, F., *et al.*, *The effect of poloxamer 188 on nanoparticle morphology, size, cancer cell uptake, and cytotoxicity.* Nanomedicine: Nanotechnology, Biology and Medicine, 2010. **6**(1): p. 170-178.

89. Chen, Y., *et al.*, *Pluronic mixed micelles overcoming methotrexate multidrug resistance: in vitro and in vivo evaluation.* International journal of nanomedicine, 2013. **8**: p. 1463-1476.

90. Croy, S.R. and G.S. Kwon, *Polymeric Micelles for Drug Delivery.* Current Pharmaceutical Design, 2006. **12**(36): p. 4669-4684.

91. Lohcharoenkal, W., *et al.*, *Protein Nanoparticles as Drug Delivery Carriers for Cancer Therapy.* BioMed Research International, 2014. **2014**: p. 12-24.

92. Nogueira, E., *et al.*, *Design of liposomal formulations for cell targeting.* Colloids and Surfaces B: Biointerfaces, 2015. **136**: p. 514-526.

93. Daraee, H., *et al.*, *Application of liposomes in medicine and drug delivery.* Artificial Cells, Nanomedicine, and Biotechnology, 2016. **44**(1): p. 381-391.

94. Kulthe, S.S., *et al.*, *Polymeric micelles: authoritative aspects for drug delivery.* Designed Monomers and Polymers, 2012. **15**(5): p. 465-521.
95. MaHam, A., *et al.*, *Protein-Based Nanomedicine Platforms for Drug Delivery.* Small, 2009. **5**(15): p. 1706-1721.
96. Talekar, M., *et al.*, *Targeting of nanoparticles in cancer: drug delivery and diagnostics.* Anti-Cancer Drugs, 2011. **22**(10): p. 949-962.
97. Huang, J., *et al.*, *Magnetic Nanoparticle Facilitated Drug Delivery for Cancer Therapy with Targeted and Image-Guided Approaches.* Advanced Functional Materials, 2016. **26**(22): p. 3818-3836.
98. Prabhu, R.H., V.B. Patravale, and M.D. Joshi, *Polymeric nanoparticles for targeted treatment in oncology: current insights.* International Journal of Nanomedicine, 2015. **10**: p. 1001-1018.
99. Salehi, N.S.B.D.A.B.T.A.S.A., *Target Nanoparticles: An Appealing Drug Delivery Platform.* Nanomedic Nanotechnol, 2012. **4**(9): p. 1-9.
100. Fahmy, T.M., *et al.*, *Targeted for drug delivery.* Materials Today, 2005. **8**(8, Supplement): p. 18-26.
101. Blanco, E., *et al.*, *Nanomedicine in cancer therapy: Innovative trends and prospects.* Cancer Science, 2011. **102**(7): p. 1247-1252.
102. Rychahou, P., *et al.*, *Colorectal cancer lung metastasis treatment with polymer–drug nanoparticles.* Journal of controlled release : official journal of the Controlled Release Society, 2018. **275**: p. 85-91.
103. Yewale, C., *et al.*, *Proteins: emerging carrier for delivery of cancer therapeutics.* Expert Opinion on Drug Delivery, 2013. **10**(10): p. 1429-1448.
104. Teng, L., *et al.*, *Clinical translation of folate receptor-targeted therapeutics.* Expert Opinion on Drug Delivery, 2012. **9**(8): p. 901-908.
105. Assaraf, Y.G., C.P. Leamon, and J.A. Reddy, *The folate receptor as a rational therapeutic target for personalized cancer treatment.* Drug Resistance Updates, 2014. **17**(4): p. 89-95.
106. Low, P.S., W.A. Henne, and D.D. Doorneweerd, *Discovery and Development of Folic-Acid-Based Receptor Targeting for Imaging and Therapy of Cancer and Inflammatory Diseases.* Accounts of Chemical Research, 2008. **41**(1): p. 120-129.

107. Langer, D.P.J.M.K.S.H.O.C.F.R.M.R., *Nanocarriers as an emerging platform for cancer therapy.* nature nanotechnology, 2007. **2**: p. 751-760.

108. Brannon-Peppas, L. and J.O. Blanchette, *Nanoparticle and targeted systems for cancer therapy.* Advanced Drug Delivery Reviews, 2004. **56**(11): p. 1649-1659.

109. Loureiro, A., *et al.*, *Folic acid-tagged protein nanoemulsions loaded with CORM-2 enhance the survival of mice bearing subcutaneous A20 lymphoma tumors.* Nanomedicine: Nanotechnology, Biology and Medicine, 2015. **11**(5): p. 1077-1083.

110. Loureiro, A., *et al.*, *Functionalized protein nanoemulsions by incorporation of chemically modified BSA.* RSC Advances, 2015. **5**(7): p. 4976-4983.

111. Abolmaali, S.S., *et al.*, *Sequential optimization of methotrexate encapsulation in micellar nano-networks of polyethyleneimine ionomer containing redox-sensitive cross-links.* International journal of nanomedicine, 2014. **9**: p. 2833-2848.

112. Gulfam, M., *et al.*, *Bioreducible cross-linked core polymer micelles enhance in vitro activity of methotrexate in breast cancer cells.* Biomaterials Science, 2017. **5**(3): p. 532-550.

113. Chabner, B.A. and T.G. Roberts Jr, *Chemotherapy and the war on cancer.* Nature Reviews Cancer, 2005. **5**: p. 65-73.

114. Gorlick, R., *et al.*, *Intrinsic and Acquired Resistance to Methotrexate in Acute Leukemia.* New England Journal of Medicine, 1996. **335**(14): p. 1041-1048.

115. Choi, G., *et al.*, *Emerging nanomaterials with advanced drug delivery functions; focused on methotrexate delivery.* Coordination Chemistry Reviews, 2018. **359**: p. 32-51.

116. Brown, P.M., A.G. Pratt, and J.D. Isaacs, *Mechanism of action of methotrexate in rheumatoid arthritis, and the search for biomarkers.* Nature Reviews Rheumatology, 2016. **12**: p. 731-742.

117. Wong, P.T. and S.K. Choi, *Mechanisms and Implications of Dual-Acting Methotrexate in Folate-Targeted Nanotherapeutic Delivery.* International Journal of Molecular Sciences, 2015. **16**(1): p. 1772-1790.

118. Wibowo, A.S., *et al.*, *Structures of human folate receptors reveal biological trafficking states and diversity in folate and antifolate recognition.* Proceedings of the National Academy of Sciences of the United States of America, 2013. **110**(38): p. 15180-15188.

119. Suksiriworapong, J., *et al.*, *Synthesis and properties of a biodegradable polymer-drug conjugate: Methotrexate-poly(glycerol adipate).* Colloids and Surfaces B: Biointerfaces, 2018. **167**: p. 115-125.

120. Meloun, M., Z. Ferenčíková, and A. Vrána, *The thermodynamic dissociation constants of methotrexate by the nonlinear regression and factor analysis of multiwavelength spectrophotometric pH-titration data.* Central European Journal of Chemistry, 2010. **8**(3): p. 494-507.

121. Loureiro, A., *et al.*, *Absence of Albumin Improves in Vitro Cellular Uptake and Disruption of Poloxamer 407-Based Nanoparticles inside Cancer Cells.* Molecular Pharmaceutics, 2018. **15**(2): p. 527-535.

122. ATCC. *Caco-2 [Caco2] (ATCC® HTB-37™)*. 2016; Available from: https://www.lgcstandards-atcc.org/Products/All/HTB-37.aspx?geo_country=pt#characteristics.

123. Promega. *CellTiter 96® AQueous One Solution Cell Proliferation Assay (MTS)*. 2018; Available from: https://worldwide.promega.com/products/cell-health-assays/cell-viability-and-cytotoxicity-assays/celltiter-96-aqueous-one-solution-cell-proliferation-assay-_mts_/?catNum=G3582.

124. Noro, J., *et al.*, *Ultrasound-assisted biosynthesis of novel methotrexate-conjugates.* Ultrasonics Sonochemistry, 2018. **48**: p. 51-56.

125. Potangale, C.N. and S.K. Pardeshi, *Quantification of Drugs by Proton NMR Incorporated Internal Standard Method.* Eurasian Journal of Analytical Chemistry, 2014. **9**(1): p. 1-7.

126. Tseng, M.-C., *et al.*, *Dihydrobenzoic Acid Modified Nanoparticle as a MALDI-TOF MS Matrix for Soft Ionization and Structure Determination of Small Molecules with Diverse Structures.* Journal of the American Society for Mass Spectrometry, 2010. **21**(11): p. 1930-1939.

127. Kanakapura, B., P. Nagegowda, and V. Ramakrishna, *Determination of Drug Content of Pharmaceuticals Containing Ranitidine by Titrimetry and Spectrophotometry in NonAqueous Medium*. 2018.

128. Raveendran, R., G.S. Bhuvaneshwar, and C.P. Sharma, *In vitro cytotoxicity and cellular uptake of curcumin-loaded Pluronic/Polycaprolactone micelles in colorectal adenocarcinoma cells.* Journal of Biomaterials Applications, 2012. **27**(7): p. 811-827.

129. Stetefeld, J., S.A. McKenna, and T.R. Patel, *Dynamic light scattering: a practical guide and applications in biomedical sciences.* Biophysical Reviews, 2016. **8**(4): p. 409-427.

130. Bhattacharjee, S., *DLS and zeta potential – What they are and what they are not?* Journal of Controlled Release, 2016. **235**: p. 337-351.

131. Wilhelm, S., *et al.*, *Analysis of nanoparticle delivery to tumours.* Nature Reviews Materials, 2016. **1**: p. 16014.

132. Cámara, A.L.-S.R.M.O.J.S.L.C., *Nanoparticles: a global vision. Characterization, separation, and quantification methods. Potential environmental and health impact.* Anal. Methods, 2014. **6**(38): p. 38-56.

133. Rios-Ramírez, E.T.a.A., *Biodegradation of Medical Purpose Polymeric Materials and Their Impact on Biocompatibility.* Biodegradation—Life of Science, 2013.

134. Fukami, T. and T. Yokoi, *The Emerging Role of Human Esterases.* Drug Metabolism and Pharmacokinetics, 2012. **27**(5): p. 466-477.

135. Kunzmann, A., *et al.*, *Toxicology of engineered nanomaterials: Focus on biocompatibility, biodistribution and biodegradation.* Biochimica et Biophysica Acta (BBA) - General Subjects, 2011. **1810**(3): p. 361-373.

136. Li, W., J. Zhou, and Y. Xu, *Study of the in vitro cytotoxicity testing of medical devices.* Biomedical Reports, 2015. **3**(5): p. 617-620.

137. Couvreur, P., *Nanoparticles in drug delivery: Past, present and future.* Advanced Drug Delivery Reviews, 2013. **65**(1): p. 21-23.

138. Karimi, M.A., *et al.*, *A new simple method for determining the critical micelle concentration of surfactants using surface plasmon resonance of silver nanoparticles.* Journal of Analytical Science and Technology, 2015. **6**(1): p. 35-43.

139. Patist, A., *et al.*, *On the measurement of critical micelle concentrations of pure and technical-grade nonionic surfactants.* Journal of Surfactants and Detergents, 2000. **3**(1): p. 53-58.

140. Topel, Ö., *et al.*, *Determination of critical micelle concentration of polybutadiene-block-poly(ethyleneoxide) diblock copolymer by fluorescence spectroscopy and dynamic light scattering.* Journal of Molecular Liquids, 2013. **177**: p. 40-43.

141. Dominguez, A., *et al.*, *Determination of Critical Micelle Concentration of Some Surfactants by Three Techniques.* Journal of Chemical Education, 1997. **74**(10): p. 1227-1232.

142. Chakraborty, T., I. Chakraborty, and S. Ghosh, *The methods of determination of critical micellar concentrations of the amphiphilic systems in aqueous medium.* Arabian Journal of Chemistry, 2011. **4**(3): p. 265-270.

143. Qian, C. and D.J. McClements, *Formation of nanoemulsions stabilized by model food-grade emulsifiers using high-pressure homogenization: Factors affecting particle size.* Food Hydrocolloids, 2011. **25**(5): p. 1000-1008.

144. Silva, H.D., M.A. Cerqueira, and A.A. Vicente, *Influence of surfactant and processing conditions in the stability of oil-in-water nanoemulsions.* Journal of Food Engineering, 2015. **167**: p. 89-98.

145. Jaiswal, M., R. Dudhe, and P.K. Sharma, *Nanoemulsion: an advanced mode of drug delivery system.* 3 Biotech, 2015. **5**(2): p. 123-127.

146. Yuan, Y., *et al.*, *Characterization and stability evaluation of β-carotene nanoemulsions prepared by high pressure homogenization under various emulsifying conditions.* Food Research International, 2008. **41**(1): p. 61-68.

147. Abbas, S., *et al.*, *Fabrication of polymeric nanocapsules from curcumin-loaded nanoemulsion templates by self-assembly.* Ultrasonics Sonochemistry, 2015. **23**: p. 81-92.

148. Charcosset, C., *et al.*, *Preparation of liposomes at large scale using the ethanol injection method: Effect of scale-up and injection devices*, 2015. **94**: p. 508-515.